Fundamental interactions driving the coil-to-globule transition and LCST behavior of poly(N-isopropylacrylamide) in water.

An Abstract
Submitted On The Seventh Day Of April, 2015
To The Department Of Physics and Engineering Physics
Of The Graduate School Of
Tulane University
In Partial Fulfillment Of The Requirements
For The Degree Of
Doctor Of Philosophy
By

Colin A. McFaul

Approved:

Wayne F. Reed, Ph.D.
Chairman

Ryan Glasser, Ph.D.

Scott M. Grayson, Ph.D.

Charles L. McCormick, Ph.D.

Abstract

I introduce and demonstrate a novel detector for characterization of lower critical solution temperature (LCST) behavior during synthesis. This new detector acts in concert with Automatic Continuous Online Monitoring of Polymerization (ACOMP) to correlate LCST behavior with other properties of the polymer system. As a result, the new detector system is called "Second generation ACOMP" (SGA). This allows me to observe, for the first time ever, LCST behavior of a polymer during synthesis.

ACOMP works by extracting a small stream of sample from a polymerization reaction, diluting it, and passing it through several detectors. This allows rapid characterization of molecular weight (M_w), radius of gyration (R_g), second virial coefficient (A_2), and viscosity. For copolymers, ACOMP also characterizes the comonomer composition and comonomer composition drift.

The SGA detectors consist of three temperature-controlled single-angle light scattering flow cells. These allow the characterization of polymer aggregation due to LCST effects. The onset and temperature of this effect can be correlated to the more basic properties (primarily composition) of the polymer.

I use this detector to characterize the composition dependence of the LCST of poly(N-isopropyl acrylamide) (pNIPAM). I copolymerize NIPAM with the neutral, hydrophilic comonomer Acrylamide (Am), the anionic comonomer styrene sulfonate (SS), and the cationic comonomer [2-(acryloyloxy)ethyl]-trimethylammonium chloride (Q9). The effect of each of these comonomers on the LCST is compared. In addition, I compare the effect of ionic strength on the LCST of each of the copolymer systems.

Fundamental interactions driving the coil-to-globule transition and LCST behavior of poly(N-isopropylacrylamide) in water.

A Dissertation
Submitted On The Seventh Day Of April, 2015
To The Department Of Physics and Engineering Physics
Of The Graduate School Of
Tulane University
In Partial Fulfillment Of The Requirements
For The Degree Of
Doctor Of Philosophy
By

Colin A. McFaul

Approved:

Wayne F. Reed, Ph.D.
Chairman

Ryan Glasser, Ph.D.

Scott M. Grayson, Ph.D.

Charles L. McCormick, Ph.D.

© Copyright by Colin A. McFaul, 2015

All Rights Reserved

Acknowledgments

I would like to begin by thanking my committee members. Prof. Reed has provided research guidance, career advice, and financial support throughout my time here at Tulane. Profs. Grayson and McCormick have both provided wise chemical and career insights. Prof. Glasser stepped in to serve on my committee at the very last minute.

In addition to my committee, the other members of the Reed Research group have supported me. Mike Drenski and Curt Jarand provided much technical assistance with instrumentation and experimental design. Tomasz Kreft helped me settle into the group upon my arrival, and introduced me to New Orleans. Zheng and Zifu have provided camaraderie, support, and an inquisitive perspective on American culture. Brooke has provided encouragement and new energy.

The Hollygrove Market and Farm, has provided me with delicious and healthy food via delivery every Tuesday during the past 15 months. Several mental health professionals have assisted me with their expertise. They have all allowed me to persevere through the various psychological difficulties that come with graduate school and the sciences.

My family has loved and supported me for over thirty years. This includes all four of my mothers, my three fathers, four brothers, and four sisters. My dog and cats have calmed me and kept me company at various times. Finally, my wife Nora is an amazing partner, protector, and lifelong companion. She has been incredibly patient, supportive, and understanding throughout this entire process.

Contents

1 Introduction **1**

2 Theory **4**

2.1 Introduction 4

2.2 Polymers 4

2.2.1 Degree of polymerization and molecular weight 4

2.2.2 Chain conformation 6

2.2.3 Architecture and composition 7

2.2.4 Polymerization kinetics 8

2.3 Polyelectrolytes 15

2.4 Light scattering theory 18

2.4.1 Static light scattering 18

2.4.2 Dynamic light scattering 24

2.5 Viscosity 26

2.6 UV-Vis spectroscopy 29

3 Lower critical solution temperature **31**

3.1 Introduction 31

3.2 Phenomenology 33

3.3 Observation of LCST 35

3.4 Thermodynamics of mixing 38

3.5 Hofmeister Effect 44
3.6 Overall Picture 46

4 Materials and Methods **47**

4.1 Introduction 47
4.2 Detectors 47
4.2.1 Multi-Angle Light Scattering 47
4.2.2 Differential Refractometry 49
4.2.3 UV-Vis Spectroscopy 50
4.2.4 Dynamic Light Scattering (DLS) 54
4.2.5 Simultaneous Multiple Static Light Scattering (SMSLS) 54
4.2.6 Viscometer 55
4.3 Multi-Detector Techniques 55
4.3.1 Gel Permeation Chromatography 55
4.3.2 ACOMP 57
4.3.3 Automatic Continuous Mixing (ACM) 59
4.3.4 Second Generation ACOMP (SGA) 60

5 Results **64**

5.1 Introduction 64
5.2 Second generation ACOMP 67
5.3 Simultaneous multiple sample light scattering 70
5.4 Nonionic comonomer: Acrylamide 73
5.4.1 Introduction 74
5.4.2 Materials and methods 75
5.4.3 Results and discussion 83
5.4.4 Conclusions 104

5.5 Anionic comonomer: Styrene sulfonate 105
5.5.1 Introduction 105
5.5.2 Materials and Methods 109
5.5.3 Results and discussion 116
5.5.4 Conclusion 132
5.6 Cationic comonomer: Q9 133
5.6.1 Introduction 133
5.6.2 Materials and Methods 135
5.6.3 Results and Discussion 137

6 Conclusion **148**

References **150**

List of Figures

2.1 A typical random walk conformation of a polymer. 7

2.2 The light scattering experiment. 24

2.3 A shear force. 27

2.4 Capillary flow. 28

3.1 A photo of pNIPAM clouding in water. 35

3.2 LCST depends on M_w. 36

3.3 Spinodal and binodal curves. 40

4.1 The differential refractometer. 50

4.2 Permeation of the chains through the GPC column. 56

4.3 The GPC detector train. 57

4.4 Automatic continuous online monitoring of polymerizations (ACOMP). 58

4.5 The ACM instrumentation setup. 61

4.6 The SGA flow cells. 62

4.7 The SGA flow arrangement. 63

5.1 Acrylamide. 64

5.2 Styrene sulfonate. 65

5.3 [2-(acryloyloxy)ethyl]-trimethylammonium chloride. 65

5.4 Potassium Persulfate. 66

5.5 2,2'-Azobis(2-methylpropionamidine)dihydrochloride (V50). 66

5.6 Tetramethylethylenediamine. 66

5.7 Voltage-Temperature response of the peltier devices. 68
5.8 Flow cell temperature due to heating block temperature. 69
5.9 Stability of BSA at different pH's in water. 71
5.10 Protein aggregation by SMSLS. 72
5.11 The SMSLS cells with meshes for dissolution studies. 73
5.12 Dissolution observed by SMSLS. 74
5.13 Typical ACOMP raw data. 79
5.14 Raw ACOMP data for reaction A7. 82
5.15 $F_{\text{inst,NIPAM}}$ for the batch reactions. 87
5.16 Molecular weight versus conversion. 90
5.17 Conversions and composition of reaction A7. 91
5.18 The widths of LCST transitions. 92
5.19 LCST as a function of composition, at several salt concentrations. . . 97
5.20 Composition distributions. 100
5.21 End product LCST's. 103
5.22 Stability and reversibility 104
5.23 UV spectra of NIPAM, SS, and Am monomers 112
5.24 The effect of smoothing. 115
5.25 Raw ACOMP data. 116
5.26 Scattering versus conversion. 118
5.27 Conversion, viscosity, M_w, SGA light scattering. 120
5.28 The onset of LCST in Reaction S2. 121
5.29 The onset of LCST in Reaction S3. 122
5.30 The onset of LCST in Reaction S4. 122
5.31 Reaction S5 shows no LCST behavior. 124
5.32 Composition drift can go either way. 125

5.33 Viscosity shows no abnormality. 127
5.34 Immediate onset of LCST in an Am/NIPAM copolymer. 128
5.35 The polymer blend shows no LCST behavior. 130
5.36 NaCl can induce LCST. 131
5.37 Computed monomer concentrations from Reaction Q2. 138
5.38 Raw UV, light scattering, and SGA light scattering from Reation Q3. 139
5.39 The $F_{\text{inst,Q9}}$ data from Reaction Q3. 140
5.40 Raw UV data from Reaction Q4. 141
5.41 Finst data from Reaction Q4. 142
5.42 A GPC trace of Reaction Q1. 144
5.43 Reaction Q2 and Q3 LCST's as a function of ionic strength. 145
5.44 Semi-batch samples in 1 M NaCl. 146

List of Tables

2.1 Some reactivity ratios. 15

3.1 Enthalpy of the coil-to-globule transition. 43

5.1 Flow cell temperature under different conditions. 70

5.2 The batch reactions used in the NIPAM/Am study. 78

5.3 The semi-batch reaction. 81

5.4 Reaction A7 aliquots. 81

5.5 First generation ACOMP results. 83

5.6 Semi-batch ACOMP results. 89

5.7 SGA results of the NIPAM/Am batch reactions. 102

5.8 SS batch reactions. 109

5.9 Dual-wavelength UV extinction coefficients for NIPAM and SS monomer, and their polymers. 114

5.10 The batch reactions used in the Q9 study. 135

5.11 The semi-batch reaction used in the Q9 study. 136

5.12 The samples taken from the waste stream of Reaction Q4. 146

Chapter 1

Introduction

The word "polymer" refers to any high molecular weight, long chain-like molecule. The chain is made up of smaller, repeating units called "monomers." For some time, it was controversial whether polymers were single covalently bonded molecules, or aggregates of smaller molecules connected together through some other interaction [1]. Staudinger was awarded the 1953 Nobel Prize in Chemistry for demonstrating that polymers are actual covalently-bonded molecules. Each individual polymer chain can have an essentially unlimited molecular weight. In practice, chains of molecular weight over 1 MDa are easily made.

Natural and synthetic plastics and oils are polymers. In addition, the macromolecules of biology can be considered polymers: DNA, RNA, proteins. These have much different uses in the world than the non-biological polymers. Many of the properties that make biopolymers useful biologically interferes with their use for other purposes. However, there are sufficient underlying principles that describe all polymers that it is useful to lump together the two classes.

Most polymers follow a motif in which the monomers in the chain are nearly identical. Some chemical functionality allows them to chain together. The side groups that stick out from the backbone can be different. Nearly any functionality can be attached in this manner. It is this flexibility that makes polymers so useful; the added

functionalities can be mixed and matched to nearly any desired proportion. This allows a chemist to design a polymer with nearly any desired macroscopic solution or solid-state properties.

This is in sharp contrast to small molecules: a functional group makes up a large fraction of a small molecule, and has a correspondingly large impact on several physical and chemical properties at once. For example, the difference between ethanol and methanol is only one ethyl group. The addition of this group into the molecule drastically raises the boiling point of the liquid phase, and lowers the toxicity. Adding an ethyl group (or even a whole monomer) to a polymer chain would have only a very small effect on the macroscopic properties of the chain.

Stimuli-responsive polymers is a rapidly developing sub field of polymer science. This is a class of polymers which react to changes in their environment, usually quite drastically. pH, temperature, ionic strength, electric or magnetic fields, and light irradiation are all stimuli known to induce these changes in certain polymer systems. The exact physical interaction that causes this behavior varies with the stimulus. Light of the appropriate frequency causes certain double bonds to undergo a cis-trans isomerization. Some polymers can protonate or deprotonate with changes in pH.

One prominent stimuli-responsive polymer is the temperature responsive poly(N-isopropyl acrylamide) (pNIPAM) [2]. NIPAM displays a lower critical solution temperature (LCST) in water: when heated above 32 °C, the polymer chains become hydrophobic, collapse into a globule and fall out of solution. Below 32 °C, the polymer chains are in an expanded coil configuration and readily soluble in water. This unusual behavior is caused by the balance of hydrophobic and hydrophilic groups in the NIPAM monomer, and is completely reversible. Several past studies have demonstrated that adding hydrophilic or hydrophobic comonomers to pNIPAM lowers and

raises the LCST, respectively [3, 4]. In addition, adding ions to the solution lowers the LCST [5].

Automatic continuous online monitoring of polymerization (ACOMP) is a technique that allows the measurement of several fundamental polymer properties during polymer synthesis. ACOMP can measure monomer conversion, copolymer composition and drift, intrinsic viscosity $[\eta]$, molecular weight M_w, and radius of gyration R_g. A dilution stage between the reactor and the detectors allows the detectors to measure the single-chain average properties of the polymer in a model-independent fashion. In this way, the polymer is "born characterized."

The goal of this dissertation is to use ACOMP and its associated techniques to study the effect of electrostatic interactions on the LCST of NIPAM. I copolymerize NIPAM with the hydrophilic monomer Acrylamide (Am), the negatively-charged monomer styrene sulfonate (SS), and the positively-charged monomer [2-(acryloyloxy)ethyl]-trimethylammonium chloride (Q9). Each of these has a different reactivity with NIPAM, and a different effect on the LCST of the resulting polymer chains. I also report several improvements to the ACOMP technique.

The work presented in this thesis has been published in the following papers:

1. McFaul, C. A., Alb, A. A., M. F. Drenski, and W. F. Reed, "Simultaneous multiple sample light scattering detection of LCST during copolymer synthesis", *Polymer* **52** (2011), no. 21, 4825–4833.

2. McFaul, C. A., M. F. Drenski, and W. F. Reed, "Online, continuous monitoring of the sensitivity of the LCST of NIPAM-am copolymers to discrete and broad composition distributions", *Polymer* **55** (2014), no. 19, 4899–4907.

Chapter 2

Theory

2.1 Introduction

This chapter outlines the basic theory of polymers themselves, and describes the chemical theory of their synthesis. The underlying chemistry predicts that the polymer chain population will have certain properties. Understanding that theory requires some vocabulary specific to polymer science. There are several techniques used for the characterization of polymers; this chapter also discusses the background theory behind each of the techniques used in this dissertation.

2.2 Polymers

2.2.1 Degree of polymerization and molecular weight

Polymers are long-chain molecules. They are made up of several repeating units called monomers. The monomers are covalently bonded to each other to form the chain. The number of repeating units in the chain is known as the degree of polymerization, and is denoted N. The molecular weight of the chain, denoted M, can be approximated as the degree of polymerization multiplied by the molecular weight of an individual monomer, $M_p = NM_m$. Strictly speaking, the molecular weight of the polymer should also account for the end groups terminating each end

of the chain. But for long chains, this is not a measurable effect.

One major difference between polymers and small molecules is that not all polymer chains in a given population will be identical. There will typically be some variation of molecular weight within the population. Therefore, we use averages to describe the population. The simplest average is the number average molecular weight, M_n. In this average, all chains count equally. This is given by

$$M_n = \frac{1}{N} \sum_i M_i \tag{2.1}$$

The next average is the weight average molecular weight,

$$M_w = \frac{\sum_i N_i M_i^2}{\sum_i N_i M_i} \tag{2.2}$$

This average weights each polymer chain according to its weight, so it is more sensitive to higher molecular weight chains. As we will discuss below, this is the average measured by light scattering. Another average sometimes used is the z-average molecular weight,

$$M_z = \frac{\sum_i N_i M_i^3}{\sum_i N_i M_i^2} \tag{2.3}$$

These are, respectively, the first, second, and third moments of the mass distribution. Higher-order moments also exist, and can be computed given the full mass distribution. But these moments are not easily measured experimentally, and are only rarely used.

A basic result of statistics is that the i^{th} moment of a distribution is lager than the $(i-1)^{\text{th}}$ moment. Therefore, $M_n < M_w < M_z$. The ratios M_w/M_n and M_z/M_w can be used as measures of the polydispersity of the population. M_w/M_n is the more typical choice, and is called the polydispersity index, or PDI. Note that PDI ≥ 1. Rarely, the quantity PDI $- 1$ is used as a measure of polydispersity.

2.2.2 Chain conformation

A second major difference between polymers and small molecules is that polymers' configurations change much more readily than those of small molecules. The chain conformation can be described using several measures of chain size. Two common measures are the end-to-end length R_n, the distance between the two ends of the chain, and the radius of gyration R_g, the root mean squared distance of the monomers in the chain to the chain's center of mass. R_g is the second moment of the mass distribution, equivalent to the moment of inertia from classical mechanics. These two measures of chain dimension will in general have the same scaling behavior with respect to molecular weight, but the exact relationship between them will depend on the conformation of the chain. In addition, the chain conformation is in constant flux; as a result, the only meaningful chain dimensions of an individual chain are averages over time. In the case of a population, the chain dimension will also be an average over the population of chains.

The simplest model to describe a polymer conformation is the random walk model. This follows the same $\langle R_n \rangle \propto \sqrt{n}$ scaling behavior as the random walk model for ideal gasses. The pre-factor can be changed by adding more detail to the model, such as C−C bond angles, C−C−C dihedral angles, and other effects of steric hindrance. None of these short-term effects affects the scaling behavior with respect to the number of monomers in the chain; this remains proportional to $\sqrt{n}$. But real polymer chains cannot intersect themselves; accounting for this excluded volume effect gives the self-avoiding random walk model, in which the end-to-end distance scales as $\langle R_n \rangle \propto n^{3/(2+d)}$ if the polymer lives in a d-dimensional space. In three dimensions, this becomes $\langle R_n \rangle \propto n^{3/5}$ [6]. In all cases, the scaling behavior of the radius of gyration $\langle R_g \rangle$ is the same as the scaling behavior of the end-to-end distance. In addition, any measure of the conformation is an average over time and the chain

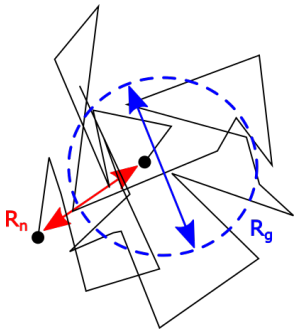

Figure 2.1: A typical random walk conformation of a polymer. Each step is shown as a straight line. R_n is defined as shown. R_g as shown is approximate.

population, and will vary from solvent to solvent.

2.2.3 Architecture and composition

In addition to molecular weight and conformation changes, polymers can also have a wide array of architectures. The simplest architecture is the simple linear chain, in which the polymer chain forms a simple chain. This architecture has been implicitly assumed in the previous sections, and is the only architecture I use in this dissertation. Some polymers can, however, branch. This happens when an atom in the chain backbone connects to three functional groups instead of just two. This causes the chain to branch, forming a Y-shaped backbone. If the branch is composed of a different monomer than the main branch, then this is called a graft copolymer. There is no general limit to the amount of branching a polymer can have. If the polymer has such a high degree of branching that each branch is only a few monomers long, then this is called a cross-linked polymer. The polymer chain can also re-connect to itself, forming a loop or a cyclic polymer [7]. The polymer can even have more than one loop [8].

Copolymers are polymers with two different constituent monomers, called comonomers. Terpolymers have three different monomers. There is no specific name for a copolymer with more than three comonomers. There is no limit to the number

of different comonomers in the polymer. For example, DNA and RNA have four comonomers, the nucleic acids; proteins have 20, the amino acids. The presence of more comonomers brings more interesting properties, and a wider variety of configurations. As mentioned above, graft copolymers are copolymers where a chain of a second monomer branches from the middle of a chain of the first monomer. Block copolymers are made of blocks of each monomer. A section of the chain is made entirely of one monomer ("A"), while the next section is made of another monomer ("B"); these blocks are then joined together to form a single chain. Many blocks can be joined together in any fashion. The easiest copolymers to make are random, or statistical, copolymers. In these copolymers, the monomers are allowed to react and add to the chain according to the statistics and kinetics of the reaction. The result is that the chain will have both comonomers present at nearly all points along the chain. The exact pattern and ratio is determined by the ratio of the two comonomers in the reaction vessel (the "feed ratio"), and the reactivities of the monomers present (the "reactivity ratios"). All of the copolymers in this dissertation are random copolymers. I describe these in more detail in Section 2.2.4.

2.2.4 Polymerization kinetics

Free radical chain reactions form the basis of many polymerization techniques. One of the simpler is free radical polymerization; this is the only polymerization method I use in this dissertation. Both because of the importance of this method as a basis for other methods, and my use of it in this thesis, this subsection will review the kinetics of free radical polymerization in detail.

Polymerization reactions are sometimes divided into step-growth and chain-growth reactions. In step-growth reactions small chains are made initially out of monomers, and get larger as the reaction progresses. As a result, high molecular weight chains require that the reaction run to near completion. In contrast, chain-

growth reactions produce high molecular weight chains early in the reaction, and lower molecular weight chains later in the reaction. The free-radical reactions I used in this thesis are all chain-growth reactions, so I will not consider step-growth reactions any further. Chain-growth reactions have three major steps: initiation, propagation, and termination.

In the initiation step, the initiator is broken down into free-radicals. This is represented as $\mathrm{I} \longrightarrow \mathrm{I}\cdot$. This can be done thermally, as in the case of peroxides and azos, via a redox coupling reaction, as in the case of peroxides or persulfates, or photochemically. For thermal decomposition, we can write down the kinetic law for the process as

$$\frac{d[[\mathrm{I}\cdot]}{dt} = 2k_d[\mathrm{I}] \tag{2.4}$$

where k_d is the rate constant for the process. For a redox process, this becomes

$$\frac{d[\mathrm{I}\cdot]}{dt} = k_d[\mathrm{Ox}][\mathrm{Red}] \tag{2.5}$$

In both cases, k_c follows an Arrhenius law

$$k_d \propto \exp(-E^*/RT) \tag{2.6}$$

where E^* is the activation energy. Of note is that increasing the temperature of the reaction greatly speeds up reactions initiated both by thermal decomposition and redox coupling. There is no such temperature effect in photoinitiated reactions. In this dissertation, I use thermal decomposition with Azobisisobutyronitrile (AIBN) and redox coupling with Potassium persulfate (KPS) and Tetramethylethylenediamine (TEMED).

Propagation is the process of propagating the radical while a chain builds up.

This is described by the kinetic equation

$$R_p = \sum_i k_p^i [\mathrm{P_i} \cdot][\mathrm{M}] = k_p[\mathrm{P} \cdot][\mathrm{M}] \tag{2.7}$$

The second equality holds under the assumption that all chain lengths propagate at the same rate. Under the additional assumption that the number of monomers involved in propagation is much larger than the number of monomers involved in initiation, we can also say that

$$-\frac{d[\mathrm{M}]}{dt} \propto R_p = k_p[\mathrm{P} \cdot][\mathrm{M}] \tag{2.8}$$

In this work, $[\mathrm{M}]_0/[\mathrm{I}] = 150$, so this assumption is valid.

Termination is the process by which a propagating chain ceases propagation. This can be due either to combination of two chains, or by disproprotionation. Combining the two cases into one kinetic equation gives

$$R_t = -\frac{d[P*]}{dt} = 2k_t[\mathrm{P} \cdot]^2 \tag{2.9}$$

where $k_t = k_{t,c} + k_{t,d}$; $k_{t,c}$ and $k_{t,d}$ are the rate constants for combination and disproprotionation, respectively. If we take $E^*_{t,c}$ and $E^*_{t,d}$ to be the activation energies for the two termination processes, we can write the relative importance of the two processes as

$$\frac{k_{t,c}}{k_{t,d}} = \frac{A_{t,c}}{A_{t,d}} \exp\left(\frac{-(E^*_{t,c} - E^*_{t,d})}{RT}\right) \tag{2.10}$$

Typically, $E^*_{t,d} > E^*_{t,c}$, so combination is more important at lower reaction temperatures. As the reaction temperature increases, both processes tend to become equally important.

In practice, we use the quasi-steady state approximation (QSSA) to relate the

kinetics of these three reactions and use the kinetics to make predictions about the products of the reaction. QSSA assumes that the rate constants k_t and k_p are independent of chain length and monomer concentration. It also assumes that monomer is consumed only by propagation, and that the concentration of free radicals is constant. These assumptions are not strictly true at all times during the reaction, but it is believed that the reaction quickly enters the quasi-stead state, and that these assumptions hold for most of the reaction [9]. The initiator dissociates completely into its radical form quickly, and the total radical concentration remains approximately constant from that point on. Under the QSSA,

$$R_i = R_t \Rightarrow 2fk_d[\mathrm{I}] = 2k_t[\mathrm{P}\cdot]_S^2 \tag{2.11}$$

where f is the efficiency of the initiator in creating propagating chains ($0 < f < 1$). Then the free-radical concentration at steady-state is

$$[\mathrm{P}\cdot]_S = \left(\frac{fk_d}{k_t}\right)^{1/2}[\mathrm{I}]^{1/2} \tag{2.12}$$

We can plug equation 2.12 in to equation 2.8 to get

$$R_p = \sqrt{\frac{2fk_dk_p^2}{k_t}}[\mathrm{M}][\mathrm{I}]^{1/2} = -\frac{d[\mathrm{M}]}{dt} \tag{2.13}$$

We can then define a kinetic chain length as

$$v_n = R_p/R_i = \frac{k_p[\mathrm{M}]}{k_t[\mathrm{P}\cdot]} = \frac{k_p[\mathrm{M}]}{(2fk_dk_t[\mathrm{I}])^{1/2}} \tag{2.14}$$

Now, termination by disproprotionation causes each kinetic chain to produce 1 polymer chain, so $X_n = v_n$. But termination by combination creates two polymer chains for each kinetic chain, so $X_n = 2v_n$. Knowing the relative amounts of combination

and disproprotionation allows us to infer $\langle X_n \rangle$, and therefore $\langle M_w \rangle$, as a function of [I] and $[\mathrm{M}]_0$.

Following Hiemenz [10], we can derive the molecular weight distribution produced by this reaction. Under the QSSA, the kinetic equation

$$\frac{d[\mathrm{P_i} \cdot]}{dt} = k_p[\mathrm{M}][\mathrm{P_{i-1}} \cdot] - k_p[\mathrm{M}][\mathrm{P_i} \cdot] - 2k_t[\mathrm{P_i} \cdot][\mathrm{P} \cdot] = 0 \tag{2.15}$$

The three terms on the left correspond to the reactions $\mathrm{P_{i\text{-}1}}\cdot + \mathrm{M} \longrightarrow \mathrm{P_i}\cdot$, $\mathrm{P_i}\cdot + \mathrm{M} \longrightarrow \mathrm{P_{i+1}}\cdot$, and $\mathrm{P_i}\cdot + \mathrm{P} \longrightarrow \mathrm{P_{i+k}}\cdot$. This be rearranged to give

$$\frac{[\mathrm{P_i} \cdot]}{[\mathrm{P_{i-1}} \cdot]} = \frac{k_p[\mathrm{M}]}{k_p[\mathrm{M}] + 2k_t[\mathrm{P} \cdot]} = \frac{v_n}{1 + v_n} \tag{2.16}$$

where the last equality is from plugging in the definition of kinetic chain length, Equation 2.14. This is a recursive relation, so we can multiply it $i - 2$ times:

$$\frac{[\mathrm{P_i} \cdot]}{[\mathrm{P_1} \cdot]} = \frac{[\mathrm{P_i} \cdot]}{[\mathrm{P_{i-1}} \cdot]} \left(\frac{v_n}{1 + v_n} \right)^{i-2} \tag{2.17}$$

Canceling the common $[\mathrm{P_i} \cdot]$ terms rearranging, and relabeling the dummy variable $i - 1 \to i$ yields

$$[\mathrm{P_i} \cdot] = [\mathrm{P_1} \cdot] \left(\frac{v_n}{1 + v_n} \right)^{i-1} \tag{2.18}$$

From the kinetic equation 2.15, we can write

$$[\mathrm{P_1} \cdot] = \frac{2fk_d[\mathrm{I}]}{k_p[\mathrm{M}] + 2k_t[\mathrm{P} \cdot]}, [\mathrm{P} \cdot] = \frac{2fk_d[\mathrm{I}]}{2k_t[\mathrm{P} \cdot]} \tag{2.19}$$

for the initiation and termination steps. Their ratio is

$$\frac{[\mathrm{P_1} \cdot]}{[\mathrm{P} \cdot]} = \frac{2k_t[\mathrm{P} \cdot]}{k_p[\mathrm{M}] + 2k_t[\mathrm{P} \cdot]} = \frac{1}{1 + v_n} \tag{2.20}$$

Using equations 2.20 and 2.18, we can define the molar ratio of the i-mer to be

$$x_i = \frac{[\mathrm{P_i} \cdot]}{[\mathrm{P} \cdot]} = \frac{1}{v_n}\left(\frac{v_n}{1+v_n}\right) \tag{2.21}$$

Polymerization reactions done in pure monomer, called bulk reactions, are subject to a phenomenon called the Trommsdorff effect [11]. This occurs because the polymer solution becomes very highly concentrated in polymer, and therefore becomes very viscous. The high viscosity prevents heat transfer within the bulk solution. Because the reactions are all exothermic, heat builds up at the propagation centers. This build-up of heat causes the reaction to auto accelerate, leading to the polymer gelling in the reactor. The result is very difficult and expensive to clean. The Trommsdorff effect is very difficult to predict, and is therefore a risk when polymerizing in bulk. The polymerizations I conduct in this thesis are all done in bulk, so the Trommsdorff effect is not a risk here. I will ignore it from now on.

When the polymer is a copolymer rather than a homopolymer, we must also consider the composition of the chain in addition to the molecular weight. The simplest model that is chemically plausible is the chain-end effect model. The probability of each monomer to attach to a chain is modeled as a function of both the relative concentration of the two monomers in the reactor, and on the most recent monomer to attach to that chain. This is a first-order Markov model. In this case, there are four rate constants k_{11}, k_{12}, k_{21}, and k_{22}, describing the four propagation steps

$$\mathrm{M_1} \cdot + \mathrm{M_1} \longrightarrow \mathrm{M_1} \cdot \tag{2.22a}$$

$$\mathrm{M_1} \cdot + \mathrm{M_2} \longrightarrow \mathrm{M_2} \cdot \tag{2.22b}$$

$$\mathrm{M_2} \cdot + \mathrm{M_1} \longrightarrow \mathrm{M_1} \cdot \tag{2.22c}$$

$$\mathrm{M_2} \cdot + \mathrm{M_2} \longrightarrow \mathrm{M_2} \cdot \tag{2.22d}$$

The two kinetic equations describing the consumption of the monomers are

$$\frac{-d[\mathrm{M}_1]}{dt} = k_{11}[\mathrm{M}_1][\mathrm{M}_1\cdot] + k_{21}[\mathrm{M}_1][\mathrm{M}_2\cdot] \tag{2.23}$$

$$\frac{-d[\mathrm{M}_2]}{dt} = k_{12}[\mathrm{M}_2][\mathrm{M}_1\cdot] + k_{22}[\mathrm{M}_2][\mathrm{M}_2\cdot] \tag{2.24}$$

Under the steady state condition, $k_{21}[\mathrm{M}_1][\mathrm{M}_2\cdot] = k_{12}[\mathrm{M}_2][\mathrm{M}_1\cdot]$. Using this, and diving 2.23 by 2.24, we obtain

$$\frac{d[\mathrm{M}_1]}{d[\mathrm{M}_2]} = \frac{[\mathrm{M}_1]}{[\mathrm{M}_2]}\frac{r_1[\mathrm{M}_1] + [\mathrm{M}_2]}{[\mathrm{M}_1] + r_2[\mathrm{M}_2]} \tag{2.25}$$

r_1 and r_2 are called the reactivity ratios, and are defined to be $r_1 = k_{11}/k_{12}$, $r_2 = k_{22}/k_{21}$. In general, the reactivity ratios depend on the pair of monomers, the solvent, and other reaction conditions.

We can define the mole fraction of monomer 1 in the reaction feed as $f_1 = [\mathrm{M}_1]/[\mathrm{M}_2]$, and the mole fraction of monomer 1 in a chain as $F_1 = d[\mathrm{M}_1]/d[\mathrm{M}_2]$. We can also define $f = f_1/f_2$ and $F = F_1/F_2$. Then

$$F_1 = \frac{r_1 f_1^2 + f_1 f_2}{f_1 f_2 + r_2 f_2^2} \tag{2.26}$$

and

$$\frac{f(1-F)}{F} = r_2 - \frac{f^2}{F} r_1 \tag{2.27}$$

This last form allows a particularly simple method of determining the reactivity ratios, due to Fineman and Ross [12]. Table 2.1 shows some reactivity ratios that inspired the work in this thesis. In general, the reactivity ratios are most stronly influenced by the chemical groups closest to the reacting group. Because NIPAM and Am are both acrylamides, they have identical groups near the reacting vinyl bond; they therefore have very similar reativity ratios. Q9 has a similar, but not quite identical group,

Table 2.1: Some reactivity ratios

m1	m2	solvent	r_1	r_2	source
Am	SS	0.1 M NaCl	0.18	2.0	[13]
Am	Q9	5 mM NaCl	1.1	0.47	[14]
Am	Np	water	1.0	1.0	[15]
BA	MMA	butyl acetate	0.4	2.58	[16]

near its reacting vinyl bond; its reactivity ratios with NIPAM or Am will therefore be a bit different. SS has a styrene group instead of the acrylamide group, so it will have a much different reactivity ratio when copolymerized with the acrylamides.

A few qualitative descriptions can be derived from the reactivity ratios. If $r_i > 1$, then a chain ending in a radical of monomer i prefers to add monomer i; if $r_i < 1$, then the chain prefers to add the other monomer. If $r_1 r_2 = 1$, then the chain is called an ideal random chain. If, in addition, $r_1 = r_2 = 1$, then $F_i = f_i$, producing a perfectly random copolymer. If $r_1 r_2 < 1$, then the chain will tend towards alternation of the two monomers. If $r_1 r_2 > 1$, then the chain will tend away from alternation and towards "blockiness." In the extreme case of $r_1 = r_2 = 0$, the chain will deterministically alternate between the two monomers. In the opposite extreme of $r_1 = r_2 = \infty$, the monomers will form a blend of two homopolymers. This last case is extremely rare, however.

2.3 Polyelectrolytes

Polymer chains with electric charges are called polyelectrolytes. Positively charged polyelectrolytes are called polycations, while negatively charged polyelectrolytes are called polyanions. Polyelectrolytes with both positive and negative charges are called polyzwitterions. Polyzwitterions are much more complicated than polyanions and polycations, and are beyond the scope of this dissertation.

These charges cause long-range interactions that have dramatic effects on the

physical and chemical properties of the polymer chains. The most apparent effect is that the charges repel each other; this causes polyelectrolytes to have a more stretched conformation than electrically neutral chains of similar monomer and degree of polymerization. This more elongated conformation has the effect of greatly increasing the intrinsic viscosity of the polymer. In addition, the charges on different chains repel each other; this interchain repulsion causes a large virial effect (the virial coefficient A_2 is defined in Section 2.4.1). Both of these effects are largely suppressed by the addition of small molecular weight ions to the solution.

When a salt is added to the solution, it dissociates into its constituent ions. These small molecular weight ions are free to move through the solution; the ions with the opposite charge as the polyion move closer to the polyion, and "screen" the electric potential from the ions farther away. One way to see this is to model the polyelectrolyte chain as an imobile charge at the origin, and the small ions as free to move [17]. At temperature T the mobile ions arrange themselves according to the Boltzmann distribution, with the energy given by the electrostatic interaction between a given ion's charge q_i and the electric potential φ at its location. The Poisson-Boltzmann equation describes the electric potential outside the polyelectrolyte chain:

$$\nabla^2\varphi = -\sum_i \frac{q_i n_i}{\varepsilon} e^{-\frac{q_i\varphi}{kT}} \tag{2.28}$$

i is a dummy index to identify the ions in the solution and n_i is the bulk density of the ions far away from the polyion. ε is the electric permitivity of the solution. If the ionic strength is low enough that $\frac{q_i\varphi}{kT} << 1$, then the exponential term can be approximated by a linear term, and the Poisson-Boltzmann equation can be approximated by the Debye-Hückel equation

$$\nabla^2\varphi = \left(\sum_i \frac{q_i^2 n_i}{\varepsilon kT}\right)\varphi \stackrel{\text{def}}{=} \kappa\varphi \tag{2.29}$$

Then the potential can be analytically solved for as

$$\phi(r) \propto \frac{e^{-\kappa r}}{r} \tag{2.30}$$

where r is the distance from the polyion. The Debye screening length is given by

$$\lambda_D = \kappa^{-1} = \left(\frac{\epsilon kT}{\sum_{j=1}^{N} n_j q_j^2} \right)^{1/2} \tag{2.31}$$

We can define the charge density as

$$\xi = \frac{e^2}{\epsilon kTb} \tag{2.32}$$

with $b = L/P$. L is the total contour length of the polymer. P is the total number of charged groups on the polymer. Counterion condensation is the phenomenon in which free ions in the solution are attracted to oppositely signed charges on the chain [18]. The free ions are called the "counterions," and they are said to have "condensed" onto the chain. This phenomenon ensures the condition

$$\xi \leq 1 \tag{2.33}$$

This establishes a lower bound on the spacing between charges of $\lambda_b = e^2/(4\pi\varepsilon kT)$, called the Bjerrum length, for the given solution.

The Bjerrum length can also be derived by equating the electrostatic interaction of two charges with the thermal energy kT:

$$\frac{q_1 q_2}{4\pi\varepsilon\lambda_b} = kT \tag{2.34}$$

For water, the relative permitivity is $\varepsilon_r = 78.54$ at 25 °C [19]. The Bjerrum length for

monovalent ions is therefore $\lambda_b = \frac{e^2}{4\pi\varepsilon kT} = \frac{(1.602\times10^{-19})^2}{4\pi\times78.54\times8.854\times10^{-12}\times1.38\times10^{-23}\times298} = 7.135\,\text{Å}$ at 25 °C.

Polyelectrolytes exhibit some interesting properties that neutral polymer chains do not. One such phenomenon is called the electroviscus effect. Polyelectrolyte solutions tend to have higher intrinsic or reduced viscosity than neutral polymers in the same solution. This is because the electrostatic repulsion elongates the chains; this elongated configuration has a much higher drag on the surrounding fluid. The electroviscus effect is greatly reduced with increasing ionic strength. Electrostatic repulsion between chains causes very high values of the virial coefficients A_2 and A_3 at very low ionic strength. Again, this effect is greatly reduced by added ionic strength; 0.1 M NaCl is typically sufficient to suppress this effect [20, 21]. Virial effects have a large impact on light scattering measurements. For light scattering measurements, therefore, either the large A_2 values must be taken into account, or the light scattering measurements must be made in a moderate to high ionic strength solvent in order to eliminate this effect.

2.4 Light scattering theory

2.4.1 Static light scattering

The light emitted from an accelerated charge is a result of basic electrodynamics, and is derived, for example, in Jackson [22] and van de Hulst [23]. Jackson gives the power radiated over unit solid angle in SI units as:

$$\frac{dP}{d\Omega} = \frac{c^2 Z_0}{32\pi^2} k^4 |\mathbf{p}|^2 \sin^2\chi \tag{2.35}$$

In equation 2.35, χ is the angle between the axis of the oscillation of the dipole and the angle at which the radiation is directed. In the typical light scattering experiment,

the incoming light is vertically polarized so that all the oscillating dipoles are directed in the up-down direction. The scattered light is all measured in the horizontal plane, so that $\chi = 90\,^\circ$ for all detectors, and Equation 2.35 becomes

$$\frac{dP}{d\Omega} = \frac{c^2 Z_0}{32\pi^2} k^4 |\mathbf{p}|^2 \tag{2.36}$$

The magnitude of the induced dipole $|\mathbf{p}|$, is determined by the polarizability α of the solution and the magnitude of the incoming wave: $|\mathbf{p}|^2 = \alpha^2 |\mathbf{E_0}|^2$. Note that this assumes that the polarizability is isotropic and linear and that the scattering volume is small enough that the incoming wave can be considered to be constant. This gives

$$\frac{dP}{d\Omega} = \frac{cZ_0}{4\pi} k^4 \alpha^2 \left(\frac{c}{8\pi} |E_0|^2 \right) \tag{2.37}$$

The expression in parentheses is equal to the incoming power I_0. We can plug that in, and the definitions $k = 2\pi/\lambda$ and $Z_0 = \sqrt{\mu_0/\epsilon_0} = 1/c\epsilon_0$. This produces

$$\frac{dP}{d\Omega} = \frac{16\pi^4 \alpha^2}{(4\pi\epsilon_0 \lambda^4)} I_0 \tag{2.38}$$

Time-averaging, and taking the power per volume element δV produces

$$\frac{\overline{I_s}}{\overline{I_i}} = \frac{16\pi^2 \langle \alpha_V \rangle^2}{(4\pi\epsilon_0)^2 \lambda_0^4 R^2 \delta V} \tag{2.39}$$

Now, we can write $\langle \alpha_V \rangle^2 = (\langle \alpha_V^0 \rangle + \delta\alpha_V)^2 = \langle \alpha_V^0 \rangle^2 + 2\langle \alpha_0^V \rangle \langle \delta\alpha_V \rangle + (\delta\alpha_V)^2$. But a uniform polarizability doesn't scatter, so we ignore the $\langle \alpha_V^0 \rangle$ term. $\langle \delta\alpha_V \rangle = 0$ by definition, so we make the replacement $\langle \alpha_V \rangle^2 \rightarrow (\delta\alpha_V)^2$ in equation 2.39. Most techniques don't measure the polarizability directly, so those should be eliminated. The change in polarizability is related to a change in the local solute concentration

by

$$\overline{(\delta\alpha_V)^2} = \left(\frac{\partial\alpha}{\partial c}\right)^2_{T,V} \overline{(\delta c)^2} \tag{2.40}$$

Recall the Clausius-Clapeyron equation

$$n^2 - n_0^2 = \frac{\alpha}{(\delta V)\epsilon_0} \tag{2.41}$$

Differentiating equation 2.41 with respect to c gives

$$2n\frac{\partial n}{\partial c} = \frac{\partial\alpha}{\partial c}\frac{1}{(\delta V)\epsilon_0} \Rightarrow \frac{\partial\alpha}{\partial c} = 2n\epsilon_0(\delta V)\frac{\partial n}{\partial c} \tag{2.42}$$

Plugging equation 2.42 into equation 2.40 then gives

$$\overline{(\delta\alpha_V)^2} = \overline{(\delta c)^2}\left(\frac{\partial n}{\partial c}\right)^2 (\delta V)^2\epsilon_0^2(2n)^2 \tag{2.43}$$

We can relate the concentration fluctuations δc to the concentration and the molecular weight via the chemical potential by expanding the Helmholtz free energy in a series around $\delta c = 0$. Start with

$$\delta A = \frac{\partial A}{\partial c}_{T,V}\delta c + \frac{1}{2!}\frac{\partial^2 A}{\partial c^2}(\delta c)^2 + \ldots \tag{2.44}$$

The first term on the right hand side is zero because the system is at equilibrium. One of Maxwell's relations of elementary thermodynamics (see for example [24]) relates the Helmholtz free energy to the chemical potential as:

$$\left(\frac{\partial^2 A}{\partial c^2}\right)_{T,V} = \frac{\delta V}{c\overline{V_1}}\left(\frac{\partial\mu_1}{\partial c}\right)_{T,V} \tag{2.45}$$

The definition of the chemical potential is

$$\mu_1 - \mu_1^0 = k_B N_A T \ln(1 - X_2) = k_B N_A T V_1 c \left(\frac{1}{M} + \frac{V_1^0 c}{2M^2} \right) \tag{2.46}$$

Differentiating this with respect to c gives

$$\left(\frac{\partial \mu_1}{\partial c} \right) = (k_B N_A T V_1^0) \left(\frac{1}{M} + 2A_2 c + \dots \right) \tag{2.47}$$

where $A_2 = \frac{V_1^0 c}{4M^2}$ is called the second virial coefficient.

Substituting equation 2.47 into 2.45, 2.45 into 2.44, 2.44 into 2.43, and 2.43 into 2.39 gives the correction to the light scattering for molecular weight and concentration, producing

$$\frac{I_s}{I_i} = \frac{4\pi^2 n^2 c (\partial n / \partial c)^2}{\lambda_0^4 R^2 N_A (1/M + 2A_2 c + \dots)} \tag{2.48}$$

It is typically more convenient to work with this equation in a rearranged form

$$\frac{Kc}{I_R} = \frac{1}{M} + 2A_2 c + \dots \tag{2.49}$$

I_R is the Rayleigh ratio defined above;

$$K = \frac{4\pi^2 n^2 (\partial n / \partial c)^2}{\lambda_0^4 N_A} \tag{2.50}$$

is called the optical constant for the particular system under study. A_2 is the second virial coefficient for the polymer in that particular solvent; there are further virial coefficients (A_3, A_4, etc) but they are not used in this dissertation. In some of the results in this dissertation, $2A_2 M C_p << 1$, so it can be ignored. But in some on my semi-batch reaction, C_p is high enough that the A_2 cannot be ignored. The higher-order virial coefficients are several orders of magnitude smaller than A_2, so

they require much higher concentrations before they become important.

In order to account for the physical extension of the particles, we need to account for interference effects due to light scattering off of different points within a given particle. Consider a single particle at a fixed orientation at a location $\vec{p_j}$. If the light scatters elastically at an angle θ to the incoming direction, then we can define the scattering vector as $\vec{q} = \vec{k}_f - \vec{k}_i$, where $\vec{k}_f$ and $\vec{k}_i$ are the wavevectors of the scattered and incident waves. The magnitude of the scattering vector is $|\vec{q}| = \frac{2\pi}{\lambda} \sin \frac{\theta}{2}$. The scattered field is then

$$E_t = \sum_{j=1}^{P} E_j = E_0 \exp(-i\omega_0 t) \sum_{j=1}^{P} a_j \exp(i\vec{q} \cdot \vec{p_j}) \tag{2.51}$$

where P is the number of scattering elements in the particle. The scattered intensity is then

$$I_s = \vec{E_t}^* \vec{E_t} = \frac{c\epsilon_0}{2} \left| \sum_j a_j \exp(i\vec{q} \cdot \vec{p_j}) \right|^2 E_0^2 \tag{2.52}$$

For N particles, averaging over all possible orientations gives

$$I_s = N \frac{c\epsilon_0}{2} \left\langle \left| \sum_j \right|^2 \right\rangle_{\text{angle}} E_0^2 \tag{2.53}$$

There is no scattering in the forward direction, where $\theta_s = 0$. In that case, we can let

$$a_j = a \Rightarrow I_s = \frac{c\epsilon_0}{2} |a|^2 P^2 E_0^2 N \tag{2.54}$$

This allows us to define the structure factor of the chain as

$$P(\vec{q}) = \left\langle \left| \frac{1}{P} \sum_j \right|^2 \right\rangle_{\text{angle}} = \frac{1}{P^2} \left\langle \left\langle \sum_i \sum_j \exp(i\vec{q} \cdot \vec{r_{ij}}) \right\rangle \right\rangle \tag{2.55}$$

where

$$\vec{r_{ij}} = \vec{p_i} - \vec{p_j} \tag{2.56}$$

Now, the average over all angles is

$$\langle \exp(iqr_{ij}\cos\alpha\rangle_\alpha = \frac{1}{2}\int_0^\pi \exp(iqr\cos\alpha)\sin\alpha d\alpha = \frac{\sin(qr_{ij})}{qr_{ij}} \tag{2.57}$$

$$x = qr_{ij} << 1 \Rightarrow \frac{\sin x}{x} = \frac{1}{x}\left(x - \frac{1}{3!}x^3 + \dots\right) = 1 - \frac{x^2}{6} \tag{2.58}$$

Then

$$P(\vec{q}) = \frac{1}{P^2}\left\langle \sum_i \sum_j (1 - \frac{qr^2}{6} + \dots)\right\rangle = 1 - \frac{q^2}{6P^2}\left\langle \sum_i \sum_j r_{ij}^2 \right\rangle \tag{2.59}$$

Note that

$$\left\langle \sum_i \sum_j r_{ij}^2 \right\rangle = \left\langle \sum_i \sum_j (r_i^2 + r_j^2)\right\rangle = 2P^2\langle S^2\rangle \tag{2.60}$$

Where $\langle S^2\rangle = \frac{1}{P}\sum r_i^2$ is the second moment of inertia of the mass distribution of the chain. $R_g = \sqrt{\langle S^2\rangle}$ has dimensions of length, and is called the radius of gyration. The structure factor is then

$$P(\vec{q}) = 1 - \frac{q^2\langle S^2\rangle}{3} \Rightarrow P^{-1}(\vec{q}) = 1 + \frac{q^2\langle S^2\rangle}{3} \tag{2.61}$$

for $q\langle S^2\rangle << 1$. Zimm [25] applies the structure factor to equation 2.49 as

$$\frac{Kc}{I} = \frac{1}{MP(\vec{q})} + 2A_2c \tag{2.62}$$

Finally, putting everything together, we have the Zimm equation

$$\frac{Kc}{I} = \frac{1}{M}\left(1 + \frac{q^2\langle S^2\rangle}{3}\right) \tag{2.63}$$

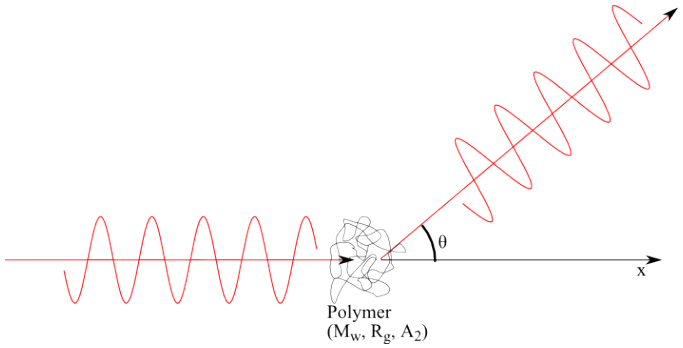

Figure 2.2: The laser (colored red in the diagram) comes in, and is scattered off of the polymer in the solution. The scattering angle θ is measured relative to the direction of the incident light, as shown. The laser is polarized vertically, so the scattering plane would come out of the paper in this diagram.

The geometry of the light scattering instrument is given in Figure 2.2.

The above derivation (starting from equation 2.35) assumes the radiation regime: that is, when the source of the scattering is much smaller than the wavelength of the light. In addition, it assumes a linearly polarized source. In polymers, the radiation regime means that $R_g << \lambda$. Thsi assumption can be relaxed while still assuming a linearly polarized source; the more general case is called Mie scattering, and is much more difficult to discuss. Kerker has the most thorough discussion of the full Mie scattering problem [26]. van de Hulst also discusses some other limiting cases of Mie scattering [23].

This derivation has been carried out in SI units, as notied above. However, polymer scientists typically use the CGS system of units. The above equations are valid in the CGS system, as long as the lengths are all given in cm, and the concentrations given in g/mL.

2.4.2 Dynamic light scattering

Dynamic light scattering (DLS) begins with the Zimm equation (2.63). DLS is sensitive to the fluctuations in the local concentration of polymer. These fluctuations

cause the local index of refration to vary, due to the $\frac{dn}{dc}$ term in equation 2.63. This in turn causes the scattered intensity $I(t)$ to vary. From Equation 2.48, we know that the scattering intensity varies as $I_s \propto c$. This variation is partially random, but partially predictable. If we have a model for the motion of the polymer chain in the solution, then we can use the fluctuations in the scattering intensity to extract information about the chains in terms of that model.

A solid sphere in a solvent of viscosity η_{solv} diffuses with a diffusion coefficient D_t given [10] by

$$D_t = \frac{kT}{f} = kT6\pi\eta_{\text{solv}}R \tag{2.64}$$

Polymer chains in general are not solid spheres, but we can define an equivalent solid sphere with a radius R_h called the hydrodynamic radius, and given by

$$R_h = \frac{kT}{6\pi\eta_{\text{solv}}D_t} \tag{2.65}$$

Fick's second law of diffusion says that

$$\frac{\partial c}{\partial t} = D_t\frac{\partial^2 c}{\partial x^2} \tag{2.66}$$

This describes a diffusive flow from a region of high concentration c to a region of low concentration. For a homogeneous solution with statistical fluctuations, equation 2.66 is better written in terms of the fluctuations of concentration δc. It is these fluctuations that give rise to the fluctuations in excess scattering.

DLS measures the diffusion coefficient by measuring the local fluctuations in the polymer concentration. For a time-dependent variable $A(t)$ with some variation, we can define an autocorrelation as the average of $A(t)$ and $A(t+\tau)$:

$$C(\tau) = \langle A(t)A(\tau)\rangle = \lim_{t\to\infty}\frac{1}{T}\int_0^T A(t)A(t+\tau)dt \tag{2.67}$$

In the case of polymer diffusion, the autocorrelation function becomes

$$C(\tau) = \left(\langle I_s^2 \rangle - \langle I_s \rangle^2\right) \exp\left(-q^2 D_m \tau\right) + \langle I_s \rangle^2 \tag{2.68}$$

The way to understand this conceptually is to recall that the signal will be perfectly correlated with itself at $\tau = 0$, and that it will be perfectly uncorrelated with itself at $\tau \to \infty$. Between those two extremes, the autocorrelation function will decay exponentially due to the polymer diffusion. The decay of the autocorrelation function is exponential because the diffusion is exponential. The time constant of this exponential decay gives the diffusion coefficient, and therefore R_h.

If all the diffusing particles have the same R_h and D_t, an exponential decay will fit the autocorrelation function. More typically, there is a distribution of values of R_h in the solution, and the autocorrelation function will be more complicated than a single exponential. The full distribution of diffusion coefficients, and therefore R_h, can in general be extracted from the autocorrelation function via Fourier transform [27].

2.5 Viscosity

Viscosity is a measure of the resistance of a fluid to movement. A few basic definitions are illustrated in figure 2.3. A force F acts on an area of fluid A at some position y. The segment of fluid immediately against the bottom wall on the x-axis is held fixed. The shear stress is then defined as $\tau = F_x/A$. The fluid can be divided up into layers of thickness dy; the applied force acts on the top layer, the force from the top layer acts on the second layer, and the force propagates down the layers through the fluid. The result is a velocity gradient dv/dy along the y-direction [28].

$$\tau = \eta \frac{dv}{dy} \tag{2.69}$$

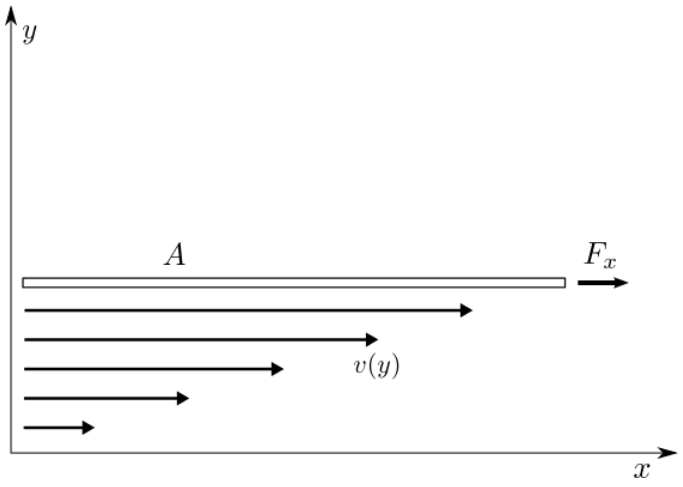

Figure 2.3: The geometry of a shear force.

This equation defines η, the coefficient of viscosity, and is called Newton's law of viscosity. Fluids that obey Equation 2.69 are called Newtonian fluids. Pure water is a Newtonian fluid. Water with a significant polymer content is, in general, non-Newtonian.

The definition of coefficient of viscosity can be used to derive the shape of a viscous fluid flow in a capillary. In this case, we will consider a fluid of density ρ and viscosity η to be flowing vertically under the force of gravity in a capillary of radius R. The fluid at the wall of the capillary is held to zero flow. This results in a parabolic flow profile, shown in figure 2.4.

The total flow rate through the capillary is given by Poiseuille's equation:

$$\eta = \frac{\pi R^4 \Delta p}{8QL} \tag{2.70}$$

Δp is the drop in pressure along the length L. R is the radius of the capillary. Q is the flow rate. By substituting the pressure drop along the capillary for the density and acceleration due to gravity, Equation 2.70 can be used for any capillary flow under constant force or pressure, not just under gravity. Equation 2.70 provides a

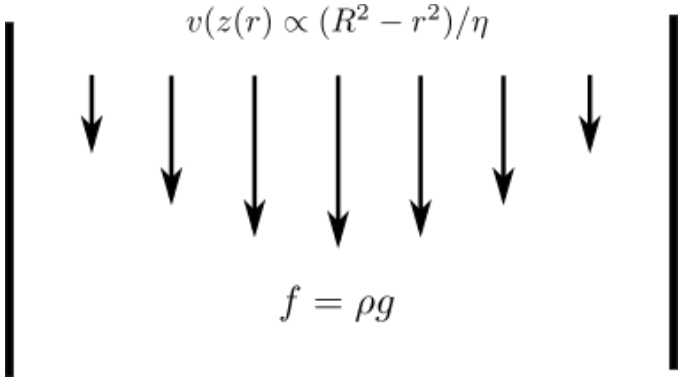

Figure 2.4: The flow profile of a fluid in a cylindrical capillary under the force of gravity is proportional to $(R^2 - r^2)$. The total flow rate through the capillary is then proportional to R^{-4}.

very simple method for calculating the rheological properties of a given polymer in a given solvent. The solution is pushed through a capillary at fixed flow rate. The drop in pressure Δp along the length L of the capillary is measured. This method will be further described in section 4.2.6.

The most general equation describing the flow and viscosity of an incompressible fluid is called the Navier-Stokes equation. This equation summarizes the findings of fluid dynamics; all the previous equations I have presented are special cases. In vector form the Navier-Stokes equation is written as [28]:

$$\frac{d\vec{v}}{dt} + \frac{1}{\rho}\nabla p = -\nabla U + \frac{\eta}{\rho}\nabla^2\vec{v} \tag{2.71}$$

ρ is the denity of the fluid, $\vec{v}$ is the velocity, p is the pressure, and U is the relative velocity of the boundaries of the fluid.

A quantity called the intrinsic viscosity can be defined for a given polymer in a given solvent. This is done by expanding the total viscosity of the solution as a Taylor series in terms of the polymer concentration.

$$\eta = \eta_{\text{solv}}(1 + [\eta]c + \kappa[\eta]^2c^2 + \dots) \tag{2.72}$$

$[\eta]$ is the intrinsic viscosity, and is is a description of how an individual polymer chain interacts hydrodynamically with the solvent. Operationally, the reduced viscosity

$$\eta_{\text{red}}(c) = \frac{\eta(c) - \eta_{\text{solv}}}{\eta_{\text{solv}} c} \tag{2.73}$$

is easier to measure than the intrinsic viscosity. The intrinsic viscosity can be found from the reduced viscosity as

$$[\eta] = \lim_{c \to 0} \eta_{\text{red}}(c) \tag{2.74}$$

2.6 UV-Vis spectroscopy

As in other spectroscopic techniques, UV-Vis works by shining some sort of electromagnetic radiation through the sample. The radiation transmitted through the sample is then measured and compared to the intensity of radiation used. From this, we can compute the radiation absorbed by the sample.

Typical wavelengths used in UV-Vis are 200–800 nm, which ranges from ultraviolet (UV), through the visible part of the spectrum, to infrared (IR). The energy of a photon in this range is approximately 1.5–6.2 eV, similar in value to the energy involved in electronic transitions in molecules. UV-Vis spectroscopy is useful for the study of polymers because many polymers have an electronic transition in this range, and thus an absorption band near the visible region of light. The exact souse of this absorption band in many polymers is the C=C vinyl bond in the monomer form. This bond breaks during the polymerization reaction, allowing UV-Vis to directly distinguish monomers from polymers. The exact shape of this absorption band will depend on the structural details of the rest of the monomer molecule, so UV-Vis can distinguish between different monomers.

The total absorption has been found to be directly proportional to the con-

cnetration c of the absorbing material, and directly proportional to the thickness L of the aborbing sample. This is summarized by Beer's Law $A = \varepsilon cL$. ε is called the extinction coefficient. A is dimensionless, so in CGS units, ε has the dimension of cm^2/g. The intensity of light transmitted through a thickness of x is then given by $I_t = I_0 \exp(-Ax)$.

Chapter 3

Lower critical solution temperature

3.1 Introduction

p(NIPAM) has been known for some time to undergo a coil-to-globule transition followed by a LCST at an appropriate temperature [2]. This transition is driven by a competition between hydrogen bonding between the polar groups and the water molecules, and the hydrophobic interaction between water and the alkyl group. In the homopolymer in pure water, the transition happens at 32 ℃. The transition point can be manipulated by several changes in the environment: adding salt lowers the transition temperature, [5] adding another polar solvent lowers the transition temperature [29, 30], inserting hydrophilic comonomers raises the transition temperature [4, 15], and inserting hydrophobic comonomers lowers the transition temperature [4, 31]. Finally, the transition is a segment-by-segment phenomenon: if the architecture allows one segment to collapse, but not others, then only part of the chain will collapse. For example, block copolymers of NIPAM and hydrophilic comonomers form micelles when heated above the LCST of the NIPAM block [32]. Graft polymers show a similar effect [33].

p(NIPAM) is an example of a temperature-responsive polymer. The temperature-responsive polymers are polymers that respond to changes in temperature. Many of

them behave in the same manner as NIPAM; they undergo a coil-to-globule transition when heating in aqueous solution. Temperature-responsive polymers are themselves part of a larger class of materials, called stimuli-responsive polymers [34, 35]. These are polymers that respond in a similar manner to other stimuli. For example, there are pH-responsive polymers [36–38], light-responsive polymers [39], and electric and magnetic field responsive polymers [40–42]. Each of these stimuli-responsive behaviors has its own set of causes and phenomenology. Temperature-responsive polymers differ from other stimuli-responsive polymers in that the temperature dependence makes the LCST phenomenon an inherently thermodynamic process. That means that we must consider both the energy interactions and the entropy effects of the transition. Because the entropy term in the expression for the free energy contains a factor of T, changing the temperature changes the relative importance of the entropy and the internal energy of the system. In other stimuli-responsive polymers, the temperature is held constant, so the relative importance of entropy and energy doesn't change. Most of these phenomena, therefore, work by changing the energy interactions, or by inputting into or extracting energy from the system. For example, in pH-responsive systems, changing the pH of the solution causes acidic and basic groups to gain or lose charge. This either increases or decreases the electrostatic interactions within and between chains in the solution [32, 36, 37, 43–47]. In light-responsive systems, an incoming photon adds energy to the polymer, causing a cis-trans isomerization. Light of a different frequency can also be used to extract energy from the polymer, causing the inverse cis-trans isomerization [39]. In glucose-responsive polymers, the presence of the diol group in the glucose affects the solubility of a boronic acid group in the polymer [48, 49].

In remainder of this chapter, I will only discuss temperature-responsiveness.

3.2 Phenomenology

NIPAM is a member of a homologous series of alkyl acrylamides. The acrylamide group is extremely hydrophilic, while the alkyl group is extremely hydrophobic. The lower critical solution temperature comes from the balance of these two effects. At one extreme of this series is acrylamide, with no added alkyl side-chain. This is highly soluble in water over the full temperature range of liquid water. At the other extreme is N-n-ayl acrylamide, with an alkyl group of length $n \to \infty$. At this extreme the polymer becomes approximately equivalent to a branched hydrocarbon. The hydrophobicity of the alkyl chain dominates the hydrophilicity of the acrylamide, and the chain is insoluble in liquid water at all temperatures. Insolubility occurs for N-n-propyl and longer alkyl chains [3]. NIPAM falls between those two extremes; the hydrophobicity of the isopropyl group approximately balances the hydrophilicity of the acrylamide. As a result, pNIPAM is soluble in water at some temperatures and insoluble at other temperatures. In addition to pNIPAM, a few alkyl acrylamides with similar alkyl chain lengths also show an LCST in liquid water, though at different temperatures [3]. The utility of pNIPAM in particular comes from the fact that its LCST (32 °C) is close to the temperature of a human body (37 °C).

The above paragraph suggests one manner in which to vary the LCST of the polymer chain: inclusion of comonomers that are more hydrophobic (-philic) than NIPAM will shrink (extend) the range of solubility, thus lowering (raising) the LCST, respectively [4]. The alkyl acrylamide homologs are particularly facile comonomers; several authors have reported results for copolymerization of NIPAM with acrylamide [15], dodecyl acrylamide [50], and others [51].

Bergbreiter has reported that salts lower the LCST; this phenomenon is known as salting out [5,52,53]. The salting out of pNIPAM appears to follow the well-known Hofmeister series: the more chaotropic ions in that series are more effective at salting

out pNIPAM than the more cosmotropic ions [5].

The coil-to-globule transition is the change in conformation of the chain from a random coil to a globule or a molten globule [54, 55]. Collapse from the coil to the globule lowers both R_g and R_h. In the random coil conformation, the chain is fully soluble in the solution, and views the solution as a good solution. This conformation is characterized by a ratio of radius of gyration to hydrodynamic radius of $R_g/R_h = 1.52$ [56]. The globule and molten globule conformations are characterized by a ratio of $R_g/R_h = 0.62$ [56]. In these conformations, the chain is hydrophobic overall, and wraps tightly around itself in order to shield its hydrophobic groups from the bulk water. The hydrophilic groups are on the outside of the globule, where they can interact with polar water molecules. This reduces the free energy of the resulting system. In order to further reduce the free energy of the solution, the globules aggregate to each other; aggregation causes an increase in the apparent M_w [43, 57]. This aggregation leads to the phase separation, and is observed as the lower critical solution temperature. The speed and degree of the aggregation depends on the concentration of the polymer in the solution. If the concentration is high enough, the aggregation and phase separation can be seen visually, as in Figure 3.1, a photo of one of my samples clouding. In a sufficiently dilute solution, the chains remain unaggregated after the coil-to-globule transition. In this case, the coil-to-globule transition can be measured by light scattering: static light scattering measures the reduction in R_g, while dynamic light scattering measures the reduction in R_h. Either of these is suggestive of the transition; both together confirm the change in conformation [56]. The aggregation can be measured by light scattering (either dynamic or static) as an increase in the observed molecular weight. The aggregation can also be measured by any of the other techniques discussed in Section 3.3, below. This process fully reverses when the solution is cooled back to below the LCST.

Figure 3.1: At sufficient concentration, the clouding and phase separation is visible to the human eye. This sample is taken directly out of the reactor final product; the polymer concentration is 17 mg/mL. The thermometer is used to monitor the temperature, and to estimate the cloud point temperature.

The LCST of pNIPAM depends on M_w; this is a very weak but measurable effect [58]. This effect becomes more noticeable at very low molecular weights (degree of polymerization less than 20) [59, 60]. At such low degree of polymerization, end-group effects also affect the LCST [58]. Figure 3.2 summarizes the molecular weight dependence as measured by Furyk, et al. and Xia et al. [58,61]. I do not examine the molecular weight effects in this dissertation. Because my polymers are all synthesized by free-radical polymerization, the molecular weights are above 100 kg/mol. The LCST change over this range is less than the uncertainties in the measurements, so the M_w dependence can be ignored.

3.3 Observation of LCST

Many researchers have reported several different experimental techniques for observing LCST. The easiest method is turbidity or cloud point measurement. In this technique, light is shown through the solution. The wavelength chosen varies,

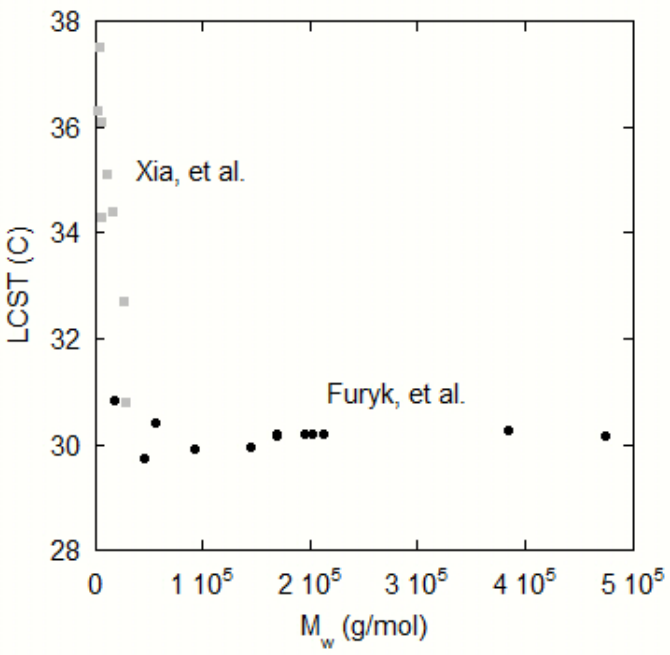

Figure 3.2: The LCST is approximately inversely dependent on the molecular weight of the chains.

but is typically in the range 400–600 nm. It is preferable that the solution not have a measurable absorption at the chosen wavelength. The intensity of the transmitted light is measured as a function of temperature. As the chains pass through the LCST, the transmitted intensity decreases. The turbidity of the solution is defined as the fraction of transmitted light that is lost. Some arbitrary loss of transmission is taken to define the LCST. Different authors use different thresholds; typical thresholds are 1% loss [52] or 50% loss [61]. One difficulty with this method is that the resulting LCST can depend on the threshold if the transition is not perfectly sharp. The small dependence of the LCST on the molecular weight can also cause a broadening of the transition [61], further complicating the interpretation of the results.

The loss of transmitted light in turbidimetric measurements is due to the scattering of the light by the polymer aggregates. As described in section 4.2.1, light scattering is very sensitive to molecular weight, and thus to the presence of

high molecular weight aggregates. If the molecular weight of the individual chains is known, then the apparent molecular weight of the aggregates immediately gives the aggregation number. If A_2 effects can be ignored, then this aggregation number is simply the ratio of the absolute light scattering intensity of the aggregated and unaggregated solutions. The results I present in Chapter 5 use this method. I use single angle light scattering, and approximate that A_2 and angular effects can be ignored. In addition to reporting M_w, light scattering can also report R_g [62] and/or R_h [27]. Either of these by itself indicates that the polymer shrinks in on itself upon heating through the LCST. Both together help describe the change of shape from a random coil to a molten globule [56].

Because the LCST transition involves the breaking of hydrogen bonds, differential scanning calorimetry (DSC) can measure the change in enthalpy as the chain undergoes the transition [5,30,51,63–66]. This technique confirms that the de-mixing transition is endothermic, and that the breaking of these hydrogen bonds is a necessary part of the transition. Several reports agree that the enthalpy change of the transition is approximately 1.5 °C, which suggests a loss of one hydrogen bond per repeat unit [64]. The peak of the DSC endotherm is more well-defined than an arbitrary point on a turbidity curve, so DSC has the advantage of giving a better defined and more reproducible measurement of LCST. DSC measurements generally agree with turbidity measurements to within the precision implied by the arbitrariness of the turbidity definition.

Finally, LCST can be measured by flourimetry. In this technique, a fluorescence probe is added to the solution [67]. When the pNIPAM chains undergo their conformational change, they envelop the probe in a hydrophobic environment. The probe fluoresces at a different wavelength in this hydrophobic environment than it does in the hydrophilic environment of the bulk water. Again, the LCST as mea-

sured by fluorescence is in general agreement with that measured by other techniques [31, 68]. Flourimetry has the advantage of measuring the conformational change directly, but has the potential disadvantage of possibly altering the state of solution.

Recently, some high-throughput methods have been developed based on one or more of the above techniques. These high-throughput methods allow researchers to more rapidly characterize the phase space of the LCST behavior. The LCST is influenced by many factors, so these methods are necessary to rapidly study the interactions between different input parameters. Bergbreiter's group at Texas A&M has developed a linear temperature gradient capillary [58]. This works by heating two ends of a cover glass to different temperatures, and allowing the glass to equilibrate. The resulting temperature increases linearly from the lower temperature at one end of the glass to the higher temperature at the other end. The polymer solution sample is then placed on the glass, and optically imaged with a CCD camera. Position in the CCD image is a function of temperature. The CCD allows imaging of the light transmission as a function of position. Several such cover glasses can fit inside the apparatus, allowing the researchers to study several samples at the same time. This has allowed them to study the effect of Hofmeister ions [5, 53] and molecular weight [53, 58] on the LCST of pNIPAM. Jana modified this idea to a 384 well microplate [69]. Because the microplate arranges its wells in a two-dimensional pattern, the temperature gradient can be set up along one direction, while the other direction is used to modify the sample concentration or added cosolute.

3.4 Thermodynamics of mixing

When the polymer chain undergoes its coil-to-globule transition, it demixes from the solution. In order to understand this transition we need to look at the

thermodynamics of mixing and phase separation.

The phase behavior of two species systems are typically shown by a phase diagram. This plots the spinodal and binodal curves as functions of composition and temperature. The binodal and spinodal curves partition the phase space into three regions. In one region, bounded by the spinodal, a single phase is stable, containing both species fully mixed. In a second region, outside the binodal, two phases are stable, each rich in one species and poor in the other. The third region is the region bounded by the spinodal and the binodal; this region is called the "meta-stable" region. In this region, the mixture is thermodynamically unstable, but kinetically stable: an activation energy is required to separate the species. If such an energy is added, the two phases will de-mix. two species can remain mixed unless the mixture is agitated in some way. If it is stirred or bumped or otherwise agitated, the two phases will de-mix. A schematic of spinodal and binodal curves for a general system is shown in Figure 3.3.

While Figure 3.3 shows the general case, the concentrations I discuss in this dissertation do not cover nearly the full concentration space. The concentrations I discuss are all in the range 0–10 mg/mL, or $0 \leq x_1 \leq 0.01$. In addition, the LCST is not known to depend on concentration, so the curve is very flat in this range.

Basic thermodynamic considerations (see, for example, Prigogine [70]) demonstrate that non-ideal entropy of mixing is required for the existence of an LCST at all. A critical point is given by the condition that

$$\left(\frac{\partial^2 g}{\partial x_2^2}\right)_c = 0 \tag{3.1}$$

If this critical point is an LCST, then

$$\left(\frac{\partial^2 h}{\partial x_2^2}\right)_c \geq 0, \left(\frac{\partial^2 s}{\partial x_2^2}\right)_c \geq 0 \tag{3.2}$$

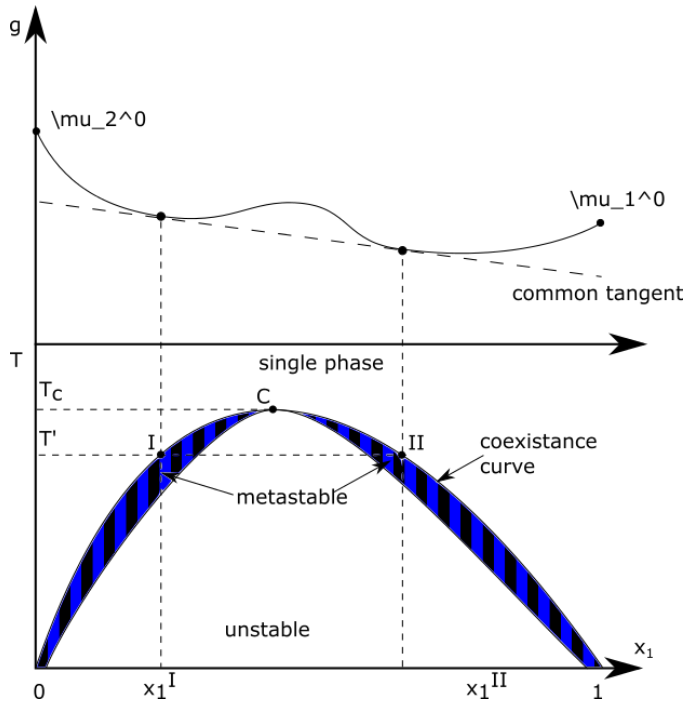

Figure 3.3: The general picture of the spinodal and binodal curves for a binary system.

The signs are reversed if the critical point is an upper critical solution temperature (UCST). Points representing the LCST and UCST are labeled in Figure 3.3. These are defined to be the temperatures above and below which no ratio of components will mix. A given system typically has either an LCST or a UCST, but not both. It is possible for a system to have both an LCST and a UCST; in this case the UCST is lower than the LCST.

In an ideal solution, the presence of one component does not affect the entropy of the other component. Therefore, the total entropy can be calculated by adding the entropies of the two components. In any mixture, the entropy of mixing is the change in entropy in going from the two unmixed components to the mixture. For an ideal solution, the entropy of mixing is given by

$$s^{\text{ideal}} = -R(x_1 \ln x_1 + x_2 \ln x_2) \tag{3.3}$$

producing

$$\left(\frac{\partial^2 s^{\text{ideal}}}{\partial x_2^2}\right)_c = -\frac{R}{x_1 x_2} < 0 \tag{3.4}$$

The inequality holds because $0 < x_{1,2} < 1$; therefore $x_1 x_2 > 0$. As a result, any mixture with an ideal entropy of mixing can only have a UCST; it cannot have an LCST. The presence of an LCST in the pNIPAM/water solution therefore requires that the entropy of mixing be non-ideal. Specifically, the presence of the pNIPAM chains affects the entropy of the water.

There are three kinds of non-ideal solutions [71]. Athermal solutions have $\Delta H_{\text{mixing}} = 0$, but ΔS_{mixing} is non-ideal. Regular solutions have $\Delta H_{\text{mixing}} \neq 0$, and ΔS_{mixing} ideal. Irregular solutions have $\Delta H_{\text{mixing}} \neq 0$, and ΔS_{mixing} non-ideal. As we have seen, the presence of the LCST requires that ΔS_{mixing} be non-ideal. In addition, the DSC results referenced in section 3.2 show that $\Delta H_{\text{mixing}} > 0$. Therefore, the pNIPAM/water mixture is an irregular mixture. Most polymer solutions are irregular.

A simple model to describe the mixing of a polymer chain in solution is the Flory-Huggins theory [72,73]. This model places the solution onto a lattice, and mixes the polymer chain into the lattice. The major result of the Flory-Huggins model is that the mole fraction of the two components can no longer be used to calculate the entropy of mixing; the volume fraction must be used instead. The overall form of the entropy of mixing is similar:

$$s_{\text{mixing}} = -k(n_1 \ln \phi_1 + 2_2 \ln \phi_2) \tag{3.5}$$

Here, $n_{1,2}$ are the number fractions of the solvent and polymer chains (equivalent to $x_{1,2}$ in equation 3.3), and $\phi_{1,2}$ are the volume fractions of solvent and polymer. This is an improvement over the naïve theory of ideal mixtures, because the volume fraction is capable of including interactions between the solvent and the solute.

The Flory-Huggins model defines an interaction parameter χ such that the enthalpy of mixing in excess of the ideal case is given by

$$\Delta H_{\text{mixing}}^{\text{excess}} = x_1 x_2 \chi k T \tag{3.6}$$

Flory and Krigbaum break this down into two interaction parameters: an enthalpy parameter κ and an entropy parameter ψ [74]. At the Θ point, $\psi = \kappa \Leftrightarrow \Delta H^E = T\Delta S^E$. The Θ temperature is then $\Theta = T\kappa/\psi$. Typically, $\chi > 0$ is assumed. One major result of this formalism is that, for $T > \Theta$, the chain expands; for $T < \Theta$, the chain collapses. This is qualitatively inconsistent with the empirical behavior in the LCST system; the Flory-Huggins theory with $\chi > 0$ is unable to capture this result. One other result of the Flory-Huggins model is that, because the entropy of mixing is lower than ideal, $\psi < 0$. This means that $\kappa < 0$ at the critical temperature. Both this result, and the result that $\chi < 0$ for an LCST system are in agreement: the mixing process must be exothermic in all LCST systems. In other words, mixing is enthalpically favored in systems showing an LCST. This conclusion is consistent with the DSC evidence discussed in Section 3.3 that the de-mixing is endothermic: if de-mixing is endothermic, then mixing is exothermic. In addition, the presence of an LCST in a system is actually a very natural result of having $\psi < 0$, $\kappa > 0$ [10].

The evidence from DSC provides estimates of the enthalpy of interaction between pNIPAM and water. There is a bit of a range to these estimates, but they are consistent with each other. Freitag reports an enthalpy change of $\Delta H = 16.5\,\text{kJ/g}$ of polymer. [75] Ding reports $\Delta H = 60\,\text{J/g}$ for $C_p = 1\,\text{mg/mL}$ and $M_w = 1.6 \times 10^6\,\text{g/mol}$. [65] This converts to $6.8\,\text{kJ/mol}$ of monomer. Schild reports $\Delta H =$ 3–15 cal/g of polymer, which equals 0.3–1.7 kcal/mol of monomer [30]. This is 1.2–7.1 kJ/mol of monomer. Kujawa reports an enthalpy change of 1.5 kcal/mol for chains of $M_w = 300\,\text{kg/mol}$, $C_p = 1\,\text{mg/mL}$ [76]. This is 6.3 J/g of monomer. Because the

Table 3.1: Enthalpy of the coil-to-globule transition.

Author	ΔH as reported	ΔH (kJ/mol monomer)	source
Schild	0.3–1.7 kcal/mol	1.2–7.1 kJ/mol	[30]
Freitag	16.5 J/g	1.9 kJ/mol	[75]
Ding	60 J/g	6.8 kJ/mol	[65]
Kujawa	1.5 kcal/mol	6.3 kJ/mol	[76]

authors use different units to report their results, the results are summarized in Table 3.1, both in the units the original author used, and in a consistent set of units, J/mol monomer. Note that that Freitag also converts their results into J/mol, but that conversion leaves off the kilo- prefix. Schild points out that this enthalpy change corresponds to the breaking of one hydrogen bond per monomer group [30]. Therefore, the enthalpically favorable mixing is due to hydrogen bonding of the acrylamide group with water. In addition, Kujawa's enthalpy value does not change when 0.5–1 mol % of decane or tetradecane is inserted into the chains in place of the isopropyl group [76]. This hydrogen bonding appears to be largely independent of the hydrophobic alkyl chain.

We can define a cooperative unit as the group of monomers in the chain that collaborate in the collapse. Tiktopulo reports that a larger cooperative unit leads to a sharper DSC peak. Based on their data, they estimate a cooperative group of approximately 60 kg/mol [77]. Based on the formula weight of the NIPAM monomer, this corresponds to approximately 530 monomer units. This is close to Schild's estimate of 430 repeat units per cooperative unit [30]. Freitag reports an LCST with chains of degree of polymerization of 20 [75]. Tiktopulo's and Schild's results then require that multiple chains are involved with the collapse and aggregation process. This requirement is qualitatively consistent with my light scattering results, described in Chapter 5, that apparent molecular weight increases at the LCST.

Kawasaki observed a decrease of ΔH with added styrene sulfonate (SS) in

NIPAM/SS copolymer gels [78]. This suggests a picture in which the increased energy penalty of the ionic groups moving closer together outweighs any increased energy bonus from breaking sulfonate-water bonds.

Ben-Naim described results that show how mixing pNIPAM and water reduces the entropy of the entire system. Solvation studies reveal that the entropy of solvation of ethane and methane into water is negative [79, 80]. The difference in solvation energy between one ethane molecule and two methane molecules is called the hydrophobic interaction. This hydrophobic interaction measures the favorability of attaching those two methane molecules together, versus leaving them unattached. That the entropy of this interaction is negative is the source of the negative entropy of mixing of the pNIPAM chain with water. Increasing hydrophobic chain length increases the strength of the hydrophobic interaction. This is consistent with the finding that LCST decreases with a longer alkyl group in the monomer [3]. This is also consistent with the finding that LCST decreases with increasing M_w [59].

3.5 Hofmeister Effect

Small ions follow a series called the Hofmeister series in regards to their thermodynamic properties when dissolved in water. This series describes the enthalpy and entropy of mixing of these ions in water. Ions at one end of the series are called kosmotropes ("order-makers") because they induce order in the aqueous solution. Ions at the other end of the series are called chaotropes ("order-breakers") because they reduce order in the aqueous solution. The Hofmeister series is typically (see, for example, [5]) given for anions as:

$$\begin{aligned} {CO_3}^{2-} > {So_4}^{2-} > {S_2O_3}^{2-} > {H_2PO_4}^{-} > F^{-} \\ > Cl^{-} > Br^{-} \approx {NO_3}^{-} > I^{-} > {ClO_4}^{-} > SCN^{-} \end{aligned} \tag{3.7}$$

with more cosmotropic species being to the left, and more chaotropic species on the right [75]. The boundary between chaotropes and kosmotropes is typically given as being between F^- and Cl^- (I have split the line at this point for ease of viewing). The ordering is inferred from the ability of the ions to precipitate proteins out of solution.

The terms chaotropes and kosmotrope come partially from the effect of these ions on the solubility of proteins in aqueous solution; kosmotropes stabilize the protein in solution, while chaotropes lower the solubility of a protein. These effects are called "salting-in" and "salting-out," respectively. This particular difference between chaotropes and kosmotropes does not exist with pNIPAM. At sufficient concentration all ions in the Hofmeister series lower the LCST of pNIPAM [5]. The chaotropes operate on pNIPAM by a different mechanism than the kosmotropes however. This causes the chaotropes to elevate the LCST slightly at very low concentrations. In this dissertation, I use only NaCl, which acts as a chaotrope with respect to pNIPAM, and therefore always lowers the LCST.

Using DSC, Kawasaki reports that ΔH of NIPAM/styrene sulfonate copolymer gels increases with added NaCl [78]. This is consistent with a picture of the ions binding either to the polar bonds in the NIPAM residues, or to the ionic SS residues. This is also consistent with the observed increase in LCST with added SS content. They did not, however, measure the change in ΔH for added NaCl with pNIPAM homopolymers or homopolymer gels. This makes it impossible to tell which interaction raises the enthalpy of the de-mixing. Yaacobi and Ben-Naim found that several small-molecule salts lower the entropy of the hydrophobic interaction [79]. This result is consistent with the empirical finding that these salts salt-out pNIPAM.

3.6 Overall Picture

The results from Sections 3.4 and 3.5 suggest the following picture. Mixing the pNIPAM chain and water lowers the entropy of the water by approximately $17\,\mathrm{J/(mol\,K)}$ [81]. Hydrogen bonds are formed between the water molecules and the polar acrylamide group. Adding polar, non-ionic groups to the chain increases the hydrogen bonding between the polymer chain and the surrounding water. The polar, non-ionic groups do not significantly interact with each other when the chain forms a globule. Ionic groups also increase the bonding between the polymer chain and the surrounding water. But the ionic groups strongly repulse each other when the chain collapses into a globule, preventing that collapse until a much greater entropy penalty is incurred.

My own results in Chapter 5 are consistent with previous results, and with this picture. This picture suggests a few additional experiments, some of which are included in Chapter 5. Better verification would come with DSC studies of the NIPAM/Am copolymers, as well as with the Q9 copolymers. These DSC experiments are not included in this dissertation.

Chapter 4

Materials and Methods

4.1 Introduction

This chapter details the detectors used in this dissertation, and the different techniques for combining several detectors into a single experiment. Each detector provides a single piece of information about a polymer system; the techniques combine several detectors giving complementary information in a manner to more fully characterize the system. I describe the theory underlying each detector in Chapter 2; in this chapter, I explain how to convert the raw output voltages into meaningful physical quantities. I also explain how several detectors work together in the characterization techniques.

4.2 Detectors

4.2.1 Multi-Angle Light Scattering

Static light scattering (SLS), or multi-angle light scattering (MALS), uses a laser light to measure the weight-average molecular weight M_w z-average mean squared radius of gyration $\langle S^2 \rangle_z = R_g$, and second virial coefficient A_2 of a polymer

in solution. MALS is based on the well-known Zimm equation [25, 62],

$$\frac{Kc}{I(q,c)} = \frac{1}{M_w}\left(1 + \frac{q^2\langle S^2\rangle_z}{3}\right) + 2A_2c \tag{2.63}$$

In the Zimm equation, $I(q,c)$ is the excess Rayleigh scattering due to the polymer, taken to be a function of scattering vector q and concentration c. The scattering vector is $q = \frac{4\pi n}{\lambda}\sin(\theta/2)$. Where λ is the wavelength of the laser, n is the refractive index of the pure solvent, and θ is the scattering angle. K is the optical constant describing the experimental setup. For vertically polarized incident light, $K = \frac{4\pi^2 n^2 (dn/dc)^2}{N_A \lambda^4}$.

A particular instrument must be normalized and calibrated in order to convert the raw voltage output into absolute Rayleigh scattering values. Normalization accounts for the fact that the detectors may not respond to the same scattering. To normalize the instrument, a known isotropic scatterer (for example, NIST-traceable 2nm polystyrene spheres) is run through the detector. If the scattering voltage at scattering vector q is $V(q)$, then the normalization function $N(q)$, given by

$$N(q) = \frac{V_{\text{norm}}(\theta = 90^\circ) - V_{\text{solvent}}(\theta = 90^\circ)}{V_{\text{norm}}(q) - V_{\text{solvent}}(q)} \tag{4.1}$$

normalizes the detectors to a reference detector (taken to be the detector at $\theta = 90\,^\circ$in this case). The subscript "norm" refers to the voltages with the normalizing scatterer. The subscript "solvent" refers to the voltages due to the pure solvent.

Calibration converts the normalized voltages into absolute Rayleigh scattering ratios by referring them to a solvent with a known Rayleigh scattering ratio. The Rayleigh scattering ratio $I(q)$ at scattering vector q is then

$$I(q) = \frac{V_{\text{ref}}(q) - V_{\text{solvent}}(q)}{V_{\text{ref}}(\theta = 90^\circ) - V_{\text{dark}}(\theta = 90^\circ)}(I_{,\text{ref}})(F)N(q) \tag{4.2}$$

The subscript "solvent" again refers to the solvent used in the experiment. The subscript "ref" refers to the reference solvent, which is almost always toluene. The subscript "dark" refers to the response of the detectors with the laser turned off. I_{ref} is the Rayleigh scattering ratio of the reference solvent. F is a geometrical factor [82], and accounts for the shape of the scattering volume; it is between 0 and 1, and is usually only a little less than 1.

Both the normalization and the calibration depend on the particular instrument and the particular solvent chosen for the experiment. The particular instrument used in this work is a BI-MwA, (Brookhaven Instruments Corporation, Holtzville NY). This is a seven-angle detector, operating at $\lambda = 663\,\text{nm}$. At this wavelength, $I_{\text{tol}} = 1.1 \times 10^{-5}\text{cm}^{-1}$. For this particular instrument, $F = 0.892$.

4.2.2 Differential Refractometry

The differential refractometer used in this dissertation is model RID-10A (Shimadzu Corporation, Kyoto Japan).

Differential refractometry measures the fractional difference in refractive index n between two solutions. Typically, one cell contains a reference solution of known index of refraction (n_0), so that the detector reports the index of refraction (n) of the test sample, as long as $(n - n_0)/n_0 \ll 1$ (see Figure 4.1. A laser passes through the two cells, and refracts slightly at the interface between the two samples. The deflection due to this refraction is proportional to $(n - n_0)/n_0$. This has several uses in polymer science. An important input parameter to the Zimm Equation is the differential refractive index dn/dc of the polymer/solvent system. By keeping the reference solvent unchanged, and adding a known concentration of polymer or solvent the test solvent, one can measure the dn/dc. The dn/dc of the polymer is often larger than that of the monomer; if both are known, then the change in RI during the reaction can tell how much monomer has been polymerized.

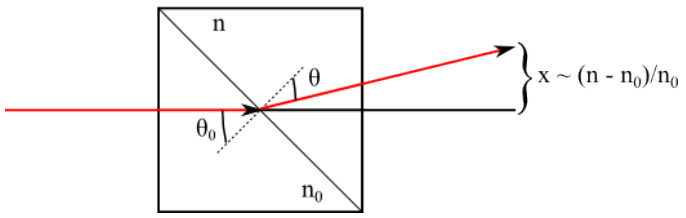

Figure 4.1: The light (shown in red) passes through the cell with the reference solvent (index of refraction n_0). It is refracted at the interface between the reference solvent and the test solvent (index of refraction n). The angle of refraction is usually quite small. The small angle approximation then gives the final result.

4.2.3 UV-Vis Spectroscopy

Two types of UV-Vis spectrometers were used in this dissertation: model SPD-M20A (Shimadzu) is a full-spectrum diode array spectrometer. It measures absorption from 190 nm to 800 nm. This was used with a 0.01 cm path length cell. The other is a dual-wavelength model (SPD-10AVvp Shimadzu). It measures absorption at two specified wavelengths; these can range from 190 nm to 370 nm. This was used with a 1.0 cm path length cell.

Ultraviolet-visible spectroscopy (UV-Vis) derives its utility to polymer science from the fact that many monomers have a carbon-carbon double bond (vinyl bond) in the monomer form, which is broken into a single bond in the polymerization reaction. The vinyl bond absorbs strongly in the UV, particularly between 200 and 300 nm. This bond does not exist in the polymer form (though other vinyl bonds in the side groups may still exist), so the UV absorption in this region is greatly reduced as the polymerization reaction progresses. For this class of polymers, UV-Vis spectroscopy can accurately report the conversion of each monomer species, and the relative composition of each monomer in the resulting polymer. In order to distin-

guish the monomers present, it is necessary that their UV spectra differ sufficiently. For some pairs of comonomers, the spectra are sufficiently different that only two wavelengths are necessary. An example is the NIPAM/SS pair: SS absorbs much more strongly at 260 nm than does NIPAM. In this case, the signal at 260 nm can be used to determine the SS monomer present, and this information can be combined with a lower wavelength can to determine the NIPAM monomer present. For other pairs of monomers, the spectra are similar enough that many wavelengths must be used; an example of this is the pair NIPAM/Am. In such cases, an error minimization technique can be used to fit the experimental spectra to the two monomer spectra, using the monomer concentrations as the fit parameters. In this section, I will explain the two-wavelength solution first, then the error-minimization method.

The general expression for UV absorption at time t and wavelength λ is $UV^{\lambda}(t) = \varepsilon_1^{\lambda} c_1 + \varepsilon_2^{\lambda} c_2 + \varepsilon_p^{\lambda}[c_{0,1} + c_{0,2} - c_1(t) - c_2(t)]$, where UV is the UV absorption, ε is the mass extinction coefficient, c is the mass concentration, subscripts 1 and 2 indicate the monomer species, and subscripts $0,1$ and $0,2$ indicate the initial concentrations of the monomers. If it is assumed that the reaction goes to completion, only polymer is present at infinite time, so the UV signal at infinite time can be used to compute the extinction coefficient of the resulting polymer: $\varepsilon_p^{\lambda} = \frac{UV^{\lambda}(\infty)}{c_{0,SS}+c_{0,N}}$. If we also assume that a single absorption spectrum is sufficient to describe the polymer regardless of composition, this leaves the monomer concentrations as the only two unknowns. Therefore, two wavelengths are sufficient. The associated matrix equation

$$\begin{pmatrix} UV^{\lambda_1}(t) - UV^{\lambda_1}(\infty) \\ UV^{\lambda_2}(t) - UV^{\lambda_2}(\infty) \end{pmatrix} = \begin{pmatrix} \varepsilon_1^{\lambda_1} - \varepsilon_p^{\lambda_1} & \varepsilon_2^{\lambda_1} - \varepsilon_p^{\lambda_1} \\ \varepsilon_1^{\lambda_2} - \varepsilon_p^{\lambda_2} & \varepsilon_2^{\lambda_2} - \varepsilon_p^{\lambda_2} \end{pmatrix} \begin{pmatrix} c_1(t) \\ c_2(t) \end{pmatrix} \tag{4.3}$$

can then be solved for the monomer concentrations every time step during the reac-

tion.

The above paragraph is the method used for pairs of monomers where it is sufficient. In theory, under the assumptions given, only two wavelengths should be necessary. In practice, however, more may be needed. This is because there is an inherent uncertainty in any of the UV absorption measurements. If this uncertainty is comparable to the difference in the absoprtions at the two wavelengths, then more wavelengths will be needed. In such cases, an error minimization technique can be applied to a large window of the full spectrum to determine the monomer concentrations. The expected signal at wavelength λ and time t is

$$S_{\text{calc}}(\lambda, t) = L \sum_{i=1}^{N} \epsilon_i(\lambda) c_i + \epsilon_{p,i}(\lambda) c_{p,i} \tag{4.4}$$

This allows us to define an error function as

$$M(t) = \frac{\sum_\lambda w(\lambda)(S_{\text{exp}}(\lambda, t) - S_{\text{calc}}(\lambda, t))^2}{\sum_\lambda w(\lambda)} \tag{4.5}$$

We then minimize $M(t)$ with respect to c_i as our free parameters. There are two concentrations, so $N = 2$. This algorithm is described in [16] to compute the concentrations of two monomers with similar UV spectra, and further used in [14, 83].

$$\begin{aligned} \frac{\partial M(t)}{\partial c_i} &= \frac{\partial}{\partial c_i} \frac{1}{\sum w(\lambda)} (S_{\text{exp}}(\lambda, t) - S_{\text{calc}}(\lambda, t))^2 & (4.6) \\ &= \frac{1}{\sum w(\lambda)} \sum w(\lambda)(S_{\text{exp}}(\lambda, t) - S_{\text{calc}}(\lambda, t)) & (4.7) \\ &\quad \times \frac{\partial}{\partial c_i}(S_{\text{exp}}(\lambda, t) - S_{\text{calc}}(\lambda, t)) \end{aligned}$$

Plug in equation 4.4:

$$\frac{\partial S_{\text{calc}}}{\partial c_i} = L \left(\epsilon_i(\lambda) \frac{\partial c_i}{\partial c_i} + \epsilon_{p,i} \frac{\partial}{\partial c_i}(c_{i,0} - c_i) \right) = L \left(\epsilon_i(\lambda) - \epsilon_{i,0}(\lambda) \right) \tag{4.8}$$

Then

$$\frac{\partial M(t)}{\partial c_1}\frac{2L}{\sum w(\lambda)}\sum_{\lambda} w(\lambda)\left(S_{\exp}(\lambda,t)-S_{\text{calc}}(\lambda,t)\right)\left(\epsilon_i(\lambda)-\epsilon_{p,i}(\lambda)\right)=0 \tag{4.9}$$

Making the identification $\delta_k(\lambda)=\epsilon_k(\lambda)-\epsilon_{p,k}(\lambda)$, we can simplify this to

$$\sum_{\lambda} w(\lambda)\delta_i(\lambda)\left(S_{\exp}(\lambda,t)-L\sum_{i=1}^{N}\left[\epsilon_i(\lambda)c_i+\epsilon_{p,i}(\lambda)(c_{i,0}-c_i)\right]\right)=0 \tag{4.10}$$

Rearranging terms leads to

$$\begin{aligned}&\sum_{\lambda} w(\lambda)\delta_i(\lambda)\left[S_{\exp}(\lambda,t)-L\sum_{i}\epsilon_{p,i}(\lambda)c_{i,0}\right]\\&-\sum_{\lambda} w(\lambda)\delta_i(\lambda)L\sum_{k}\left[\epsilon_k(\lambda)(c_k-\epsilon_{p,k}(\lambda)c_k)\right]=0\end{aligned} \tag{4.11}$$

and finally to

$$\sum_{\lambda} w(\lambda)\delta_i(\lambda)\left[S_{\exp}(\lambda,t)-L\sum_{i}\epsilon_{p,i}(\lambda)c_{i,0}\right]=\sum_{\lambda} w(\lambda)\delta_i(\lambda)L\sum_{k}[\epsilon_k(\lambda)(c_k-\epsilon_{p,k}(\lambda)c_k)] \tag{4.12}$$

Recalling the definition of matrix multiplication $(AB)_{ij}=\sum_k A_{ik}B_{kj}$, we can substitute $\sum_k Lw(\lambda)\delta_i\delta_k c_k=\sum_k c_k B_{ki}=(cB)_i$, Equation 4.12 can then be rewritten as

$$\vec{A}_i=(\vec{c}\underline{B})_i\Rightarrow\vec{A}=\vec{c}\underline{B} \tag{4.13}$$

with the definitions

$$A_i = \sum_{\lambda} w(\lambda)\delta_i(\lambda)\left[S_{\exp}(\lambda,t)-L\sum_{i}\epsilon_{p,i}(\lambda)c_{i,0}\right] \tag{4.14}$$

$$B_{ij} = L\sum_{\lambda} w(\lambda)\delta_i\delta_j \tag{4.15}$$

This error minimization can be seen as a generalization of the dual wavelength

method. The definition $\delta(\lambda)$ in the error minimization technique is analogous to the $\varepsilon_m + \varepsilon_p$ terms in the dual wavelength technique.

This error minimization method is typically required if the shape of the monomers' absorption spectra are similar. In this dissertation, this is the case with NIPAM and Am, and with NIPAM and Q9.

4.2.4 Dynamic Light Scattering (DLS)

As described in section 2.4.2, dynamic light scattering measures the fluctuations in light scattering due to the diffusion of the polymer chains in solution. The DLS instrument used in this dissertation is a 90Plus Particle Sizer (Brookhaven Instruments Corporation, Holtzville, NY). This uses a 26 mW, 658 nm laser. Scattering is taken at 90°. Autocorrelation functions are recorded by a BI-9000AT Digital Correlator (Brookhaven). The distribution of diffusion constants is extracted from the autocorrelation function, and the hydrodynamic radius of the polymer is calculated according to Equation 2.65. The primary output of this instrument is hydrodynamic diameter D_h, which requires no further conversion before interpretation. In addition, this instrument outputs counts per second (cps). This must be converted into absolute Rayleigh scattering ratio using the ideas of Section 4.2.1, Because there is only one angle of light scattering, the normalization step is not necessary.

4.2.5 Simultaneous Multiple Static Light Scattering (SMSLS)

The SMSLS instrument used in this work was the first version built. It has eight sample cells, each individually temperature controlled. Four cells are capable of stirring the sample, though this was not used in this dissertation. Two cells are capable of cooling; all eight are capable of heating and holding the sample at any temperature above ambient and at below at least 100 °C. Raw light scattering data

was recorded by computer, and written to a text file. This raw voltage data can be converted to the absolute Rayleigh scattering ratio using the ideas of Section 4.2.1. As in DLS, the normalization step is unnecessary because there is only one angle for each scattering cell. Temperature data was written to a separate file.

4.2.6 Viscometer

The viscometers used in this work are single-capillary bridge viscometers (P55D-28-2446, Validyne Engineering, Northridge CA). They have a range of $\pm 5\,\mathrm{kPa}$ The pressure transducer measures the pressure difference between two points in the flow along the tubing. The viscosity and flow rate of the solution cause a pressure differential at these two points according to Equation 2.70. The viscometer outputs a voltage proportional to this pressure differential. Thus, if the polymer concentration c is known, the reduced viscosity can be calculated as

$$\eta_{\mathrm{red}} = \frac{V - V_{\mathrm{solv}}}{(V_{\mathrm{solv}} - V_{\mathrm{zero}})c} \tag{4.16}$$

where V is the voltage output by the viscometer, V_{solv} is the voltage output by the viscometer for pure solvent at the given flow rate, and V_{solv} is the voltage output by the viscometer at zero flow rate.

4.3 Multi-Detector Techniques

4.3.1 Gel Permeation Chromatography

Gel permeation chromatography (GPC) is also known as size exclusion chromatography (SEC). This is a column-based technique in which a liquid sample (called the liquid phase) is forced through a column filled with a porous material. The packing material in the column is usually a polymer material; the exact polymer depends on whether the column will be used with an aqueous or an organic liquid phase. An

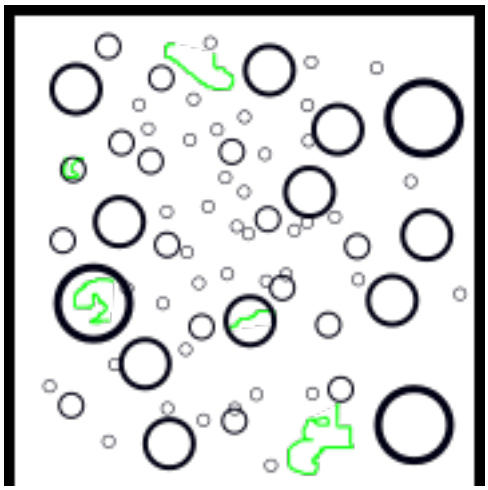

Figure 4.2: The chains (green) can only fit into pores (black circles) that have a larger radius than that chain's hydrodynamic radius. Passage through the pores slows the chains. Because smaller c chains can fit into more pores than larger chains, they elute later.

injector loop ensures that the total injected solution is of a known volume. The mass concentrated of dissolved solids is known, so the total mass injected is known. The solution is forced through the column by a pump pumping at a constant rate; this allows a one-to-one correlation between the elution time and the elution volume. One or more detectors are placed at the output of the GPC column to detect the elution of solids.

GPC separates the solids in the solution on the basis of their hydrodynamic volume: larger hydrodynamic volume solids elute earlier. This is because there is a distribution of pore sizes in the column packing. Solid particles are unable to move through pores that are smaller than they are, as illustrated in figure 4.2. As a result, smaller particles are able to more through more pores. This causes the smaller particles to spend more time in the column, and therefore elute later. It is important to note, through, that a given column has both a minimum and a maximum elution volume, and can therefore only discriminate among chains that elute within that range.

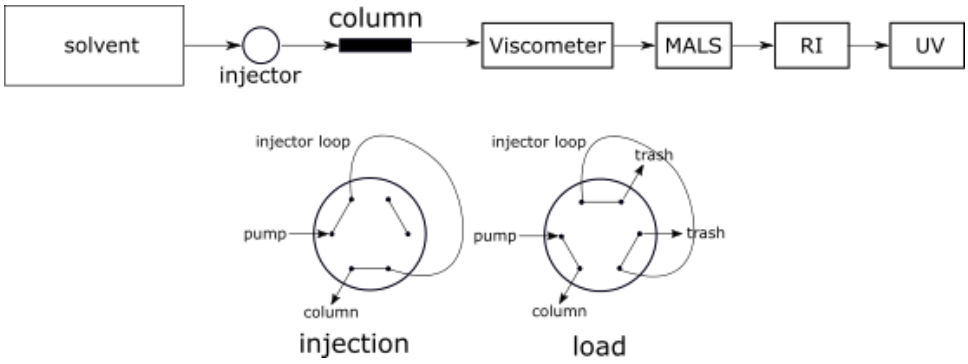

Figure 4.3: Top: a solvent pump pushes the solvent and sample through the GPC column. After the column, the solution passes through the detector train. In the GPC detector train, UV is last because it requires a 1 cm cell, which has a large delay volume. This is in contrast to ACOMP, described below.

If there is only one detector after the column, then a calibration curve is required to translate elution volume into chain size. If, however, there are multiple detectors, there is no need for a calibration curve because light scattering can measure M_w directly. The GPC system I use in this dissertation is a multi-detector system; a schematic is shown in Figure 4.3.

4.3.2 ACOMP

Automatic continuous online monitoring of polymerizations (ACOMP) is a multi-detector methods developed in the Reed lab [84, 85]. It was first reported in 1998 by Florenzano, et al [86]. The basic insight of ACOMP is that we can extract a stream of material from a polymerization reaction, dilute and condition it, and then pass it directly to characterization instruments. Reaction conditions typically have a much higher concentration of polymer than is useful for characterization; in particular, reaction conditions usually violate the assumptions required for single chain light scattering. This can be overcome by diluting the reactor eluent with solvent from a reservoir. in the simplest case, the dilution factor is not too large, and the dilution can be achieved by pumping the two streams into a mixing tee,

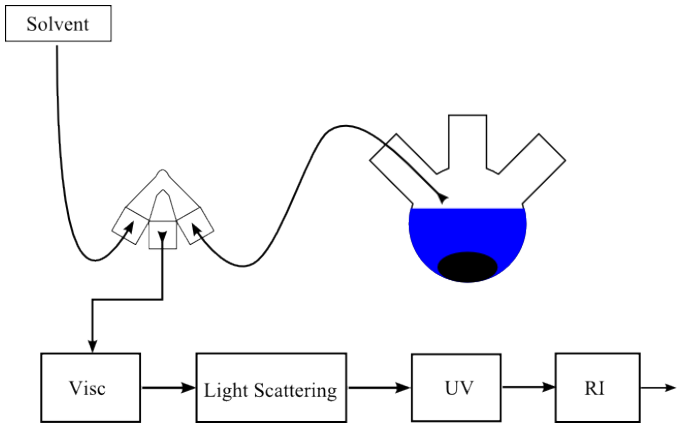

Figure 4.4: Shown is the typical order of detectors: viscometer, static light scattering UV-Vis, differential refractometer. Only one dilution stage is shown, as is used in this dissertation.

called a high pressure mixing chamber (HPMC). The output of the mixing tee is then passed to the detectors. If the dilution factor is so high that the pumps cannot precisely deliver both streams, two such dilution stages may be necessary. Figure 4.4 illustrates the setup with one dilution stage.

In a slightly more complicated situation, some time delay may be needed in the dilution stage. For example, the polymer may need to be solubilized in a surfactant, and this may take some time. In these cases, a low pressure mixing chamber (LPMC) can be used. Both streams are input to a vial, the LPMC. A third pump extracts from the LPMC. In this case, the flow rate extracted from the LPMC can be less than the combined flow rate into the LPMC; a fourth pump can extract the excess inflow to the waste. The finite volume of such an LPMC introduces a delay time; if needed, this delay time can be adjusted up or down to allow for solubilization or micellization. Mixing and/or heating can also be applied at the LPMC stage. An LPMC dilution stage can also be used to make a full solvent-to-solvent transfer. This is done by diluting the solution in one solvent into a second solvent. The mixture is then heated to boil off the original solvent, leaving the polymer in the second solvent. This transfer can be useful if the reaction solution is sub optimal for characterization.

Finally, any number of HPMC and/or LPMC dilution stages can be combined in series or parallel.

The work I present in this dissertation uses only a single-stage HPMC. The pumps used were either LC-10AD or LC-10ADvp (Shimadzu).

After the dilution and conditioning stage, the polymer solution passes through several detectors in the detector stream. The exact set of detectors will depend on the needs of the experiment. The order of the detectors is chosen for experimental simplicity. Figure 4.4 shows the typical order for the work in this dissertation.

A multi-angle static light scattering unit is almost always included, in order to measure M_w, R_g, and A_2. The MALS instrument used for the ACOMP experiments reported in this dissertation is a BIC (Brookhaven), with $F = 0.9294$ and $\lambda = 637\,\text{nm}$ A UV-Vis spectrometer can report the conversion of monomer into polymer. This is necessary both to provide the MALS detector with the polymer concentration and to calculate the reaction kinetics and progress. Depending on the exact pair of comonomers, the UV-Vis spectrometer may be a dual wavelength model or a full spectrum diode array model. A differential refractometer can report the differential refractive index dn/dc of the monomers and the polymer. The dn/dc of the polymer is needed for the MALS detector. Finally, the viscometer reports the total viscosity of the solution. Coupled with the concentration reported by the UV-Vis detector, the viscometer can report the intrinsic and reduced viscosity properties of the polymer solution.

4.3.3 Automatic Continuous Mixing (ACM)

Automatic continuous mixing (ACM) is a multi-detector technique used for post-synthesis characterization of polymers [21]. This technique uses a quarternary mixing attachment (FCV-10ALvp, Shimadzu) to an HPLC pump (LC-10AD or LC-10ADvp) to create a linear ramp of the concentration of a polymer or other solute of

interest. Typically we will ramp the polymer concentration, keeping other solution characteristics (ionic strength, pH, etc) constant. However, we can also ramp the ionic strength, keeping the polymer concentration constant. After mixing, the solution passes through a detector train.

The detectors in the ACM detector train are usually the same as those used in the ACOMP detector train. In this case, the dn/dc of the polymer is usually known, so the differential refractometer can report the polymer concentration directly. The UV-Vis spectrometer can also report the polymer concentration. The viscometer reports the viscosity as in ACOMP. The major difference between ACM and ACOMP is in the use of the light scattering detector. In ACM, the polymer concentration can be ramped to a higher concentration than in ACOMP, so the MALS detector can more accurately measure the A_2 of the polymer. ACM also ramps the polymer concentration linearly rather than according to the polymerization kinetics, so the data is more evenly distributed across the concentration range. The MALS detector used in the ACM experiments reported in this dissertation is a BI-MwA (Brookhaven) with $F = 0.9294$ and $\lambda = 637\,\mathrm{nm}$

Instead of ramping the polymer concentration, we can also ramp the ionic strength of the solution. This is particularly useful for polyelectrolytes; because the conformation of polyelectrolytes is highly dependent on the ionic strength, the exact dependence is important to know. An ACM ramp of ionic strength allows us to measure this.

Figure 4.5 shows a schematic of the ACM setup. The configuration shown allows for ramping of either polymer concentration or ionic strength.

4.3.4 Second Generation ACOMP (SGA)

Second-generation ACOMP (SGA) is a new detector that can be added on to the standard ACOMP detector stream [87]. This detector allows us to see temperature-

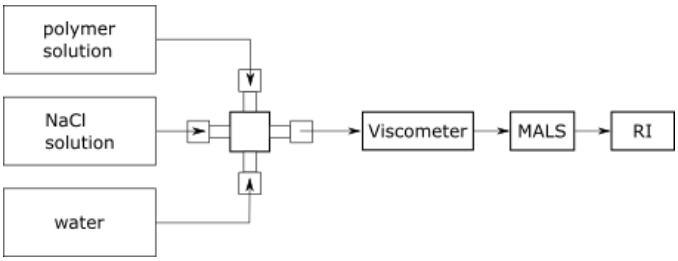

Figure 4.5: The ACM instrumentation setup. Any two of the three input solutions can be ramped. The third is used to keep one component of the resulting mixture constant. In this configuration, NaCl and water can be ramped to change the ionic strength, keeping polymer concentration constant; or polymer solution and NaCl can be ramped to change the polymer concentration, keeping ionic strength constant.

dependent properties of the polymer solution. In the current instrument, there are three single angle light scattering flow cells. In addition to the light scattering, each light scattering cell has a thermocouple measuring the temperature of the solution immediately before the solution passes through the light scattering volume. Before the light scattering cell, the solution is heated up by passing through an aluminum block heated by a peltier device. stainless steel tubing is wrapped in a serpentine fashion, and attached to the aluminum block via thermally conducting solder. The serpentine wrapping maximizes the time the sample spends in thermal contact with the heat block. The aluminum blocks are 2 in. square, and 0.5 in. thick. The tubing is stainless steel 1/16 in. inner diameter. The peltier devices are model NL2060 (Marlow Industries, Dallas). They have a maximum heat flow of 45.0 W, and can sustain a temperature differential across their thickness of over 75 °C under the conditions discussed in this dissertation.

A schematic of the flow cells is shown in Figure 4.6. The block is a $30 \times 20 \times 50$ mm block of nylon 6-6. For ease of reference, I will refer to these as the x, y, and z axes, respectively. The flow is then directed along the x-axis, the laser input along the y-axis, the 90° light scattering output along the z-axis, and thermocouple parallel to the z-axis. Along the x-axis, a 5/32 in. hole is drilled all the way through the block.

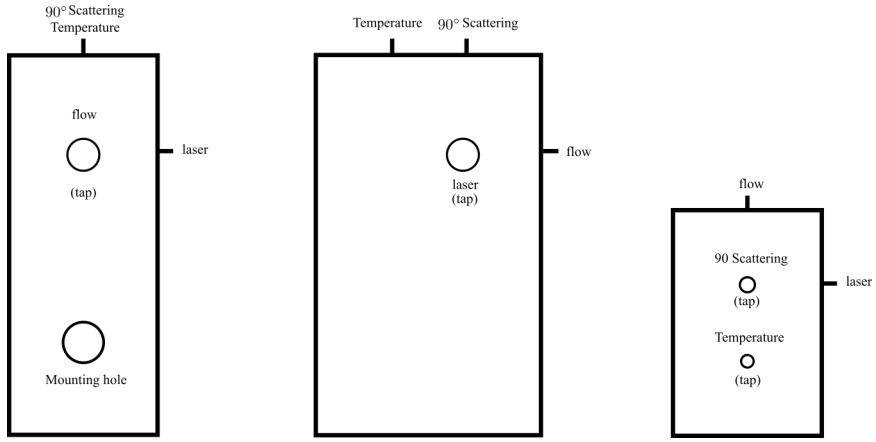

Figure 4.6: A schematic of the SGA flow cells. From left to right: looking along the z-axis, looking along the y-axis, and looking along the x-axis.

A flat drill bit is used to drill a 7/32 in. hole 1/4 in. deep on both sides. This hole is at both ends with a 1/4-28 tap. A #43 bit is used to drill through along the y-axis. The 7/32 in. flat drill bit to is used to drill 1/4 in. deep on both sides of that hole. Again, both sides are tapped with a 1/4-28 tap. A 7/64 in. drill bit has been ground to a sharper taper. This bit is used to drill 5/16 in. deep along the z-axis from one sides. A micro drill bit is drilled through to the x-y plane through that hole. That hole is tapped with a 6×32 tap. Parallel to the z-axis and offset from the z-axis by 10 mm, the #48 taper drill is drilled fully through the block. A #22 bit has been ground to a sharper taper; this bit is used to drill 7/32 in. deep into that hole. That hole is tapped with a 10×32 tap. The fittings are install into each hole as shown in figure 4.6. The light scattering intensity is carried via fiber optic cable to an electronics box, in which is mounted a photodiode board. The photodiode board outputs a voltage between -10–10 V, which is then fed into a computer via A/D board. The temperatures are recorded by an Omega (Stamford, CT) model DP472-T-C2-12VDC six-channel temperature measurement indicator. This reports the temperature at each cell with a resolution of 0.1 °C. The temperatures are recorded to a computer via the DS472 software (Omega).

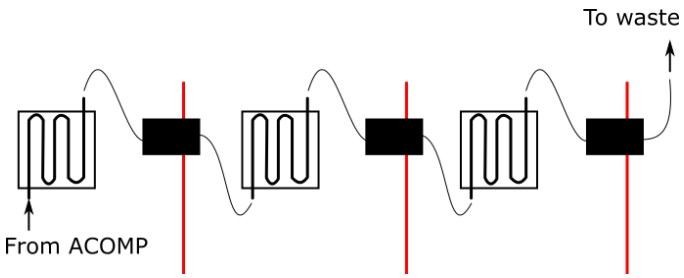

Figure 4.7: The SGA heating blocks and scattering cells are arranged in series, in alternating fashion. Each heating block is placed immediately before the corresponding scattering cell along the flow path.

The flow cells are then connected in series via PEEK tubing. The heating blocks are connected immediately before each light scattering flow cells. stainless steel tubing is used in the heating blocks to ensure optimal heat transfer to the fluid. The arrangement is shown in Figure 4.7

The polymer solution is thus heated by the heat block, and cools slightly before entering the light scattering cell. The temperature measurement is made at the light scattering cell rather than the heat block to ensure that we're actually measuring the temperature of the polymer at the light scattering. Because of this setup, there is a trade off in flow rates. Higher flow rates reduce the amount of time the polymer cools between the heat block and the light scattering cell. But higher flow rates also cause the sample to spend less time in the heating block.

For a given temperature at the heat block, there is a flow rate that will maximize the temperature of the polymer sample at the light scattering cell. For the temperatures used in this work, I found that a flow rate of $q = 2.0\,\mathrm{mL/min}$ was close to optimal. Happily, this is also a typical flow rate for the rest of the ACOMP detector stream.

Chapter 5

Results

5.1 Introduction

I used the methods outlined in Chapter 4 to characterize three NIPAM copolymer systems. The three comonomers were chosen to have varying charge and reactivity properties. Acrylamide (Am, Figure 5.1) is a a hydrophilic neutral monomer. Due to their structural similarity, Am and NIPAM are expected to be approximately isoreactive. Indeed, the reactivity ratios of the Am/NIPAM copolymerization system have been measured previously as 1.0 and 1.0 [15]. Styrene sulfonate (SS, Figure 5.2) is an anionic monomer. Because the styrene group is structurally different from the acrylamide group, SS and NIPAM are expected to have much different reactivity ratios when copolymerized. This is therefore expected to be a high drift copolymerization. The system SS/Am has been characterized previously in the Reed lab [13]. The reactivity ratios were reported as $r_{\mathrm{SS}} = 2.0$, $r_{\mathrm{Am}} = 0.18$, and a two-phase drift was seen in the copolymerization.

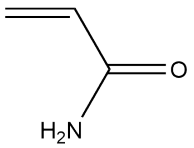

Figure 5.1: Acrylamide (Am).

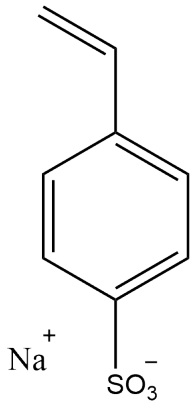

Figure 5.2: Styrene sulfonate, sodium salt (SS).

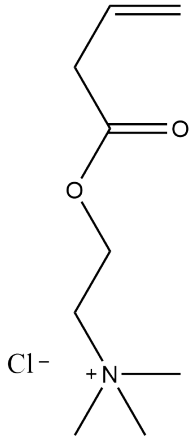

Figure 5.3: [2-(acryloyloxy)ethyl]-trimethylammonium chloride (Q9).

[2-(acryloyloxy)ethyl]-trimethylammonium chloride (Q9, Figure 5.3) is a cationic comonomer. The group at the base of the Q9 side chain is acrylic, so Q9 is expected to have a similar reactivity ratio as NIPAM, but the bulk of the side chain and the presence of the charge cause us to expect this system not to be as ideal as the NIPAM/Am system. The reactivity ratios of the Q9/Am system have been measured as $r_{\mathrm{Q9}} = 0.47$, $r_{\mathrm{Am}} = 1.10$ [14].

The reactions were initiated by either potassium persulfate (KPS, Figure 5.4) or 2,2'-Azobis(2-methylpropionamidine)dihydrochloride (V50, Figure 5.5), both of which are water-soluble free radical initiators. AIBN- and KPS-initiated polymers

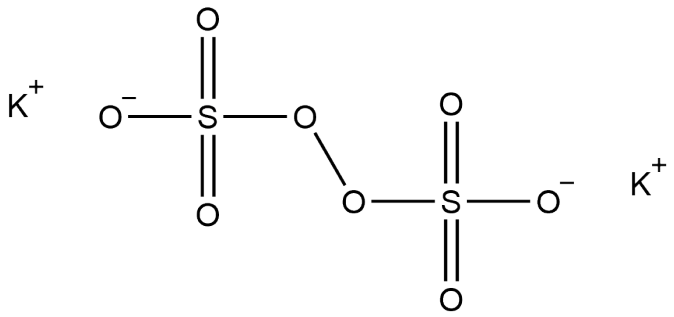

Figure 5.4: Potassium Persulfate (KPS).

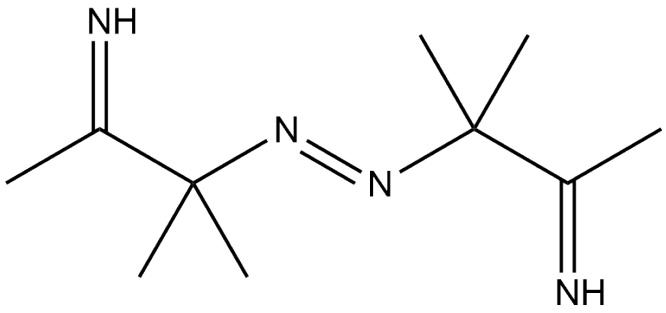

Figure 5.5: 2,2'-Azobis(2-methylpropionamidine)dihydrochloride (V50).

react slowly at room temperature. There are two possible ways to speed the reaction up: increase temperature, or use a redox catalyst. For some of the reactions discussed in this chapter, the reactor was heated. For others, this was undesirable due to the LCST of the resulting polymers. For those reactions, tetramethylethylenediamine (TEMED, Figure 5.6) was used as a redox catalyst. TEMED is water-soluble.

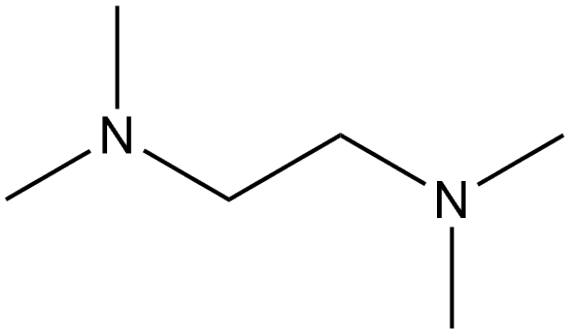

Figure 5.6: Tetramethylethylenediamine (TEMED).

5.2 Second generation ACOMP

This section presents some results from the commissioning of the second generation ACOMP (SGA) flow cells.

Peltier devices work by the thermoelectric effect: a current run through the device creates a temperature differential across the device. The temperature differential across the element is directly proportional to the current running through the element. It is easier to measure voltage, so I attempted to calibrate the voltage/temperature response curves for the peltiers. This makes it easier to set a desired temperature for each heating block. Figure 5.7 shows the results for two of the peltier devices. In both cases, the temperature measurement is from a K-type thermocouple inserted into the aluminum block attached to the hot side of the peltier; the cool side is attached to a heat sink at ambient temperature. From this, it is apparent that we can heat the peltiers to 100 °C if we hold enough voltage across the device. There is a small difference between these two particular elements; this is immaterial, as the temperature is measured directly at the scattering volume in all my experiments, and this calibration result is used only as a guide to set the voltages.

In addition to calibrating the voltage applied against the resulting block temperature, I also wanted to calibrate the block temperature to the resulting sample temperature at the scattering volume. Figure 5.8 shows that the temperature at the scattering volume is consistently lower than the temperature at the heating block. The fact that the slope of the fit line is less than 1 indicates that the loss in temperature increases as the temperature of the block increases. This loss in temperature is due to the fact that the sample fluid is exposed to ambient temperature over a length of about 10 cm between the heat block and the light scattering cell. The length of time the fluid spends in this environment depends on the flow rate. The time rate of cooling depends on the temperature of the heating block and the ambient temperature.

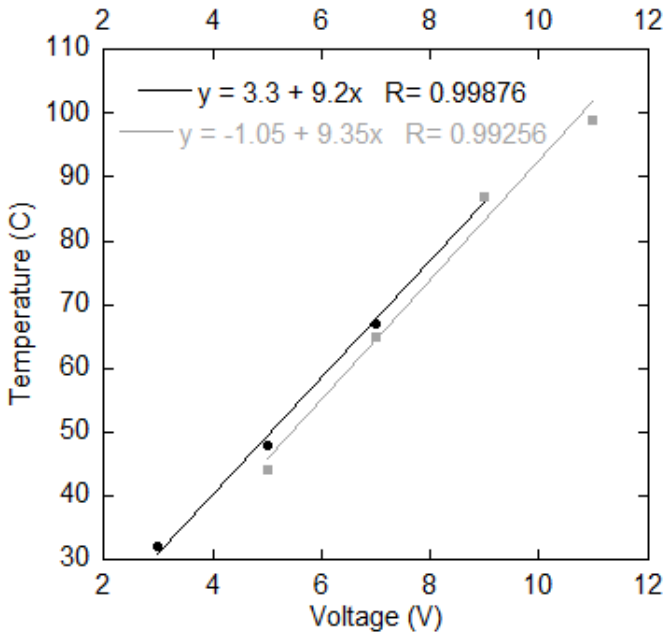

Figure 5.7: Two of the peltier devices show almost identical temperature responses to applied voltage. The actual cause of the temperature is the current, which is itself due to the applied voltage. The linear response shown here demonstrates that we can use voltage as a proxy for current.

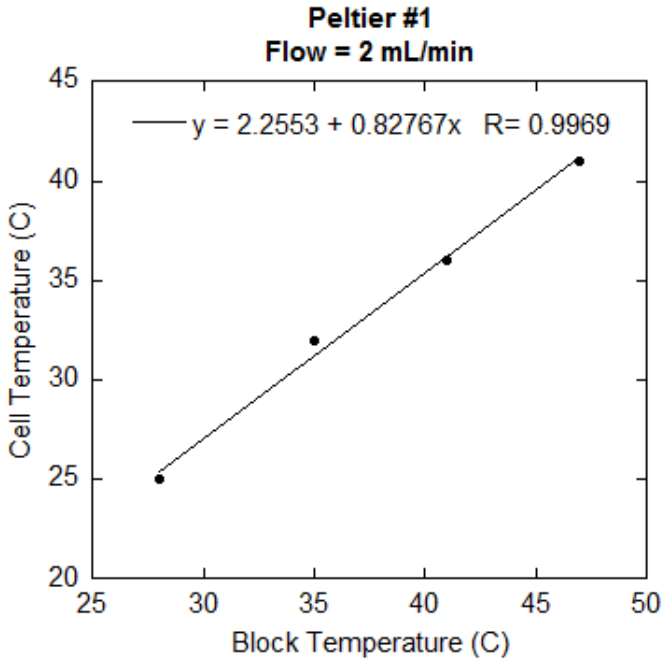

Figure 5.8: There is some loss of temperature during the trip from the heating block to the flow cell. For a given flow rate, the relation between the two temperatures is approximately linear.

Therefore, we would expect the difference between the temperatures of the heat block and the scattering cell to depend on the flow rate, in addition to the temperature of the heat block. Table 5.1 shows that this is the case. In general, lower flow rates will lead to more cooling between the heat block and the flow cell, because the fluid is exposed to ambient temperature for a longer period of time. However, the sample also takes a finite amount of time to heat up while in the heat block. At an extremely high flow rate, therefore, the sample could flow so quickly through the block that it does not come fully up to the temperature of the heat block. This can be seen, for example, when the block is at 46.3 °C, and the flow rate increases from 2.2 mL/min to 4.6 mL/min; the higher flow rate gives a lower temperature at the flow cell. Overall, I found that a flow rate of 2.0 mL/min is a good balance between these two effects, and maximizes the temperature at the scattering cell for a given temperature at the heat block. This is a typical flow rate used in the traditional ACOMP system, so it

Table 5.1: Flow cell temperature is a function of flow rate, applied voltage, and eating block temperature.

flow rate (mL/min)	applied voltage (V)	block temperature (°C)	flow cell temperature (°C)
0.8	3.02	37.2	33
2.0	3.02	37.2	35
3.0	3.02	37.2	36
1.2	5.06	46.3	46
2.2	5.05	46.2	47
4.6	5.05	46.2	46
0.8	7.02	64.6	53
1.2	7.06	65.0	57
1.2	8.36	77.1	58

is quite convenient to use.

5.3 Simultaneous multiple sample light scattering

This section presents some early results from the simultaneous multiple sample light scattering instrument. One of my initial attempts at using the SMSLS instrument to monitor protein aggregation was with bovine serum albumin (BSA) in aqueous solutions at different pH's. This is a relatively well-understood protein [88–90], so BSA was a good first step in commissioning SMSLS for protein aggregation studies.

The first experiment with BSA suggested that BSA is stable at neutral or basic conditions for up to 22 hours. This is shown in Figure 5.9. The BSA did not readily go into solution at 4 mg/mL at pH 13.6; the dissolution took over night. The samples at pH 2.76, 4.95, and 7.0 all appear to remain stable in solution for 22 hours. The large drop in the 4.95 signal at $t = 40\,000$ s is probably an artifact of the instrument. We observed this phenomenon several times in the early SMSLS prototypes; the baseline value can change drastically. We believe that this is due to errors either in the laser, or in the CCD camera. The work I discuss in Sections 5.4 through 5.6 does not suffer from this artifact.

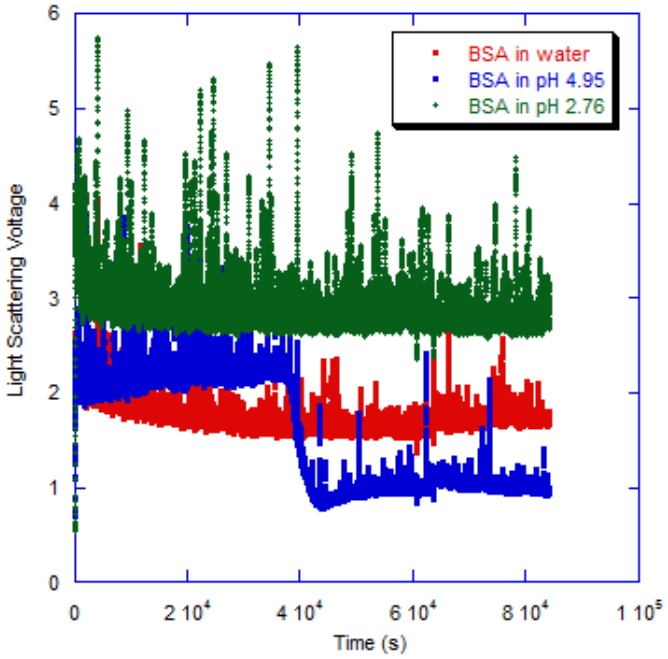

Figure 5.9: BSA is stable for 22 hours at pH 2.76, 4.95, and 7.00. The drop in the pH 4.95 signal is an artifcat of detector. The isoelectric point is 4.7.

After the introduction of better data recording software, I was able to contribute to Arrhenius plots for some protein aggregation studies for Biogen Idec (Cambridge MA). In these studies, the proteins were held in solution in SMSLS at different temperatures. The light scattering signal can be used to measure the aggregation number of the proteins. From this, we measure the rate constant of the aggregation process. As in any thermodynamically driven process, the rate constant increases exponentially with temperature; this can be shown on an Arrhenius plot. My contribution to this project was to measure some of the proteins at some temperatures in still buffer. This data is shown in Figure 5.10. Further measurements were made with stirring of the buffer. The stirring induces shear forces on the proteins, which increases the rate of aggregation.

Finally, I established that SMSLS can measure the dissolution of a protein into solution. The first project for this was a set of samples from an industrial sponsor.

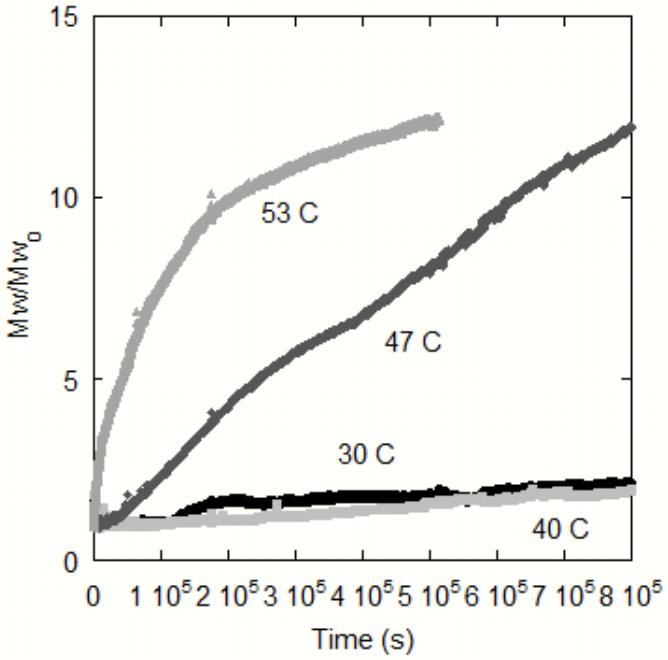

Figure 5.10: The same protein is held at several different temperatures at the same concentration in the same buffer. At higher temperatures, the protein aggregates more quickly. The aggregation rates can be plotted on an Arhennius plot to estimate the activation energy of the unfolding process that leads to the aggregation process.

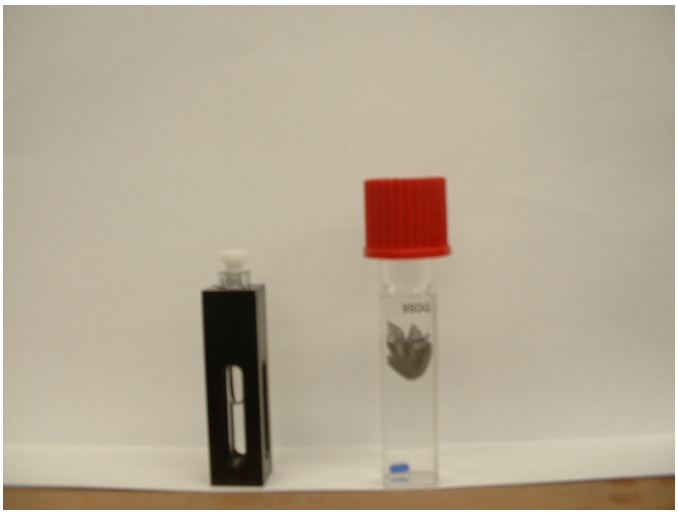

Figure 5.11: A photo illustrating how the mesh sits in the SMSLS sample cells. On the left is one of the 5 mm width cells. This cell is too small for the mesh to fit. On the right is a 10 mm width cell with the mesh installed. This cell is filled with enough fluid so that a polymer sample in the mesh will sit in the solvent. The polymer then dissolves into solution, and can be observed by light scattering.

We installed mesh baskets into each of the SMSLS sample cells, as shown in Figure 5.11. The baskets are installed so that the polymer sits at the bottom in the basket, in solution, but that the basket is above the scattering volume. As the polymer dissolves, it diffuses into the solution, and eventually into the scattering volume. the instrument measures the diffusion into the scattering volume as an increase in scattering. initially, we measured this process with no stirring of the solvent, but stirring was later added. The stirring increases the speed of the dissolution process enormously. In addition to dissolution into solution, the polymer can be left in solution for an extended period of time, allowing SMSLS to also measure the stability of the polymer in solution. I show some preliminary data from the dissolution phase of this project in Figure 5.12.

5.4 Nonionic comonomer: Acrylamide

Most of the contents of this section were published as Reference [91].

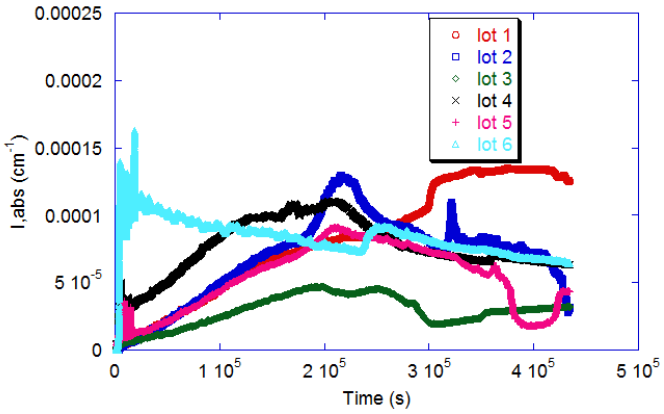

Figure 5.12: Several of the samples were set in the backets in the SMSLS sample cells, and were allowed to dissolve into solution at room temperature with no stirring. Lot 6 was from a different series, and went into solution much faster than the other lots. Lots 1 through 5 all dissolved at approximately the same rates. The difference in light scattering among those samples is due to the differing concentrations and scattering characteristics.

5.4.1 Introduction

Poly(N-isopropyl acrylamide), or pNIPAM, is a stimuli-responsive polymer. When heated to 32 °C, it undergoes a coil-to-globule transition. At high enough concentrations, the polymer chains aggregate and precipitate, producing a lower critical solution temperature (LCST) [56, 92, 93]. Two easy ways of changing the particular value of the LCST of a polymer are comonomer composition and salt. Because the balance between hydrophobic interactions and hydrogen bonding causes the coil-to-globule transition, the incorporation of comonomers that are more hydrophobic or hydrophilic than NIPAM decreases or increases the LCST, respectively. Various researchers have reported this behavior in several systems [3,4,76]. Acrylamide (Am) is an uncharged, polar, hydrophilic monomer, and so Am/NIPAM copolymers will have a higher LCST than NIPAM homopolymers [15, 94, 95]. In addition, adding salts to the solution decreases the LCST, as Bergbreiter has reported [5,96]. NaCl is a simple salt that lowers the LCST of NIPAM homopolymer [5].

As acrylamides, NIPAM and Am have similar reactivity ratios [15, 16], so batch free-radical copolymerization will synthesize random copolymers with low composition drift. Kreft recently demonstrated semi-batch methods, consisting of programmed reagent flows into the reactor during polymerization, which allow for control of instantaneous composition and average molecular weights of copolymers [83, 97]. This semi-batch technique can produce any composition distribution desired. Both batch and semi-batch polymerization allow investigation of the effect of comonomer composition on the LCST. The work in Section 5.5 shows that in a free-radical reaction of 80% NIPAM/20% Am (M/M), the LCST appears almost immediately in the reaction [87]. One weakness of the work in that section is that the reactions were carried out at 60 °C, above the LCST; because of reversibility issues, aggregation in the reactor during the reaction complicates the interpretation of those results. This section uses a redox catalyst to carry out the reactions at room temperature, keeping the reactor below the LCST and hence avoiding this difficulty. Zhang reports that the 50/50 copolymer shows no LCST in pure water [94]. Other researchers have reported very high LCST's of NIPAM/Am copolymers with 43–45 % Am [15, 95]. As a result, one would expect to be able to detect an LCST during synthesis of a copolymer with composition somewhere between 45% and 50% Am.

The object of this section is to monitor LCST and associated polymer properties both for batch reactions with given initial concentrations of Am/NIPAM and for a semi-batch reaction in which virtually all copolymer compositions are traversed in a single experiment.

5.4.2 Materials and methods

5.4.2.1 Reagents

NIPAM monomer (97% pure), Am monomer (99+%), and Potassium Persulfate (KPS, 99+%) were purchased from Aldrich. NaCl (≥99.0%) was purchased from

Sigma-Aldrich. Tetramethylethylenediamine (TEMED, min 99%) was purchased from Spectrum. All reagents were used as acquired unless otherwise noted. Water was purified by an ELGA Purlab Ultra system (18 MΩ cm). All liquid samples were further filtered through Millipore Millex 0.22 µm syringe filters before use.

5.4.2.2 ACOMP

ACOMP (automatic continuous online monitoring of polymerization reactions) monitors polymerization reactions by withdrawing a steady stream of product from the reactor, diluting it, and passing it through a series of detectors [86, 98]. Static light scattering (LS) provides polymer weight-average molecular weight M_w, the z-average radius of gyration R_g, and the second virial coefficient A_2 via the Zimm approximation [99]. UV-Vis spectroscopy provides monomer conversion and composition for copolymers. Differential refractometry provides a measure of the total refractive content of the solution with respect to pure solvent. A viscometer provides the reduced viscosity η_{red} of the polymer solution. The system here was the same as described in Reference [97], and outlined in Section 4.3.2. The current 'second generation ACOMP' uses this system, and feeds the detector output stream to three individually temperature-controlled SMSLS (simultaneous multiple sample light scattering) systems in series [100, 101].

During the reaction ACOMP monitors copolymer composition and M_w [16, 102], and the SMSLS flow cells monitor LCST-driven aggregation at different temperatures. This aggregation can then be correlated with the copolymer composition. An ACOMP system with detectors able to probe polymer stimuli-response (temperature in this case) is an example of 'Second Generation ACOMP (SGA). The SGA system consisted of two HPLC pumps (Shimadzu,10-AD VP). One extracted from the reactor at 0.1 mL/min, while the other extracted from a solvent reservoir at 1.9 mL/min. These two streams met at a high-pressure mixing chamber, producing a

dilution factor of 0.05. The diluted stream was then carried at 2.0 mL/min through (in order) a single-capillary viscometer, a differential refractometer (Shimadzu, RID-10A), a UV diode array (Shimadzu, SPD-M20A), and a static light scattering module (Brookhaven, BI-MWA). The stream then passed through the custom-built SMSLS flow cell bank consisting of three single-angle light scattering flow cells set, in order, at ambient temperature, in the range 45–50 °C, and 70 °C. The waste stream was taken after the flow cells. Work is underway to add a larger number of flow cells to increase the system's utility. The light scattering detectors record voltages for the light scattering and converts them into absolute Rayleigh scattering ratios I_{abs} (cm^{-1}) by comparing to the scattering voltage of a known Rayleigh scatterer (toluene at 90°) [86]. I_{abs} is computed with reference to toluene after subtraction of the solvent baseline scattering from the total scattering.

5.4.2.3 Stand-alone batch-cell SMSLS

A separate stand-alone custom-built SMSLS unit was used for off-line evaluation of reaction aliquots and end products. This consisted of eight batch cell samples, each sitting in an aluminum block, anodized and dyed black. Independently controlled and programmable heating elements heated each aluminum block. Continuous measurements were made of single-angle (90°) light scattering. Prior to use, this instrument was normalized using toluene and solvent samples in each batch cell. Drenski et al. have recently reported more details on this SMSLS [101].

5.4.2.4 Design of NIPAM/Am copolymer experiments

This section reports two sets of experiments. A series of free-radical copolymer reactions of NIPAM and Acrylamide, summarized in Table 5.2, established input parameters for the semi-batch controlled experiment, and confirmed previous work [15]. The major input parameter is α, the rate constant associated with the consumption

Table 5.2: The batch reactions used in the NIPAM/Am study. LCST is measured by offline SMSLS.

Reaction	$[Am_0]/[Np_0]$ (mol/mol)	$C_{Am,0}$ (mg/mL)	$C_{Np,0}$ (mg/mL)	$\alpha_{Am,0}$ $(10^{-4}/s)$	$\alpha_{Np,0}$ $(10^{-4}/s)$	$F_{ave,NP,final}$ (w/w)	$F_{ave,NP,final}$ (mol/mol)	LCST (°C)
A1	100:0	10.7	0	3.27	N/A	0.00	0.00	N/A
A2	70:30	7.46	5.09	2.51	2.86	0.41	0.30	N/A
A3	60:40	6.40	6.79	3.03	3.60	0.51	0.40	N/A
A4	50:50	5.33	8.49	2.49	2.83	0.61	0.50	N/A
A5	30:70	3.20	11.88	4.08	4.22	0.79	0.70	52.1
A6	0:100	0	17.3	N/A	6.10	1.00	1.00	33.5

of each monomer according to a first-order fit (Equation 5.1).

$$C_m = C_{m,0} e^{-\alpha t} \tag{5.1}$$

where C_m is the mass concentration (g/cm^3) of a given monomer at time t, and $C_{m,0}$ is the initial concentration of that monomer. The combined initial monomer concentration was kept at 150 mM for all reactions. All reactions were initiated at $T = 25\,°C$, with a silicon oil bath to hold the temperature constant. The reactor temperature of a reaction similar to Reaction 6 was continuously monitored with a thermocouple. The temperature in that reaction remained within 0.6 °C of the starting temperature, indicating that the oil bath was successful at maintaining an approximately constant temperature. The initiator (KPS) and the redox catalyst (TEMED) were both at a concentration of 1 mM.

The batch reactions were free-radical reactions, conducted in water. For ACOMP monitoring of the batch reactions, a water baseline was taken, followed by a baseline of the first monomer, followed by a baseline of both monomers. After the baselines, initiator and redox catalyst were added. The ACOMP detectors monitored the reaction as it proceeded. Sample raw data from Reaction A5 are shown in Figure 5.13. The origin of the time axis $t = 0\,s$ is defined to be the addition of initiator and redox catalyst. The final products of reactions A1 through A6 were kept

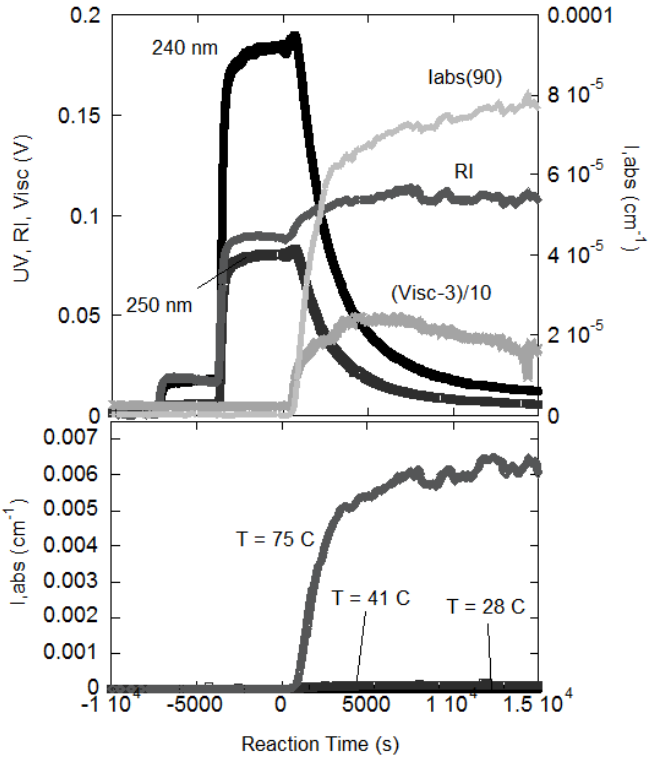

Figure 5.13: Typical raw ACOMP data (reaction A5). Top: differential refractometer, diode array (only 240 and 250 nm are shown), and viscometer raw voltages. Absolute Rayleigh scattering ratio I_{abs} is on the right hand scale. Viscosity has been scaled to fit on the graph, and referred to 0 V for solvent. All times are referenced to 0 s as the addition of initiator and redox catalyst. Bottom: I_{abs} for SGA flow cells.

for further analysis.

The final reaction was a semi-batch reaction. It began with only Am monomer present in the reactor, again at an initial concentration of 150 mM (10.7 mg/mL). When the initiator and redox catalyst were added, an HPLC pump (Knauer, Berlin) began to flow NIPAM at a rate of 0.1 mL/min from a reservoir of 1 M (113.16 mg/mL). The monomer solution feed drives the reaction towards increasing NIPAM content, almost to NIPAM homopolymer. Kreft reports [14] (Equation 12) that, for

a homopolymer, a flow rate Q_m of

$$Q_m = \frac{\alpha V_0 [m]_0}{[m'] - [m]_0} \tag{5.2}$$

will keep the total monomer concentration approximately constant, and thus will keep the molecular weight approximately constant. This is discussed further below. In equation 5.2, $V_0 = 100\,\text{mL}$ is the initial volume of the liquid in the reactor (kept constant by balancing the reservoir feed rate to the reactor with the ACOMP extraction rate), $[m]_0$ is the initial molar concentration of the monomer in the reactor, and $[m']$ is the molar concentration of the monomer in the reservoir used to feed the reactor. α is the rate constant of the batch reaction used in equation 5.1.

In this case NIPAM concentration was held approximately constant while Am constantly diminished, such that the ratio NIPAM/ Am increased continuously throughout the reaction, leading to copolymer chains ever richer in NIPAM and hence continuously lowering the LCST. The reaction time constants of the two monomers are similar across a broad range of compositions, so the homopolymer equation 5.2 was used as an approximation. For the present conditions of $[m'] = 1\,\text{M}$ and $[m] = 0.15\,\text{M}$, $\alpha = 6.1 \times 10^{-4}\,\text{s}^{-1}$ (from reaction 6 of Table 5.2) gives $Q_m = 0.65\,\text{mL/min}$. $Q_m = 0.1\,\text{mL/min}$ was chosen so that the reactor volume does not change during the reaction. Any deviations from equation 5.2 will act to increase or decrease the total monomer concentration until the rate of consumption from the reaction equals the rate of addition from the reservoir. In the present case, the total monomer concentration will decrease initially. Table 5.3 summarizes the semi-batch reaction parameters, and a few characteristics of the resulting polymer.

For the semi-batch reaction, the baselines were (in order): solvent, NIPAM monomer only, Am monomer only. The same detectors were used as in the batch reactions A1 through A6. Raw data in Figure 5.14 are discussed below; the origin

Table 5.3: The semi-batch reaction used in the Acrylamide study. This reaction was carried out in pure water.

Reaction	$C_{\mathrm{Am},0}$ (mg/mL)	$C_{\mathrm{Np},0}$ (mg/mL)	Q_{Np} (mL/min)	Q_{Np} (g/s)	final $F_{\mathrm{inst,Np}}$ (w/w)	final $F_{\mathrm{inst,Np}}$ (mol/mol)	M_w (g/mol)
A7	10.7	0	0.1	1.9×10^{-4}	1.00	1.00	379000

Table 5.4: Reaction time, polymer concentration, and instantaneous comonomer composition $F_{inst,Np}$ for samples taken from reaction A7. Time is taken relative to the addition of initiator and redox catalyst, as described in the main text. The concentration is that in the sample taken from the waste stream, accounting for the ACOMP dilution.

Sample ID	Reaction time (s)	C_p (mg/mL)	F,inst,Np (mol/mol)
As1	1164	0.0819	0.14
As2	2950	0.380	0.30
As3	3560	0.482	0.40
As4	4740	0.635	0.52
As5	5700	0.780	0.59
As6	6840	1.18	0.73
As7	8090	1.04	0.82
As8	9440	1.20	0.86
As9	11240	1.32	0.91
As10	12990	1.47	0.90
As11	15050	1.67	0.97
As12	16840	1.89	1.00

of the time axis is defined as the time when the initiator and redox catalyst were added. The NIPAM monomer feed began at this time. Several samples were taken from the waste stream of reaction A7 for further analysis, as summarized in Table 5.4. The polymer concentration C_p and the composition $F_{\mathrm{inst,NIPAM}}$ were computed as described in Section 5.4.3.2. The final product was kept for further analysis.

The product of reactions A2, A3, A4, A5, and A6 were diluted 1000-fold with NaCl stock solution to produce samples ranging from 0–5.3 M NaCl. Polymer concentration in these samples ranged from $C_p = 10.7\,\mathrm{mg/mL}$ (reaction A1) to $C_p = 17.2\,\mathrm{mg/mL}$ (reaction A6). These diluted samples were placed in the stand-alone SMSLS, and independently heated by a temperature ramp of 1 °C/min to 95 °C,

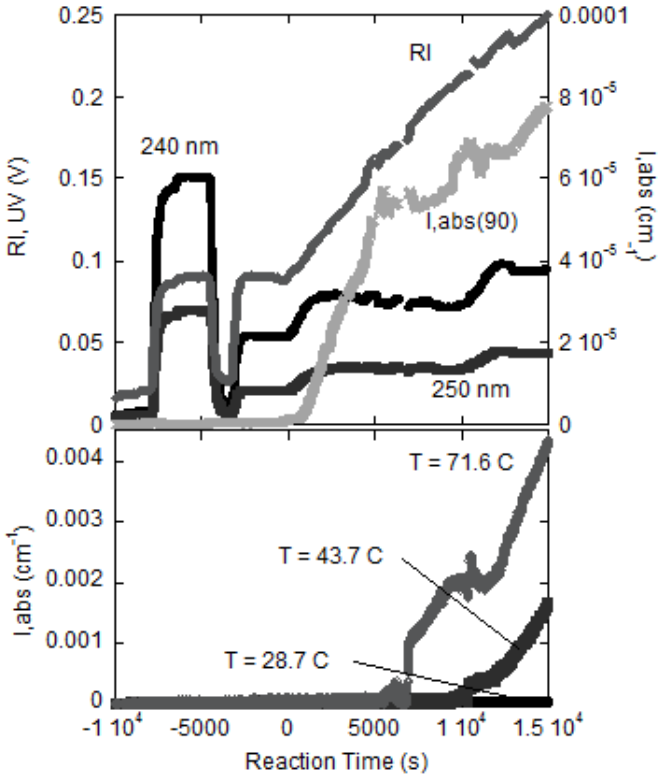

Figure 5.14: Raw ACOMP data for reaction A7. Top: first-generation ACOMP signals allow us to compute M_w, R_g, A_2, composition, and concentration of the resulting polymer. Bottom: second-generation ACOMP signals allow us to observe aggregation of polymers due to LCST.

Table 5.5: First generation ACOMP results (F_{ave}, M_w, R_g, η_r) from the batch reactions.

Reaction	$[Am_0]/[Np_0]$ (mol/mol)	$F_{\text{ave,Np,final}}$ (mol/mol)	M_w (g/mol)	R_g (nm)
A1	100:0	0.00	514000	39.6
A2	70:30	0.33	392000	37.9
A3	60:40	0.44	810000	57.7
A4	50:50	0.55	546000	56.4
A5	30:70	0.78	854000	65.9
A6	0:100	1.00	840000	41.9

while continuously monitoring the light scattering intensity at 90°. The samples from reaction A7 were already diluted 20-fold from reactor conditions to produce the concentrations listed in Table 5.4, and were diluted a further 100-fold with NaCl stock to produce samples ranging from 0–5.3 M NaCl. Polymer concentration in these samples ranged from $C_p = 0.82\,\text{mg/mL}$ (As1) to $C_p = 18.9\,\text{mg/mL}$ (As12). Each sample was heated at 1 °C/min from ambient temperature to 95 °C. One SMSLS cell has a cooling capability, allowing that sample to cool to 10 °C. For those samples with an LCST below room temperature, this cooling capability was used to measure the LCST.

5.4.3 Results and discussion

5.4.3.1 Batch reactions

Table 5.5 gives the first-generation results for the batch reactions given in Table 5.2 of Section 5.4.2.4.

5.4.3.2 Typical raw SGA data from NIPAM/Am batch copolymerization

Figure 5.13 shows an example of raw ACOMP data (from reaction A5, 70% NIPAM). The signals are typical of a batch free-radical reaction. During the solvent baseline, there is no signal in any of the detectors. The UV diode array and RI respond to the addition of the first monomer, and again to the addition of the second

monomer. The two UV wavelengths respond differently to the two monomers, due to their different absorption spectra. The full response from the UV detector allows calculation of comonomer concentrations based on swaths of wavelengths in the 190–400 nm interval. The RI also responds differently to the two monomers, due to the different values of dn/dc; $dn/dc = 0.151\,\mathrm{mL/g}$ for NIPAM, $dn/dc = 0.166\,\mathrm{mL/g}$ for pNIPAM, $dn/dc = 0.160\,\mathrm{mL/g}$ for Am, and $dn/dc = 0.177\,\mathrm{mL/g}$ for pAm (calculated from reactions A1 and A6, using the method of Brousseau [93]). 11 000 s after beginning the solvent portion of the experiment, the initiator and redox catalyst were added; this is taken as $t = 0$ on the x-axis. There is a small signal increase in the UV due to the initiator and catalyst, and then the reaction starts. The UV signals decrease as the monomers are consumed. The RI increases because the polymer has a higher dn/dc than the monomers. The LS signal increases and is concave down. This is because light scattering is proportional to polymer concentration and to M_w. Polymer concentration increases during the reaction, but at a monotonically decreasing rate, and M_w decreases monotonically.

The SMSLS signals are shown in the lower frame, on the same time scale. The two signals at lower temperatures show similar time dependence as the first generation LS signal, but this is not visible on the scale shown, which is nearly 100-fold larger than in the top figure. The higher temperature SMSLS signal shows the same qualitative behavior, but on a much higher scale because it is above the LCST of the resulting polymer. The SGA detector measures an LCST beginning at about 600 s after addition of initiator; after that, the SGA signal is very linear against the polymer concentration as measured by the first-generation detectors. The onset of LCST appears at a polymer concentration of 175 µg/mL in the detectors.

The comonomer conversions and compositions were computed from the UV-Vis data based on a previously reported error minimization technique [16]. UV wave-

lengths between 220 nm and 300 nm were used to minimize the quantity $\chi^2(t)$ at each instant in time.

$$\chi^2(t) = \sum_j \{S_{exp}(\lambda_j, t) - S_{calc}(\lambda_j, t)\}^2 \tag{5.3}$$

$S_{\text{exp}}(\lambda_j, t)$ is the measured UV signal voltage at wavelength λ_j at time t, and the summation is over all wavelengths used.

$$S_{\text{calc}}(\lambda_j, t) = L \left\{ \varepsilon_p(\lambda_j) C_p(t) + \sum_{i=1}^{N} \varepsilon(\lambda_j) C_i(t) \right\} \tag{5.4}$$

is the calculated absorbance value, based on a linear superposition over N absorbing monomers. $L = 0.01\,\text{cm}$ is the spectrometer path length. The ith monomer has an extinction coefficient at λ_j of $\varepsilon_i(\lambda_j)$, and a mass concentration (in g/cm^3) at t of $C_i(t)$. $\varepsilon_p(\lambda_j)$ is the extinction coefficient of the polymer and $C_p(t)$ is the concentration of polymer obtained by mass balance from

$$C_p(t) = \sum_{j=1}^{N} [C_{i,0}(t) - C_i(t)] \tag{5.5}$$

The extinction coefficients of the monomers are computed from monomer baselines before the reactions, and the polymer extinction coefficients are self-consistently computed from the UV data [16] . Extinction coefficients are the sum of contributions from electronic absorption and scattering.

For the work here $N = 2$, and the concentrations of Am and NIPAM at any time t, $C_{\text{Am}}(t)$ and $C_{\text{NIPAM}}(t)$, respectively, are found by the minimization procedure. The monomer concentrations resulting from this procedure are used to compute at any time t, the total polymer concentration $C_p(t)$ and the average fractional mass composition of Am and NIPAM in the copolymer, $y_{\text{Am}}(t)$ and $y_{\text{NIPAM}}(t)$, respectively.

For the NIPAM content in the homopolymer,

$$y_{\mathrm{NIPAM}}(t) = \frac{C_{\mathrm{NIPAM}}(0) - C_{\mathrm{NIPAM}}(t)}{C_p(t)} \tag{5.6}$$

The corresponding time dependent average fractional molar compositions of Am and NIPAM, $F_{\mathrm{ave,Am}}(t)$ and $F_{\mathrm{ave,NIPAM}}(t)$, respectively, can also be computed. For $F_{\mathrm{ave,NIPAM}}(t)$,

$$F_{\mathrm{ave,NIPAM}}(t) = \frac{[\mathrm{NIPAM}](0) - [\mathrm{NIPAM}](t)}{[\mathrm{NIPAM}](0) - [\mathrm{NIPAM}](t) + [\mathrm{Am}](0) - [\mathrm{Am}](t)} \tag{5.7}$$

where the molar masses of Am and NIPAM, 71.08 g/mol and 113.16 g/mol, respectively, are used to convert the mass concentrations to molar concentrations in the usual way.

The instantaneous molar compositions of Am and NIPAM, $F_{\mathrm{inst,Am}}(t)$ and $F_{\mathrm{inst,NIPAM}}(t)$, respectively, can be computed from the molar monomer concentrations at any time. For $F_{\mathrm{inst,NIPAM}}(t)$,

$$F_{\mathrm{inst,NIPAM}}(t) = \frac{d[\mathrm{NIPAM}](t)}{d\{[\mathrm{NIPAM}](t) + [\mathrm{Am}](t)\}} \tag{5.8}$$

Figure 5.15 shows $F_{\mathrm{inst,NIPAM}}(t)$ in the chains at all times during each of the batch copolymer reactions A2 through A5. This is computed from the UV-Vis data according to the above algorithm. This allows ACOMP to report the composition and composition drift of the reaction without need for post-polymerization characterization, such as by two-dimensional GPC, NMR, etc. The above method has been previously cross-checked against GPC results from periodic, manually withdrawn aliquots in similar free radical copolymer reactions [16]. The drift is measurable but not large, indicating that the reactivity ratios of Am and NIPAM are similar. This low drift

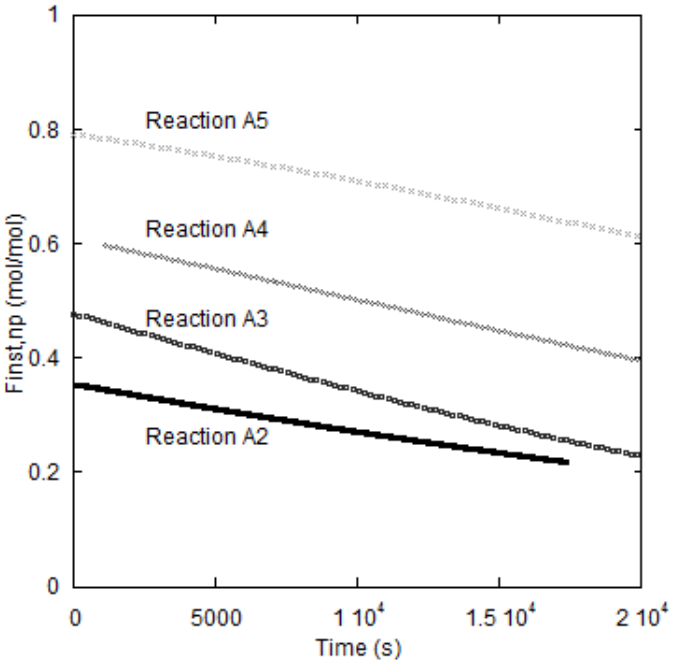

Figure 5.15: $F_{\text{inst,NIPAM}}$ measures average composition drift during each batch reaction.

makes the semi-batch approach in this work necessary if LCST behavior is to be monitored over a wide range of copolymer compositions.

Weight-average molar mass M_w , and z-average radius of gyration R_g , are calculated using the Zimm equation. A single dn/dc can be used because the dn/dc of the homopolymers are very similar to each other, and there is little drift in the reactions. As a result, dn/dc of the copolymers is computed as the weighted average of the dn/dc of the homopolymers. This gives an effective M_w , which is approximately equal to the true M_w under the conditions established by Enohnyaket [103]. The reduced viscosity η_r is determined from the combined viscometer and C_p data. The first-generation ACOMP results for M_w , R_g and η_r from the batch reactions are tabulated in Table 5.5.

5.4.3.3 ACOMP and SGA results of NIPAM/Am semi-batch reaction

Figure 5.14 shows raw ACOMP data from Reaction A7. AFter monomer baselines, the initiator and redox catalyst are added at $t = 0\,\mathrm{s}$, beginning the reaction. Also at $t = 0\,\mathrm{s}$, the NIPAM monomer flow into the reactor begins. The RI signal increases due both to the addition of NIPAM monomer, and to the conversion of both monomers into copolymer. The UV signals increase initially due to the addition of monomer. Since Am and NIPAM have the same absorption at this wavelength, the 250 nm signal indicates total monomer concentration. This signal reaches a plateau as the rate of consumption of monomer equals the rate of addition of NIPAM monomer; i.e. a steady state is reached. The signal at 240 nm slowly decreases because the Am monomer has a larger signal at this wavelength than the NIPAM monomer: the consumption of Am removes more of this signal than the addition of NIPAM adds. The flow of the NIPAM monomer was adjusted at about $t = 12\,500\,\mathrm{s}$, which leads to the UV signals repeating their initial increase. They then both reach a plateau because there is no Am monomer left in the system and NIPAM is at steady state. The ACOMP light scattering signal increases for the duration of the reaction; it begins the reaction concave down, as in the batch reactions, but becomes approximately linear after approximately $t = 6700\,\mathrm{s}$.

The three SGA signals indicate the evolution of LCST during the reaction. The $T = 29\,^{\circ}\mathrm{C}$ signal does not change, indicating that the LCST is above room temperature for the duration of the reaction. The two signals at elevated temperature begin to rise abruptly, and at different times. From these it is estimated that the LCST drops below 72 °C at $t = 5700\,\mathrm{s}$, and below 44 °C at $t = 9800\,\mathrm{s}$. As the reaction progresses to higher-NIPAM content chains, more chains participate in aggregation at each temperature.

Table 5.6 summarizes the aliquots taken from reaction A7, and gives the first-

Table 5.6: Characterization of samples taken from reaction A7.

Sample ID	Reaction Time (s)	C_p (mg/mL)	$F_{inst,Np}$ (mol/mol)	M_w (g/mol)	$2A_2C_pM_w$	R_g (nm)
As1	1164	0.081925	0.14	881000	0.08	71.2
As2	2950	0.37993	0.30	551000	0.24	62.2
As3	3560	0.48236	0.40	551000	0.30	59.3
As4	4740	0.63455	0.52	532000	0.38	54.4
As5	5700	0.78045	0.59	494000	0.40	55.5
As6	6840	1.1806	0.73	445000	0.60	53.4
As7	8090	1.0442	0.82	416000	0.50	51.7
As8	9440	1.1984	0.86	445000	0.61	50.0
As9	11240	1.3181	0.91	407000	0.61	45.0
As10	12990	1.4693	0.90	359000	0.70	44.0
As11	15050	1.6663	0.97	368000	0.70	41.9
As12	16840	1.8859	1.00	379000	0.81	41.0

generation ACOMP results for each of those samples. The molecular weight and radius of gyration decrease over the course of the reaction, as during a batch free-radical reaction, but they decrease more slowly than during batch reactions, and level off more quickly. This is discussed more fully in relation to Figure 5.16. Because the concentration of polymer in the detector train became quite large near the end of this reaction, it was necessary to correct the molecular weights for A_2 effects. This correction, using a value of $A_2 = 5.4 \times 10^{-4}\,\mathrm{cm^3\,mol/g^2}$ (only weakly dependent on mass) from poly(Acrylamide) [14], is reflected in Table 5.6. The term $2A_2C_pM_w$ is a dimensionless quatitiy; its size relative to 1 gives the effect of A_2 on the scattering. It runs from a 8% effect up to an 81% effect.

As mentioned in Section 5.4.2.4, reaction A7 is expected to produce a different molecular weight distribution than the batch reactions. Figure 5.16 shows this effect: M_w decreases very rapidly at early conversion, then levels off and remains relatively constant for most of the reaction. This is due to reaching an 'iso-reactive steady state', in which the rate of adding monomer is balanced by the rate at which it is consumed [97]. Since kinetic chain length ν is proportional to the ratio of monomer

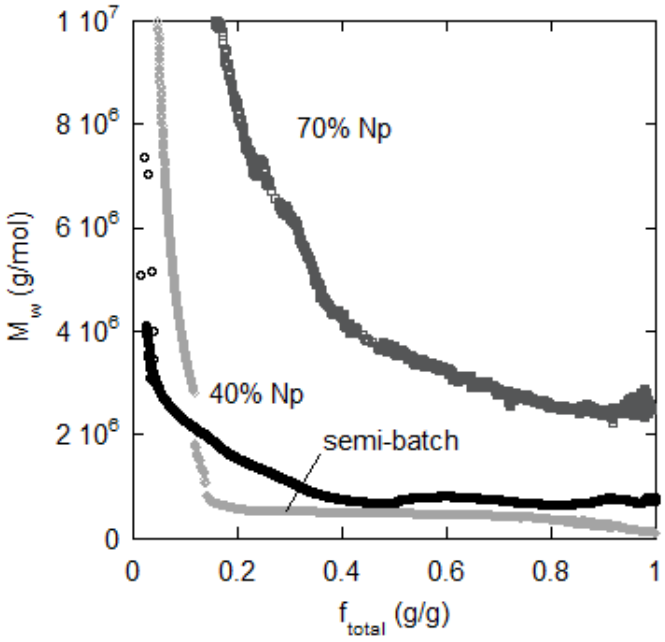

Figure 5.16: Molecular weight as a function of conversion for the semi-batch reaction and two batch reactions. M_w continues to decrease over the entire course of the reaction for the two batch reactions. For the semi-batch reaction, M_w essentially plateaus after an initial decrease.

to initiator concentrations, and the initiator concentration changes very slowly, ν will remain constant once the steady state of constant monomer concentration is reached. In contrast, the M_w trend from reactions 3 and 5 are shown as representatives of the batch series. These show the typical batch free radical behavior of decreasing M_w throughout the entire reaction. This is because the monomer concentration decreases steadily throughout the batch reactions, so that ν also decreases, and hence also M_w.

Figure 5.17 shows the resulting computed monomer concentrations and polymer composition over the course of the reaction. Comparison of the composition data with the SGA detector data allows correlation of LCST aggregation with the composition of the chains being synthesized at that time. Using the times estimated from Figure 5.14 an LCST of 72 °C at 65% NIPAM, and an LCST of 44 °C is measured at 94% NIPAM (mol/mol). These estimates are close to, but a few percent lower than,

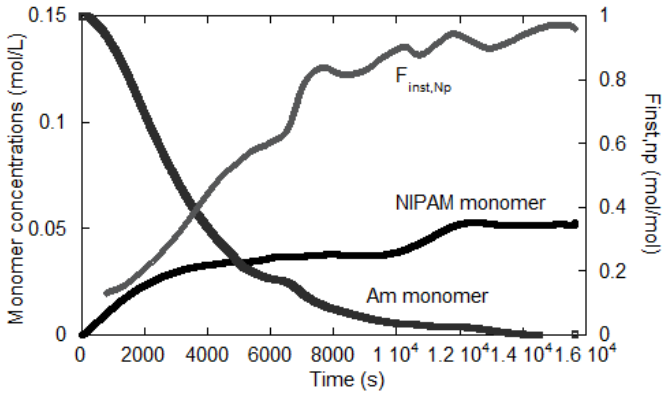

Figure 5.17: Conversions and composition of reaction A7. The monomer concentrations are computed from the UV data as explained in the main text, above. The instantaneous composition $F_{\mathrm{inst,Np}}$ is computed from the monomer compositions and mass balance.

the NIPAM content for a given LCST in previous reports [15, 94, 95]. The undulations in the trace of $F_{\mathrm{inst,Np}}$ between 6000 and 12 000 s are due to the intrinsic noise in the underlying UV data; despite smoothing, that noise is amplified by numeric differentiation of the monomer concentrations.

5.4.3.4 SMSLS measurements of LCST

The LCST behavior of NIPAM tolerates much more Am than previously found for NIPAM with styrene sulfonate [87]. The higher the Am content the higher the LCST of the resulting samples, at fixed [NaCl]. Increasing [NaCl] lowered the LCST of any given copolymer.

Figure 5.18 compares the SMSLS data for the pNIPAM homopolymer (reaction A6, Table 5.2), one batch copolymer (reaction A5, Table 5.2), and the semi-batch final product (Reaction A7, Table 5.3). These data are shown for a single heating/cooling cycle at a rate of 1 °C/min. The pNIPAM shows an abrupt increase in I_{abs} at the LCST. The copolymer from reaction A5, in contrast, shows a much broader LCST transition, reflecting some composition drift in the reaction, as was shown in Figure 5.15. Because LCST is a strong function of Am content, a broad transition results.

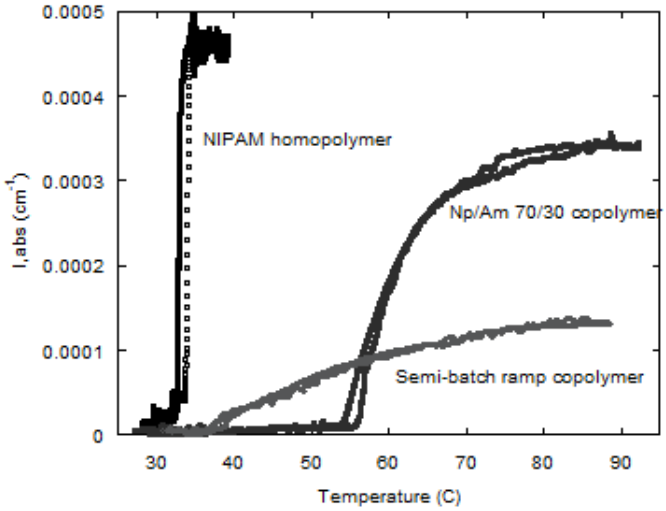

Figure 5.18: A comparison of the widths of the LCST transitions of the NIPAM homopolymer (reaction A6, $c_p = 17.26\mu$g/mL), a batch copolymer (reaction A5, $c_p = 12.56\mu$g/mL), and the semi-batch gradient copolymer (reaction A7, $c_p = 36.08\mu$g/mL). The width of the LCST transition increases with increasing composition drift.

The LCST begins at 52 °C and the LS signal continues to increase up to 95 °C. The chains in that sample are estimated to range in NIPAM content from $F_{\mathrm{inst,Np}} = 0.78$ to 0.55; previous reports of the LCST of NIPAM-Am copolymers estimate copolymers of those compositions to have exactly that range of LCST's [15, 94, 104].

The composition of the semi-batch sample in figure 5.18 ranges from Am homopolymer almost to NIPAM homopolymer, and contains copolymers of every composition in between, leading to the broadest transition of all three. The resulting sample has chains with an LCST at every temperature from near 32 °C to at least 95 °C. This can be seen as the continuous increase in light scattering with temperature for that sample. All three samples show very little difference in light scattering between the heating portion of the experiment and the cooling portion. The very small hysteresis is due to the finite heating and cooling rate, and has been reported before [66]. This very low hysteresis also indicates that the aggregation is fully reversible upon cooling, in the short term. The issue of long-term reversibility is discussed

in more detail in Section 5.4.3.5 In short, it was found that only the homopolymer in salt-free solution had long term stability (for the 5 days measured), whereas all the copolymers in salt-free solution precipitated on a time scale of tens of hours, as did the homopolymer in 0.5 M NaCl aqueous solution. Figure 5.18 also illustrates how to estimate the LCST from the light scattering data. At temperatures below the lowest LCST in the sample, light scattering is independent of temperature. When the chains in the sample begin to aggregate, the light scattering increases. This increase in aggregation is approximately proportional to the average aggregation number. For the purposes of this work, an average aggregation number of 2 is used as an estimate of the LCST. Therefore, the LCST is estimated to be that temperature at which the solvent subtracted I_{abs} is twice the value of its room temperature value.

To confirm the repeatability of the SMSLS instrument, 8 identical samples of reaction 6 end product were placed in pure water at $C_p = 65\,\mathrm{mg/mL}$. These samples were simultaneously heated to 40 °C at a rate of 1 °C/min, and allowed to cool. Toluene and water baselines allowed comparison of absolute Rayleigh scattering ratio for all 8 samples. The LCST was repeatable from one sample to the next to within 0.4 °C.

The LCST curves in Figure 5.18 suggest it may be possible to extract information on the composition distribution of the copolymer end products using the shape of I_{abs} vs T. Since $F_{\mathrm{inst,NIPAM}}$ is the fractional composition of NIPAM in the chains being produced at any instant during the reaction for the end product, the average composition distribution can be characterized by $f(F_{\mathrm{inst,NIPAM}})$ where $f(F_{\mathrm{inst,NIPAM}})dF_{inst,NIPAM}$ is the fractional concentration of copolymer chains in the end product with composition $F_{\mathrm{inst,Np}}$ in the interval from $F_{\mathrm{inst,NIPAM}}$ to $F_{\mathrm{inst,NIPAM}} +$

$dF_{\text{inst,NIPAM}}$. The normalization condition is then

$$\int_0^1 f(F'_{inst,NIPAM})dF'_{inst,NIPAM} = 1 \tag{5.9}$$

Consider the usual Zimm approximation for homopolymers [25]

$$\frac{KC_p}{I_{abs}} = \frac{1}{M_w}\left(1 + \frac{q^2\langle S^2\rangle_z}{3}\right) + 2A_2C_p \tag{5.10}$$

where K is an optical constant, given for vertically polarized incident light by

$$K = \frac{4\pi^2 n^2 (dn/dc)^2}{N_A\lambda^4} \tag{5.11}$$

where n is the pure solvent index of refraction and λ the vacuum wavelength of the incident laser beam. $\langle S^2\rangle_z$ is the z-average mean square radius of gyration of the polymer, A_2 the second virial coefficient and q the amplitude of the scattering vector given by $q = (4\pi n/\lambda)\sin(\theta/2)$, where q is the scattering angle in the scattering plane. The homopolymer approximation for Am/NIPAM has been discussed above.

The intense scattering in both the ACOMP and SMSLS experiments is due to aggregates of the copolymers when the LCST is reached. These are much more massive than the individual chains. This leads to a small A_2 for the aggregates. In addition, the concentrations of copolymer in the SMSLS experiments were very low (10–20 mg/mL). $2A_2C_pM_w \ll 1$, so the A_2 term in equation 5.10 can be ignored, and the experimental SMSLS data for I_{abs} can be expressed as

$$I_{abs} = C_p\int_0^1 K(F'_{inst,NIPAM})M_{w,0}(F'_{inst,NIPAM})f(F'_{inst,NIPAM})dF'_{inst,NIPAM} \tag{5.12}$$

where $M_{w,0}(F_{\text{inst,NIPAM}})$ is the initial mass of an aggregate composed of chains of a given composition $F_{\text{inst,NIPAM}}$.

Some approximations can be made to simplify the integral. First, by the approximation of nearly constant K for all compositions $K(F_{\text{inst,NIPAM}})$ can be removed from the integral. What is left in the integral is the product of relative concentration and mass over each differential element $F_{\text{inst,NIPAM}}$.

The aggregates form immediately in response to reaching the LCST and are quasi-stable, as mentioned above and shown in Section 5.4.3.5, so there is evidence that the aggregate mass $M_{w,0}$ is well defined for a given copolymer under given conditions of concentration and solution ionic strength and ion type [5]. Hence, the next approximation is that $M_{w,0}(F_{\text{inst,NIPAM}})$ is roughly the same for all $F_{\text{inst,NIPAM}}$. Note that this approximation may not be valid; as seen in Table 5.5 the chains with more NIPAM in them have larger molecular weights; this is in part due to the higher molecular weight of the NIPAM monomer. Higher-NIPAM content chains may produce higher M_w aggregates.

With these approximations the integral can first be re-written for a copolymer starting with the minimum value of $F_{\text{inst,NIPAM}}$ in its population that undergoes an LCST, denoted $F^*_{\text{inst,NIPAM,0}}$. Portions of the copolymer population whose NIPAM composition $F_{\text{inst,NIPAM}}$ is such that $F_{\text{inst,NIPAM}} < F^*_{\text{inst,NIPAM,0}}$ will not produce aggregates at any T and hence not contribute to the integral. This also means that this method of determining $F(f)$ will be blind towards the part of the copolymer population for which $F_{\text{inst,NIPAM}} < F^*_{\text{inst,NIPAM,0}}$. Since I_{abs} is also a function of [NaCl] that is now included. With this the integral up to any arbitrary $F_{\text{inst,NIPAM}} > F^*_{\text{inst,NIPAM,0}}$ becomes

$$
\begin{aligned}
&I_{abs}(F'_{\text{inst,NIPAM}}, [\text{NaCl}]) \\
&\quad = C_p K M_{w,0}([\text{NaCl}]) \int_{F^*_{\text{inst,NIPAM,0}}([\text{NaCl}])}^{F_{\text{inst,NIPAM}}} f(F'_{\text{inst,NIPAM}}) dF'_{\text{inst,NIPAM}} \qquad (5.13) \\
&\quad F_{\text{inst,NIPAM}} > F^*_{\text{inst,NIPAM,0}}([\text{NaCl}])
\end{aligned}
$$

To avoid cumbersome subscripts in the following, the notation is simplified to

$$F \stackrel{\text{def}}{=} F_{\text{inst,NIPAM}} \tag{5.14a}$$

$$F^* \stackrel{\text{def}}{=} F^*_{\text{inst,NIPAM,0}} \tag{5.14b}$$

$$L \stackrel{\text{def}}{=} \text{LCST} \tag{5.14c}$$

$$S \stackrel{\text{def}}{=} [\text{NaCl}] \tag{5.14d}$$

Equation 5.13 is re-written

$$I_{\text{abs}}(F,S) = C_p K M_{w,0}(S) \int_{F^*(S)}^{F} f(F')dF', F > F^*(S) \tag{5.15}$$

Now, the ordering of the integral from the SMSLS experiments is over T, not directly over F. For each composition F there is, however, an LCST (at fixed S) which decreases monotonically as F increases. Hence, there exists a monotonically decreasing function LCST(F). The ordering of I_{abs} vs F is therefore opposite the ordering in T.

The derivative of the experimental data can be expressed as

$$\left.\frac{\partial I_{\text{abs}}}{\partial T}\right|_S = \left(\frac{\partial I_{abs}}{\partial F}\frac{\partial F}{\partial T}\right)_S \tag{5.16}$$

The sought for composition distribution $f(F)$ is then related to the first partial derivative using equation 5.15 by

$$\left.\frac{\partial I_{\text{abs}}}{\partial F}\right|_S = -C_p K M_{w,0}(S) f(F) \tag{5.17}$$

where the negative sign accounts for the opposite ordering of I_{abs} in T and F.

An expression for the other partial derivative in equation 5.16, $(\partial F/\partial T)_S$, is

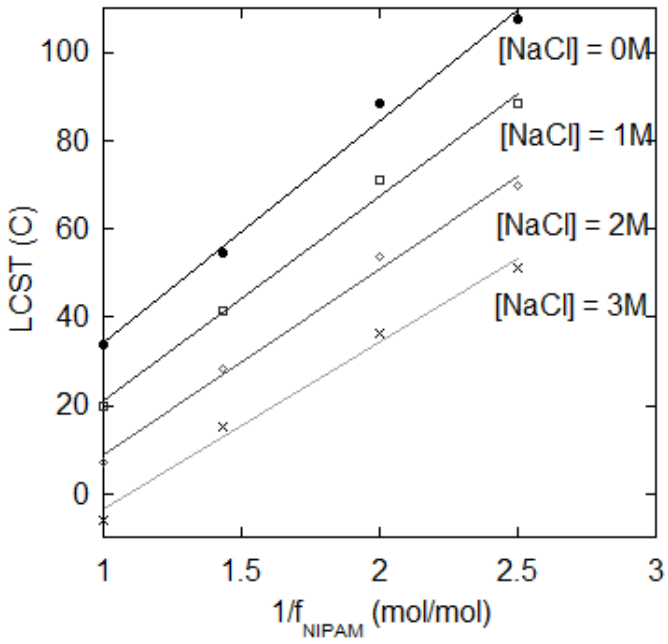

Figure 5.19: LCST as a function of $1/F$ for each [NaCl]. The lines shown are linear fits to LCST as a function of $1/F$ at constant S (= [NaCl]).

then required to complete the determination $f(F)$. The reciprocal of $(\partial F/\partial T)_S$, substituting L (LCST) for T represents the change in LCST per unit change of copolymer composition F. This can be obtained from experimental data in figure 5.19, which gives the SMSLS determination of LCST for different values of F and S.

The SMSLS data from the batch reaction end products fit well to a surface of the form

$$L(F,S) = -15.7 + \frac{50.2}{F} + (10.8F - 21.5)S \tag{5.18}$$

where, because of the low drift, F is taken as the initial mole fraction of NIPAM. The fits are shown together with the data points in figure 5.19. In addition to the data shown in figure 5.19, data from Table 4 reporting the slope of the NaCl effect on LCST were used in arriving at equation 5.18. The $50.2/F$ term dominates the $10.8FS$ term in equation 5.18, so that the surface is essentially hyperbolic in F.

Using equation 5.18 to obtain $(\partial F/\partial T)_S$, in conjunction with equations 5.16

and 5.17 yields the composition distribution of the copolymer end products:

$$f(F) = \frac{-1}{C_p K M_{w,0}(S)} \left(\frac{\partial I_{abs}}{\partial T}\right)_S \left(10.8S - \frac{50.2}{F^2}\right) \tag{5.19}$$

$f(F)$ is computed from equation 5.19 from the experimental derivative $(\partial I_{\text{abs}}/\partial T)_S$ vs T from the SMSLS temperature ramp, and equation 5.18 is used to determine the value of F which has L equal to T at each point that $(\partial I_{\text{abs}}/\partial T)_S$ is computed at. It is noted that the $1/F^2$ term in the right parenthesis is greater than the $10.8S$ term for all physically meaningful values of F and S, so that $f(F)$ is always positive. Because $f(F)$ by this method is 'blind' to $F < F^*$ and since F^* decreases with increasing S, the fullest determinations of $f(F)$ can be made at the highest values of S. In fact, this could be used as a fractionation method.

It is seen in Figure 5.19 that reliable LCST data are obtained for $F \geq 0.4$. For $F < 0.4$ high S is needed to find L below 100 °C. Hence equations 5.18 and 5.19 are meant to apply for $0.4 \geq F \leq 1$.

Equation 5.18 also allows the equivalency between changing S and F by certain amounts to be ascertained. Setting the total differential $dL = 0$ yields the total increment of dS added to the solution that would offset an increase dF, at any given F, in order to keep the LCST constant:

$$dS = dF \left(0.50S - \frac{2.33}{F^2}\right) \tag{5.20}$$

The $1/F^2$ term dominates this, so that if dF is positive then dS will be negative: salt must be decreased if the copolymer is enriched in NIPAM. This also establishes the equivalency relationship between changing S and F by taking the absolute value on the right hand side. Augmenting dF at constant S is equivalent to augmenting dS at constant F.

Figure 5.20 compares the composition distribution for reaction A5 as computed by the stand-alone SMSLS data on the end product, and as computed directly from the during-synthesis ACOMP data, using the method of Giz et al [105]. These methods are completely different, since the former makes no reference to the LCST phenomenon and computes the distribution directly from the ACOMP UV signals during the reaction, whereas the latter method uses the LCST-dependent method outlined above on the end product. In both methods, there is no salt present in the solution. These two very different methods approximately agree on the peak composition in the sample, but the ACOMP data gives a much narrower distribution than the SMSLS data. One source of the difference in width is that the ACOMP data report average behavior in the sample, while the SMSLS data are, according to this method, sensitive to the full distribution of compositions created at any time in the reaction, except those too rich in Am to have an LCST. Convolution of average comonomer composition data with Stockmayer distributions [106] was carried out previously on ACOMP data from copolymerization reactions, which broadened the ACOMP-derived distribution [105]. This suggests that the two methods are complementary: ACOMP can provide the system-wide average behavior at all times, including the critical instant during the synthesis when stimuli behavior occurs, but without information on the width of the distribution, while SMSLS can provide a more full composition distribution for discrete during-synthesis aliquots and end products.

The bottom of Figure 5.20 shows the composition distributions by ACOMP and stand-alone SMSLS for the semi-batch reaction (reaction A7). The SMSLS distribution cuts off at the lower NIPAM composition for which there is no longer an LCST under monitored conditions. Since the ACOMP method does not rely on the LCST it reports the distribution down to much lower values of NIPAM. While the distributions from the two methods are quite different, they both report a broad

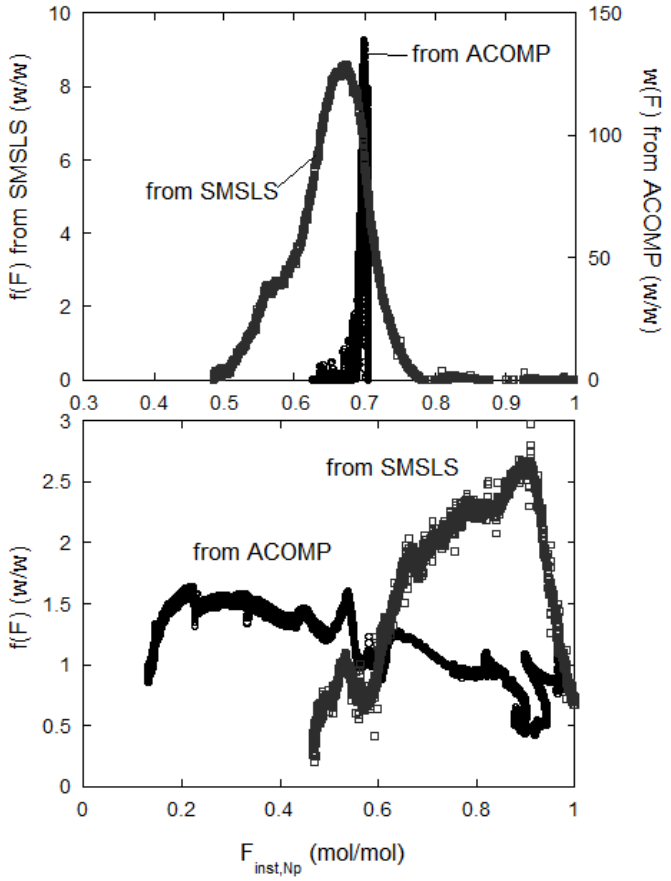

Figure 5.20: Top: Composition distribution for 70% NIPAM batch copolymer (Reaction A5) by ACOMP and stand-alone SMSLS methods. The two distributions are on separate scales, which ensure the normalization condition, Equation 5.9. Bottom: Composition distribution for semi-batch gradient copolymer (Reaction (A7) by ACOMP and stand-alone SMSLS.

composition distribution. Figure 5.20, top and bottom, hence represent first steps in using ACOMP and, separately, stand-alone SMSLS for composition distribution determination. Further work will require chromatographic separation, most likely a two-dimensional gel permeation chromatography approach.

The LCST's measured for the copolymers in pure water (Table 5.7) are consistent with previous reports [3, 4, 15, 107]. The magnitude of the salt effect for the homopolymer is consistent with measurements by Zhang et al [5]. The salt effect for the copolymers has not been measured before; in reaction A5 it is approximately the same magnitude as in the homopolymer, while it increases by about 4–5 °C/M in reactions A2 through A4, as shown in Table 5.7. This appears to be the result of a continuous process whereby increasing Am content slowly crowds out the LCST behavior. At some point between 30% Np and the Am homopolymer, the LCST behavior should completely disappear. Aliquots from reaction A7 help narrow the range of Am content that allows LCST behavior. Figure 5.21 plots the measured values of the LCST against the predictions made by Equation 5.18: the solid lines in Figure 5.21 are not fits, they are the results of using Figure 5.19 data and Table 5.7 data. This shows quite good agreement between the experimental values and the model for NIPAM content above 50%. As seen, the model begins to over-estimate the LCST around 40% NIPAM.

Figure 5.21 also shows the uncertainties in the LCST measurements as error bars. This uncertainty increases as the Am content of the chains increases. This is because the LCST becomes more gradual, and the exact onset of the transition is more difficult to measure. Note that the error bars for Reaction A6 are too small to be seen in the figure. I define the LCST itself as the point when the absolute light scattering is double the light scattering of the unaggregated polymer at room temperature. There is some ranodm variation in the light scattering signal below the

Table 5.7: The SGA results (LCST and ΔLCST/Δ[NaCl]) of the batch reactions in the NIPAM/Am study, measured on reaction end products by stand-alone SMSLS.

Reaction	$[Am_0]/[Np_0]$ (mol/mol)	$F_{inst,Np,max}$ (mol/mol)	Observed LCST in pure water (°C)	LCST in pure water from fitting (°C/M)	ΔLCST/Δ[NaCl] from fitting (°C/M)
A1	100:0	0.00	Soluble	N/A	N/A
A2	70:30	0.70	Soluble	113.8 ± 4.9	-17.8 ± 1.5
A3	60:40	0.30	Soluble	107.5 ± 2.3	-18.8 ± 0.75
A4	50:50	0.40	Soluble	85.8 ± 0.6	-15.6 ± 0.22
A5	30:70	0.50	52.1	54.2 ± 0.6	-12.6 ± 0.30
A6	0:100	1.00	33.5	33.7 ± 0.04	-11.4 ± 0.08

LCST. At some temperature, the light scattering is more than one standard deviation above the room temperature light scattering baseline. I take the uncertainty in the LCST to be the difference in temperature between this point and the temperature at which the light scattering is twice the room temperature baseline.

As mentioned before, Bergbreiter has previously reported a linear decrease in LCST of pNIPAM homopolymer with added salt; specifically, they estimated this effect to be $-10\,°C/M$ for NaCl [5]. The estimate for this parameter in this work, from the derivative of Equation 5.18 with respect to S at $F = 1$ is $-10.7\,°C$, in good agreement.

5.4.3.5 Reversibility of the aggregates formed above the LCST

Despite the short-term reversibility discussed in the main text, a separate issue is the stability of the aggregates over time. Figure 5.22 illustrates this. Four samples were held above their LCST for 4.6 days in the stand-alone SMSLS. The NIPAM homopolymer with no added NaCl formed aggregates that were stable for this entire period, and were completely re-solubilized upon cooling back to room temperature. When 0.5 M NaCl was added to the homopolymer, very highly scattering aggregates formed initially upon heating above the LCST. This was followed by a continued period of aggregation, during which light scattering fell as aggregates precipitated out of solution. The light scattering signal ultimately fell below that of the below-

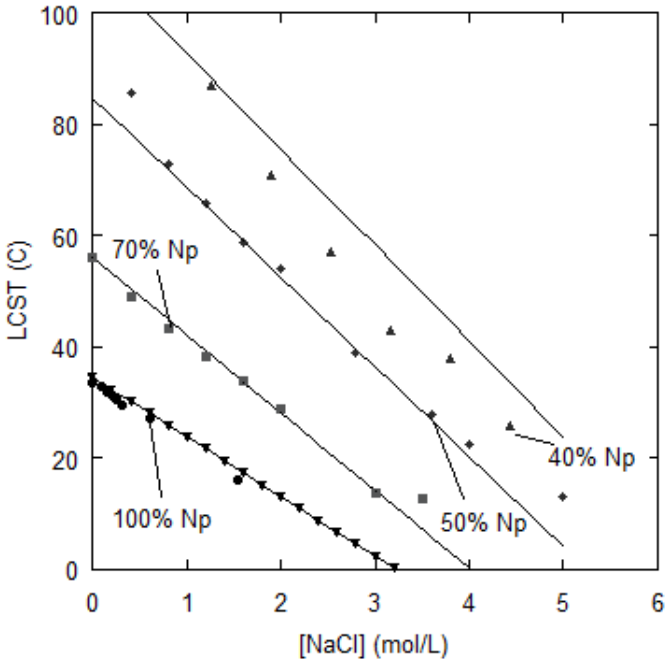

Figure 5.21: LCST of the end product of Reactions A2 through A6 vs [NaCl] (symbols), with predictions made by the model of equation 5.18 (lines). Polymer concentrations range from $C_p = 17.65\,\mu g/mL$ (Reaction A6) to $C_p = 12.56\,\mu g/mL$ (Reaction A2).
The error bars are the uncertainties as described in the main text. Note that the uncertainties in the Reaction A6 points are too small to be seen in this figure.

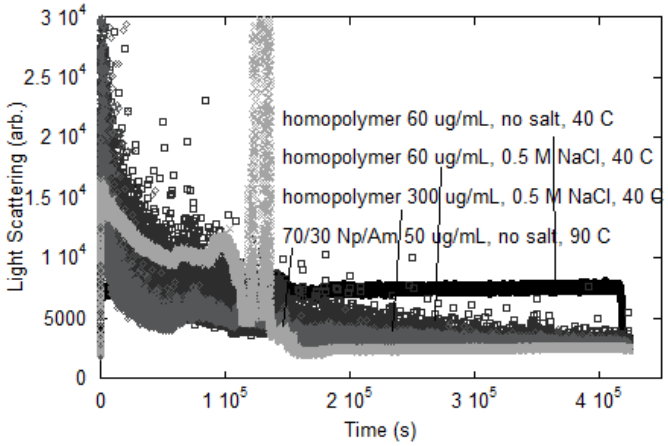

Figure 5.22: The homopolymer with no added salt is stable above the LCST for 4.6 days and the transition is reversible. Adding 0.5 M NaCl caused the homopolymer to fall irreversibly out of solution. The copolymer remained aggregated in solution for about a day, and then rapidly fell out of solution.

LCST signal of the unaggregated polymer chains. The aggregates did not return to solution upon cooling; this transition appears to be irreversible. The 70/30 copolymer with no added salt remained aggregated in solution for a little over a day, and then underwent a rapid, high scattering transition before precipitating completely out of solution. This transition also appears to be irreversible. The irreversibly of these three samples appears to occur only if the samples are held above their LCST for longer than a day. All other heating-cooling cycles reported in this work are on a scale of a few hours or less, so the aggregation phenomena are reversible.

5.4.4 Conclusions

This section demonstrates how ACOMP can be coupled to multiple light scattering flow detectors in series, at different temperatures, to monitor LCST during copolymerization of NIPAM and Am. The use of semi-batch feed adds the powerful capability of sweeping the entire span of compositions from one comonomer to the other in a single experiment, thus passing through a series of LCST's, monitored by the LS flow cells in series. Addition of more scattering detectors will allow finer de-

termination of LCST as a function of composition, or, conversely, in the case where LCST as a function of composition is known from previous experiments, copolymer composition drift and distribution could be followed during the reaction.

As a complementary method, the use of stand-alone batch cell SMSLS with controlled temperature ramps allowed detailed LCST behavior of aliquots and end products to be measured. This leads to an equation LCST = LCST($F_{\mathrm{inst,Am}}$, [NaCl]), which yields an approximate method for determining copolymer composition from the shape and breadth of light scattering intensity vs T. Agreement of compositions using the ACOMP and SMSLS/LCST methods is only qualitative at this point. The function LCST = LCST($F_{\mathrm{inst,Am}}$, [NaCl]) further allows the equivalency between copolymer composition and [NaCl] to be determined; i.e. how much the NIPAM composition must decrease in order to counteract a unit increase in [NaCl] and hold the LCST constant.

In general, the second generation ACOMP effort is aimed at building a versatile platform for monitoring the onset and evolution of stimuli-responsive behavior of polymers during their synthesis. Precise knowledge of the conditions fostering specific behavior can lead both to a better understanding of the physicochemical origins of the behavior and to optimizing reaction processes for creating useful new polymeric materials. This work is a small and early step in that direction.

5.5 Anionic comonomer: Styrene sulfonate

The results of this section were published as Reference [87].

5.5.1 Introduction

Stimuli-responsive polymers are polymers that undergo conformational changes when subjected to a change in their environment. The most well-studied stimuli are temperature (T) [108–113] and pH [37, 43, 114, 115], but polymers have also been syn-

thesized that are sensitive to sugar [48, 116] and other specific agents, electric and magnetic fields [42, 117–119], light and other radiation [39], ionic strength [5, 53, 96], and cononsolvents [30, 112].

Temperature-sensitive polymers display lower critical solution temperature (LCST) behavior in some solvents, in which heating the system causes the solvent to become a poor solvent for the polymer. This leads to a sudden decrease in solubility, usually caused by a conformational change, such as coil-to-globule, and subsequent aggregation. The most well-studied such system is poly(N-isopropyl acrylamide) (pNIPAM) in water [36, 120, 121], but LCST systems involving poly(ethylene oxide) [122], 2-(2-methoxyethoxy)ethyl methacrylate, and oligo(ethylene glycol) methacrylate also exist [123].

The current model for the coil-to-globule transition is given by Wu [56,92]. The coil first shrinks to a crumpled coil, then collapses on itself to form a molten globule, then collapses further to become a globule. At the transition temperature, each chain forms intrachain hydrogen bonds and the radius of gyration drops suddenly. At higher concentrations, interchain hydrogen bonds form, causing aggregation and leading to a higher weight average molecular weight M_w. Eventually, the chain size reaches a plateau, and does not appreciably shrink any further with heating. Differential scanning calorimetry (DSC) verifies the existence of hydrogen bonding, as well as hysteresis under some conditions [64, 65]. This description is similar to the model used to describe the denaturation and aggregation of proteins, with the important distinction that the coil-to-globule transition in pNIPAM is reversible, whereas protein aggregation is usually irreversible [124].

Besides light scattering (LS) and DSC, Schild's 1992 review of early NIPAM work reported cloud point/turbidimetry, viscometry, and fluorescence as the five major traditional techniques [2]. All of these can require long equilibration times and

large sample volumes. Recent high-throughput methods attempt to alleviate these problems. The usual technique is to measure turbidity. Bergbreiter et al.'s multi-sample temperature gradient method for measuring cloud points has the advantages of being high-throughput, having good temperature resolution, and requiring very little sample [5, 53, 96]. Jana et al. have expanded Bergbreiter's idea, allowing them to study at least two variables at the same time, and with more samples in a single study [69]. While providing high throughput, these techniques cannot detect hysteresis, do not provide any information about the internal structure of the polymer, and are unable to study samples that are changing with time. These high-throughput methods are a significant improvement over traditional methods, as they allow rapid characterization of one or several thermosensitive samples. Despite this advantage, these methods are still post-reaction techniques; they only characterize the polymer after the polymerization reaction, or in discrete reaction aliquots.

The present section has as its first objective the development of an early prototype instrument that allows the onset of LCST to be monitored during polymer synthesis. The second objective is to use this new capability to assess how adding both charge and hydrophilicity to pNIPAM via copolymerization affects the LCST.

The early prototype instrument consists of several custom-built single-angle light scattering flow cells, each with independent temperature control. Sample can flow through the cells either in parallel or in series. When flowed in series, this detector can be connected to the output fluid stream of the ACOMP (Automatic Continuous Online Monitoring of Polymerization reactions) system previously developed in this group [86]. ACOMP is an online method that allows, during synthesis, direct measurement of fundamental reaction characteristics such as kinetics, comonomer conversion and composition drift, M_w, and intrinsic viscosity $[\eta]$. In this new configuration, termed Second-Generation ACOMP (SGA), the new detector can measure

the onset of LCST phenomenon during the reaction, and thus connect the LCST behavior to properties of the polymer, such as instantaneous copolymer composition. When flowed in parallel, this detector allows for the high-throughput determination of LCST for several samples under different conditions, such as ionic strength.

The primary use of the new instrument coupled to ACOMP in this work was to study LCST behavior of a system during copolymerization reactions involving NIPAM and the charged monomer styrene sulfonate (SS). It is surmised that a copolymeric polyelectrolyte will suppress the LCST of pNIPAM to some degree due to the enhanced intra- and interchain repulsive electrostatic interactions and hydrophilicity conferred on the polymer chain by the anionic SS. Previous work in this group found that SS and Acrylamide produce a very high-drift reaction, due to the large difference in the reactivity ratios, $r_{\mathrm{SS}} = 2.14$ and $r_{\mathrm{Am}} = 0.18$ [13]. Because NIPAM and Am have the same polymerizing (vinyl) group, and because the identity of the polymerizing group is usually the dominant influence in the reactivity ratios [16], the SS/NIPAM system is expected to display the same high composition drift behavior seen in the SS/Am system. This allows ACOMP and SGA to monitor the onset of the LCST behavior across a wide range of instantaneous copolymer compositions during a single copolymerization reaction. When the copolymerization reaction is carried out in 10 mM NaCl aqueous solution, this onset appears to occur consistently when the instantaneous molar fractional composition of SS, $F_{\mathrm{inst,SS}}$, is around 4%, independent of starting ratios of the two monomers. Above 4% SS content, a much higher ionic strength solvent was required to recover LCST behavior. This suggests that the presence of SS in the polymer chains interferes with the LCST collapse via electrostatic interactions.

Table 5.8: Summary of reaction conditions, and ACOMP results. Subscripts SS, NP, Am refer to styrene sulfonate, NIPAM, and Acrylamide, respectively.

Reaction	$SS_0\%$ (M)	$C_{SS,0}$ (mg/mL)	$C_{Np,0}$ (mg/mL)	$C_{Am,0}$ (mg/mL)	$\Delta F_{inst,SS}$	M_w (g/mol)	η_r (cm^3/g)	$F_{inst,SS}$ LCST onset (%)	f_{total} LCST onset (%)
S1	0	0	17.0	0	N/A	N/A	N/A	N/A	3
S2	10	3.09	15.3	0	-0.34	6.3×10^5	132	4	70
S3	20	6.19	13.6	0	-0.49	1.8×10^5	139	5	65
S4	25	7.73	12.7	0	-0.48	1.6×10^5	198	3	76
S5	30	9.28	11.9	0	-0.18	9.6×10^4	287	< 17	None Observed
S6	50	15.5	8.49	0	+0.17	6.2×10^4	135	< 40	None Observed
S7	100	30.9	0	0	N/A	6.6×10^4	153	N/A	None Observed
S8	0	0	13.6	0	2.13	N/A	N/A	N/A	9

5.5.2 Materials and Methods

NIPAM and Acrylamide (Am) monomers were purchased from Aldrich, SS monomer and 2,2'-azobis(2-amidinopropane) dihydrochloride (V50) from Fluka, and ammonium persulfate from Sigma-Aldrich. All were used as received, without further purification. The initiator for both the NIPAM/SS and NIPAM/Am copolymer reactions was V50; for the homopolymerization reaction, ammonium persulfate. All reactions were carried out in a 50 mL 3-neck round bottom reactor which fed the custom-built ACOMP system. The reaction medium was 10 mM NaCl aqueous solution at 60 °C. Water was deionized and filtered with a 0.22 µm filter in a Modulab UF/UV system. All reagents were purged with N_2 before each reaction; continuous N_2 purge of the reactor continued throughout each reaction.

Table 5.8 summarizes various features of the reactions used in this work, including instant fractional composition of SS, $F_{inst,SS}$, its total drift over the course of the reaction $\Delta F_{inst,SS} = F_{inst,SS,final} - F_{inst,SS,initial}$, and fractional conversion of all comonomers f_{total}.

The 'first generation ACOMP' has been described in detail previously [13, 20, 86, 103]. Its output flow was used to feed the multiple light scattering detector train. The custom-built ACOMP system in this work used a two-pump, one-stage dilution, yielding a 34-fold dilution factor. The dilution solvent was identical to the reaction

medium, 10 mM aqueous NaCl. Hence, except for LCST effects in the various detectors at different temperatures, the monomer and polymer in the diluted stream had the same solubility as in the reactor. The total detector flow rate was 2.06 mL/min, yielding 0.507–0.901 mg/mL of combined monomer and polymer concentration in the detector train, depending on the reaction. The ACOMP detectors used in this work were multi-angle light scattering detector, (MALS; BI-MwA, Brookhaven), differential refractometer (RID-10A, Shimadzu), custom-built single capillary viscometer [125], and UV/visible spectrophotometer (SPM-20A, 200–800 nm, Shimadzu).

After passing through the 'first generation ACOMP' detectors, the sample stream passed in series through the three custom-built temperature-controlled single-angle light scattering detectors. Each detector consisted of a peltier heat block attached to a block of aluminum, followed by a custom-machined SMSLS light scattering cell [100]. These detectors were connected so that the sample flowed through each one in series, with each successive cell set to a higher temperature than the previous cell. The peltier heat blocks set T of the sample immediately before it passed through each light scattering flow cell. Thermocouples directly measured T in each scattering cell, and the 90° scattered light from each cell passed via a fiber optic cable to a photodiode bank. A computer recorded SGA temperature and light scattering signals via an A/D board.

As noted above, the reactor remained at $T = 60\,^{\circ}\mathrm{C}$. The eluent extracted from the reactor was diluted with solvent at room T, and flowed through the detector train. At the dilution stage, the eluent was close to room temperature. Because the plumbing is very narrow gauge (0.1 mm ID), the eluent equilibrates very quickly with its environment. As a result, each ACOMP detector measures the sample at the internal temperature of that detector. This procedure assumes that the LCST is reversible within the time scale of measurement. This is true for the homopolymer, but is not

true for the copolymers. This is discussed further in Section 5.5.3.1. Rather than relying on assumptions of exponential conversion and model-dependent reactivity ratios, the UV data was used to directly compute the conversion of each monomer by solving two UV absorption equations for the two unknown monomer concentrations. For the reactions involving NIPAM and SS, the UV signals at 240 nm and 260 nm were used; for the reaction involving NIPAM and Am, 210 nm and 240 nm were used. The resulting conversion information was used to calculate the instantaneous mole fraction of SS or Am incorporated into the polymer at all times during the reaction. This is defined by

$$F_{\text{inst,SS}} = \frac{d[\text{SS}]/dt}{d[\text{SS} + \text{NIPAM}]/dt} \tag{5.21}$$

The composition drift is defined as the change, $\Delta F_{\text{inst,SS}}$, in instantaneous composition from the beginning of the reaction to the end.

Because NIPAM, SS, and Am have easily distinguishable UV spectra, it is possible to use only two wavelengths to extract the monomer concentrations from the raw UV data of a given copolymer reaction. Both monomers absorb at the chosen wavelengths with known, different, extinction coefficients (Figure 5.23). To account for possible scattering/absorption by the polymer at these wavelengths, the UV data were fit to exponential decays. The residual at infinite time was taken to be the polymer absorption at each wavelength and was small in each case compared to the initial UV signal due to monomer absorption. The known extinction coefficients for NIPAM and SS monomers, and the effective extinction coefficient for the resulting polymer were then used to solve the two equations for the two unknown monomer concentrations.

The general expression for UV absorption at time t and wavelength λ is

$$UV^{\lambda}(t) = \varepsilon^{\lambda}_{\text{Np}} c_{\text{Np}} + \varepsilon^{\lambda}_{\text{SS}} c_{\text{SS}} + \varepsilon^{\lambda}_{p} \left[c_{0,\text{N}} + c_{0,\text{SS}} - c_{\text{Np}}(t) - c_{\text{SS}}(t) \right] \tag{5.22}$$

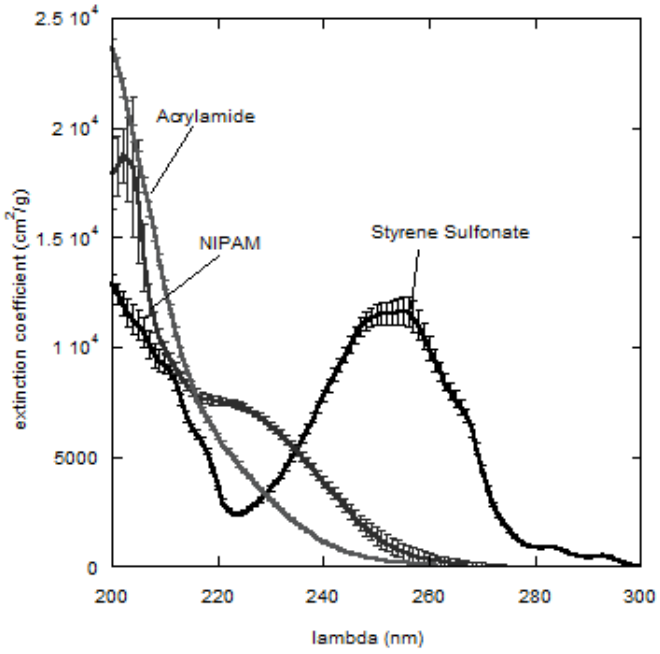

Figure 5.23: The UV spectra of the monomers. Plotted for NIPAM and SS is the average over Reactions S2 through S6 for NIPAM and SS. The error bars are the standard deviation of those five reactions. Plotted for Am is the mean of the baseline for Reaction S7; the error bars are the standard deviation of that baseline.

where UV is the UV absorption, ε is the mass extinction coefficient, c is the mass concentration, and subscripts indicate the species. If it is assumed that the reaction goes to completion, only polymer is present at infinite time, so the UV signal at infinite time can be used to compute the extinction coefficient of the resulting polymer:

$$\varepsilon_p^\lambda = \frac{UV^\lambda(\infty)}{c_{0,\mathrm{SS}} + c_{0,\mathrm{Np}}} \tag{5.23}$$

This leaves the monomer concentrations as the only two unknowns. Therefore, two wavelengths are sufficient. In order to maximize the difference between the signals from the two monomers while maintaining acceptably low errors in the spectra, the 240 and 260 nm signals for the NIPAM/SS reactions were used. For the NIPAM/Am reaction, the 210 and 240 nm signals were used. The associated matrix equation

$$\begin{pmatrix} UV^{240}(t) - UV^{240}(\infty) \\ UV^{260}(t) - UV^{260}(\infty) \end{pmatrix} = \begin{pmatrix} \varepsilon_{\mathrm{Np}}^{240} - \varepsilon_p^{240} & \varepsilon_{\mathrm{SS}}^{240} - \varepsilon_p^{240} \\ \varepsilon_{\mathrm{Np}}^{260} - \varepsilon_p^{260} & \varepsilon_{\mathrm{SS}}^{260} - \varepsilon_p^{260} \end{pmatrix} \begin{pmatrix} c_{\mathrm{Np}}(t) \\ c_{\mathrm{SS}}(t) \end{pmatrix} \tag{5.24}$$

was solved for the monomer concentrations every two seconds during each reaction. The monomer extinction coefficients are the same from reaction to reaction, to within 6.3% (NIPAM) and 3.3% (SS). The polymer extinction coefficients are smaller than the monomer extinction coefficients, but cannot be ignored. The extinction coefficients found in this section, and used in the analysis, are summarized for convenience in Table 5.9.

Because of the derivatives, small fluctuations in the raw UV data cause large fluctuations in $F_{\mathrm{inst,SS}}$. To avoid this, smoothing fits using the Stineman algorithm [126] were made to the concentration before the derivatives were computed. This algorithm was first published in a hobbyist magazine, but is the internal "smooth fit" for Kaleidagraph [127], and is also provided by R [128], Matlab [129], and Mathemat-

Table 5.9: UV extinction coefficients used in the NIPAM/SS study for each monomer, and for the polymer end product of each reaction.

Species	ε^{210} (cm^2/g)	ε^{240} (cm^2/g)	ε^{260} (cm^2/g)
NIPAM monomer	$9.3 \times 10^3 \pm 3\%$	$3.9 \times 10^3 \pm 8\%$	$4 \times 10^2 \pm 60\%$
SS monomer	N/A	$7.8 \times 10^3 \pm 3\%$	$1 \times 10^4 \pm 6\%$
Am monomer	$1.3 \times 10^4 \pm 3\%$	$1.2 \times 10^3 \pm 2\%$	N/A
S2 polymer	N/A	$2.7 \times 10^2 \pm 0.1\%$	$1.2 \times 10^2 \pm 0.1\%$
S3 polymer	N/A	$1.8 \times 10^2 \pm 3\%$	$1.4 \times 10^2 \pm 0.2\%$
S5 polymer	N/A	$1.3 \times 10^3 \pm 0.1\%$	$4.0 \times 10^2 \pm 0.2\%$
S4 polymer	N/A	$4.2 \times 10^3 \pm 0.2\%$	$2.2 \times 10^2 \pm 0.2\%$
S6 polymer	N/A	$1.3 \times 10^3 \pm 0.1\%$	$7.6 \times 10^2 \pm 2\%$
S8 polymer	$2.5 \times 10^2 \pm 0.2\%$	$3.2 \times 10^1 \pm 0.4\%$	N/A

ica [130]. The primary property of this algorithm is that the computed values are monotonic as long as the original data is monotonic, and that small changes in the original data cause similarly sized changes in the smoothed data. The effect is that there are no "wild swings" such as are sometimes seen in spline-based interpolations. An example of the effect of this smoothing is shown in Figure 5.24.

The dominant uncertainty in the conversion and $F_{\text{inst,SS}}$ is the run-to-run repeatability of the extinction coefficients of NIPAM and SS, given in 5.9. For SS, the uncertainties of the two coefficients add in quadrature. For NIPAM, the signal from 260 nm is small, and its uncertainty can be ignored. The result is that $\delta c_{\text{SS}}/c_{\text{SS}} \approx 6\%$, and $\delta c_{\text{Np}}/c_{\text{Np}} \approx 7\%$. The derivatives in $F_{\text{inst,SS}}$ are computed as a finite-difference: $dc_{\text{SS}}/dt = \Delta c_{\text{SS}}/\Delta t$. The time difference has negligible uncertainty. The absolute uncertainties in the concentration measurements add in quadrature, giving a total uncertainty of $\delta(dc_{\text{SS}}/dt) = (\sqrt{2}/2)\delta c_{\text{SS}}$. Then the fractional uncertainty is $\delta(dc_{\text{SS}}/dt)/(dc_{\text{SS}}/dt) = \sqrt{2}\delta c_{\text{SS}}/\Delta c_{\text{SS}}$. Near the onset of LCST, $\Delta c_{\text{SS}} \approx 2.1 \times 10^{-6}$ g/mL, and $\delta c_{\text{SS}} \approx 0.06 \times 5 \times 10^{-4}$ g/mL $= 3 \times 10^{-7}$ g/mL. So $\delta(dc_{\text{SS}}/dt)/(dc_{\text{SS}}/dt) \approx 20\%$.

The SGA detector also provides off-line light-scattering measurements as a stand-alone instrument. Programmed continuous mixes of polymer and/or salt were

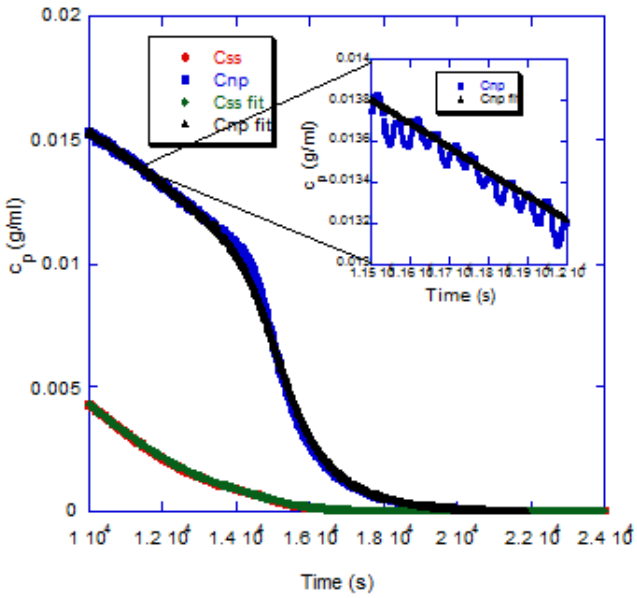

Figure 5.24: An example of the effect of the Stineman smoothing algorithm. The major effect is to make the kink in c_{Np} more gradual, and to eliminate the instrumentational oscillations.

made using a four-way programmable mixing chamber (FCV-10AL VP, Shimadzu) driven by an HPLC pump (LC-10AC, Shimadzu). This method has been frequently used in this group as part of the Automatic Continuous Mixing (ACM) technique [21]. In the present section, three inputs were used: one for each of the two species being mixed, and a solvent reservoir to keep the mixture at the desired polymer concentration. The mixing pump output stream of constantly changing ionic strength fed the sample cells in series in this mode, each at a separately fixed temperature, to explore the effects of continuously changing ionic strength.

This section follows the usual polymer science convention of cgs units. The mass concentration of species x is denoted c_{x} , and has the units g/cm^3. The one exception to this is the calculation of instantaneous fractional molar conversion, $F_{\mathrm{inst,x}}$. In this case the concentration of species x in mol/L is indicated by [x].

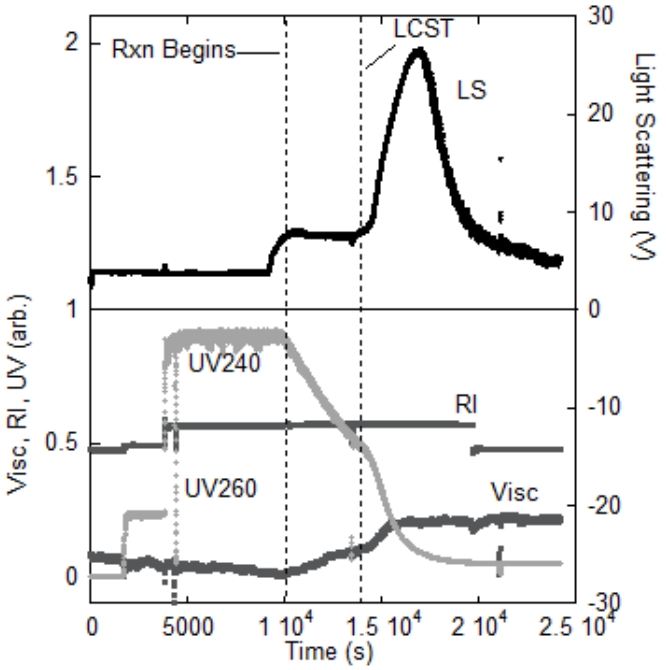

Figure 5.25: Raw ACOMP data from Reaction S2 includes data streams of RI, UV, viscosity, and LS (only 35° data is shown).

5.5.3 Results and discussion

Raw data from reaction S2 are shown in Figure 5.25. SS was added at 1700 s, followed by NIPAM at 3800 s. A strong rise in the 240 nm signal occurs with addition of SS, and again with addition of NIPAM. The 260 nm signal rises significantly only with SS, and so provides a good marker for c_{SS}. The MALS (only 35° data are shown) signals are insensitive to the presence of these dilute monomers (0.44 mg/mL NIPAM, 0.09 mg/mL SS in the detector train). Initiator is added at 8600 s, which starts the reaction. The UV signals decrease, indicating the consumption of the comonomers, while viscosity, RI, and light scattering increase with the production of polymer. At approximately 14 000 s, the light scattering signal increases very rapidly by a factor of about 80, due to the LCST behavior. The decrease in LS after 17 000 s occurs because the turbidity in the light scattering cell due to the LCST attenuates both the incident beam and scattered light.

Figure 5.25 shows two-phase behavior that has been previously observed in an Am/SS copolymer reaction [102]. In the first phase, SS is quickly consumed before the NIPAM is left in very large excess, as seen by the smooth drop of the 260 nm signal back to close to its starting point. In the second phase, the NIPAM (at that point, making up the majority of the 240 nm signal) goes through an inflection point, then a more rapid final conversion. The LCST appears before but very near the inflection point, when the concentration of SS is very low.

For convenience, the 'Second-Generation' ACOMP (SGA) results are included alongside the ACOMP results (i.e. $F_{\mathrm{inst,SS}}$, M_w and $[\eta]$) in Table 5.8. The SGA data include the computed values of $F_{\mathrm{inst,SS}}$ and f_{total} at the onset of LCST in each reaction, where applicable. The most salient feature of the tabulated values is that for the SS/NIPAM reactions that displayed an LCST in 10 mM aqueous NaCl solution, the LCST was detected when the molar SS fraction, $F_{\mathrm{inst,SS}}$, was around 3% – 5%, discussed below.

NIPAM homopolymer reaction (Reaction S1, Table 5.8) data in Figure 5.26 show that the LCST behavior is detected very early in the reaction, at about 3% conversion. This corresponds to a polymer concentration of $c = 0.015$ mg/mL in the detector ($c = 0.5$ mg/mL in the reactor) at the onset of detection. It is supposed that the intra molecular conformational change underlying the LCST is independent of polymer concentration, and that this concentration merely represents the detection limit in this particular detector scheme.

There are two obvious signatures of the LCST behavior in Figure 5.26. The light scattering signal at 45 °C increases rapidly, while the signals at 23 °C and 9 °C increase very slowly, indicating detection of single chain polymers. The increase in light scattering signal due to the LCST is approximately 80 times that due simply to polymerization. Because of this strong difference in scale, the light scattering data of

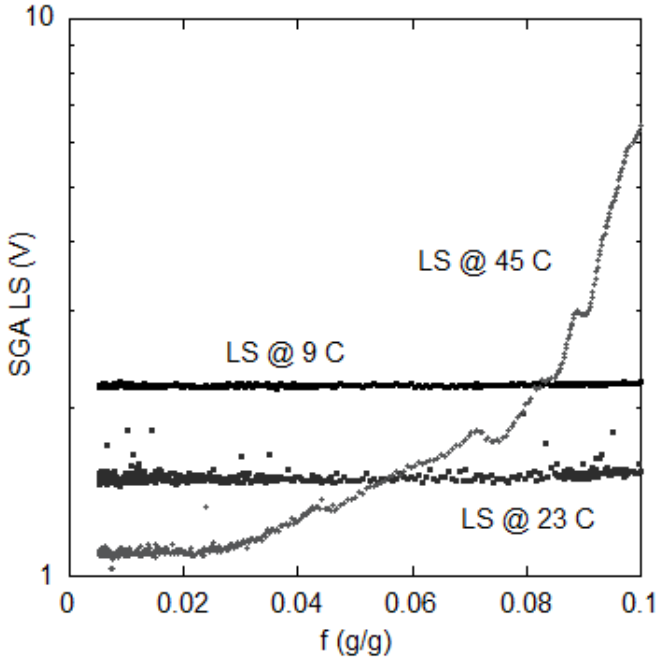

Figure 5.26: Scattering vs. fractional monomer conversion f, at three temperatures during a NIPAM homopolymer reaction (Reaction S1). The LCST of the homopolymer in water is observed here to be between 23 °C and 45 °C, which is consistent with the usually reported 32 °C. LS data at 9 °C is also shown to demonstrate the ability to cool the sample in addition to heating. The LCST behavior is first detected very early in the reaction, starting at about 3% conversion. The light scattering increase due to LCST is so strong that a logarithmic scale is used to show both the increase due to LCST and the much smaller increase due simply to polymerization.

Figures 5.26 through 5.34 are plotted on logarithmic scales to show all the relevant details. In addition, in free radical polymerization, light scattering increases with conversion as polymer concentration increases. But M_w decreases with conversion for free radical Reactions without chain transfer, such as Am, so light scattering would also be expected to have a negative second derivative with respect to conversion [97]. The light scattering signal at 45 °C is increasing and has a positive second derivative when plotted on a linear scale, indicating that apparent M_w is increasing. Thus, this light scattering behavior indicates aggregation.

As mentioned, the current use of aqueous polymerization in the heated reactor leads to an LCST in the reactor itself, when an LCST exists. The detection scheme here then relies on the reversibility of the LCST, which is robust for reaction S1 (but see below for a discussion of the robustness of this assumption for Reactions S2, S3, and S4). A means to avoid LCST in the reactor is to do the reaction in methanol, in which pNIPAM has no LCST, and to dilute the reactor product with aqueous solution. The very high ACOMP dilution with aqueous solvent would then render the methanol a tiny admixture in the detector train [30].

Figure 5.27 shows the computed quantities f_{NIPAM} , f_{SS} , which are the total fractional conversion of NIPAM and SS, respectively, reduced viscosity, η_r , and M_w from reaction S2 alongside the SGA light scattering (M_w is shown only before the LCST because the LS data gave unreliable results for M_w after the LCST). The NIPAM conversion follows the type of two-phase pattern seen in Figure 5.28 in Reactions S2, S3, and S4. Two phase behavior in another copolymer system was observed previously under ACOMP monitoring [36]. In the first phase, NIPAM conversion is approximately first-order, and co-converts with SS to produce an SS/NIPAM polyelectrolyte copolymer. The second phase begins after most of the SS has been consumed and goes on to produce quasi-homopolymer of NIPAM in a first-order fashion. The

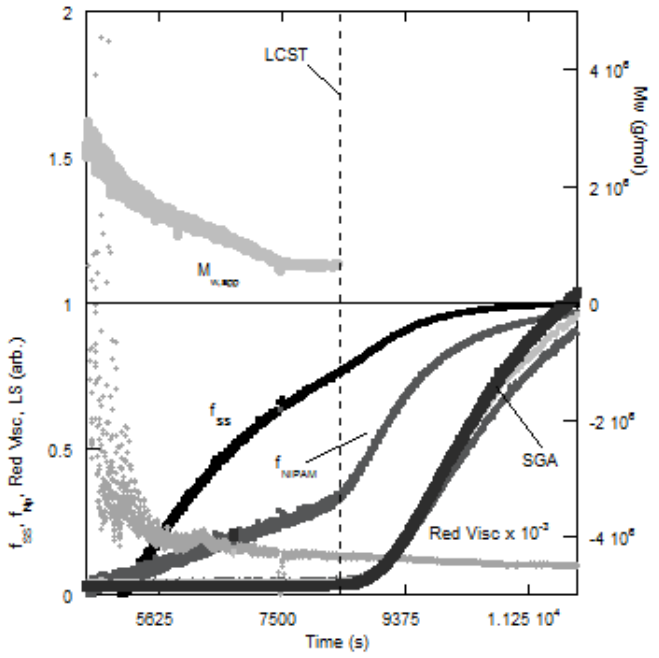

Figure 5.27: Comonomer conversions, reduced viscosity, apparent molecular weight, and SGA light scattering for Reaction S2. The onset of LCST is shown as a vertical line, and occurs at approximately the kink in f_{SS} and f_{NIPAM}. M_w after the LCST is not shown. Only one SGA detector is shown, and is scaled to the range 0–1.

most interesting thing to note about these reactions in the context of this dissertation is that the LCST behavior is suppressed during almost the entire copolymerization portion of the reaction, and only turns on near the transition from the first phase of the reaction to the second phase, at $F_{\mathrm{inst,SS}} \approx 5\%$.

Figure 5.28 shows further results of Reaction S2. The computed fractional conversion is plotted as a function of the total conversion. This reaction shows two distinct phases, as indicated distinctly by $F_{\mathrm{inst,SS}}$. In the first phase, both NIPAM and SS are consumed. $F_{\mathrm{inst,SS}}$ begins at an initial value of 0.40 mol/mol, and decreases slowly. As the reaction depletes the available SS, $F_{\mathrm{inst,SS}}$ accelerates downward, eventually producing a very sharp drop, followed by the second phase of the reaction. In this second phase, $F_{\mathrm{inst,SS}}$ decreases very slowly from 5% down to 0%, as the NIPAM continues to react. As described above, the uncertainty in $F_{\mathrm{inst,SS}}$ is

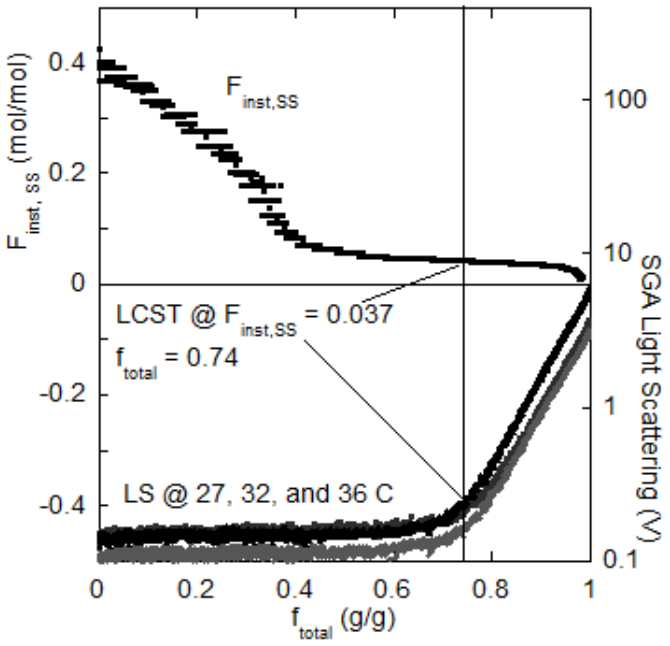

Figure 5.28: $F_{\text{inst,SS}}$ (from ACOMP) and light scattering (from SGA) plotted against f_{total} for Reaction S2. The onset of the LCST is indicated, and occurs at approximately $F_{\text{inst,SS}} = 4\%$.

approximately 0.01 mol/mol, so $F_{\text{inst,SS}}$ is measurably different from zero. The SGA light scattering signals rise slightly from their baseline values during the first phase of the reaction, a similar magnitude as for non-LCST reactions. A sharp increase in SGA light scattering signals indicates the onset of the LCST at the very low value of $F_{\text{inst,SS}} = 0.037\,\text{mol/mol}$. Similar results are seen for Reactions S3 and S4 (Figures 5.28 and 5.28.

Although the evidence is strong that the SS prevents the coil to globule transition that results in the LCST, it remains possible that inter-molecular charge-charge repulsion prevents aggregation of the copolymer chains, even if the NIPAM rich segments were able to collapse from coil to globule despite the intra-chain charge charge repulsion and high water affinity of SS. In this scenario segments of copolymer chains with high SS content could still collapse into globules but there might be too much interchain electrostatic repulsion to allow for the formation of aggregates associated

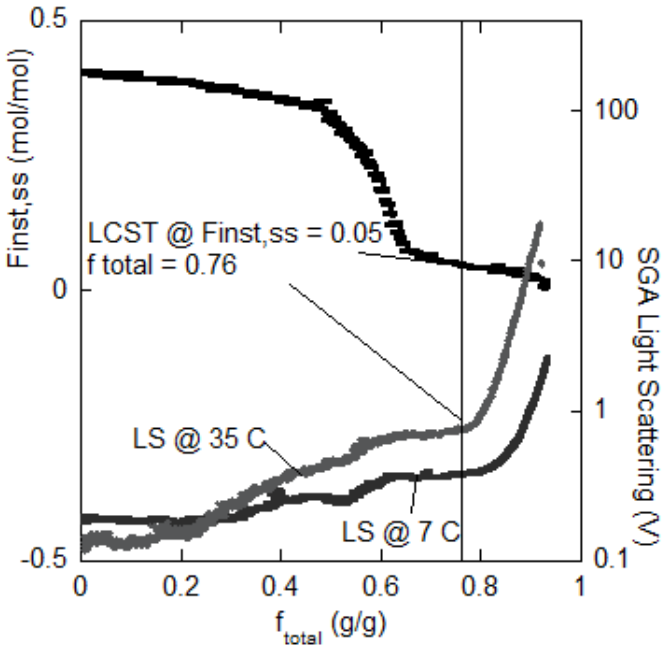

Figure 5.29: $F_{\text{inst,SS}}$ (from ACOMP) and light scattering (from SGA) plotted against f_{total} for Reaction S3. The onset of the LCST is indicated, and occurs at approximately $F_{\text{inst,SS}} = 5\%$.

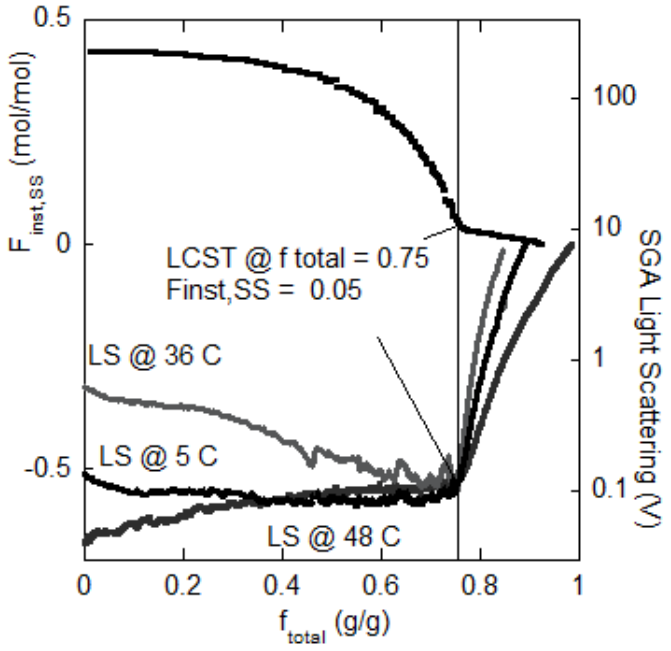

Figure 5.30: $F_{\text{inst,SS}}$ (from ACOMP) and light scattering (from SGA) plotted against f_{total} for Reaction S4. The onset of the LCST is indicated, and occurs at approximately $F_{\text{inst,SS}} = 5\%$.

with the LCST. In this scenario, at low SS content collapsed chains have weak enough inter-molecular electrostatic repulsion that they can still aggregate with each other giving the LS increase associated with the LCST. It is emphasized, however, that copolymers in this section are statistical and not block copolymers, so there are not well separated segments of SS and NIPAM in the copolymer chains, and hence no reason to assume that intra-chain segments have local coil-to-globule collapse. Tauer et al. have reported that an SS/NIPAM block copolymer has the same LCST as NIPAM homopolymer [131]. It is not surprising that a pure pNIPAM segment in a block copolymer could still collapse, whereas it would be less likely in a statistical copolymer.

One oddity seen in figure 5.28 is that all three SGA detectors indicate the onset of LCST, even the detector at 27 °C, normally below the LCST of the homopolymer. The same behavior was seen in Reaction S3: aggregation and high scattering were observed even at 9 °C. Further experiments with the end product of reaction S3 revealed high scattering down to 5 °C. The chains in the reactor at 60 °C aggregate when the SS content drops low enough; this can be seen visually in the reactor. The fact that high scattering is observed at all temperatures in the detectors is most likely due to a failure of the aggregates to dissociate within the time frame of reactor withdrawal and dilution by the front-end and detection, which is approximately 60 s for the current experimental arrangement. The observation of aggregation by the SGA detectors indicates merely that the LCST is below 60 °C. Off-line, post-reaction studies indicate that these aggregates are irreversible on the time scale of several days. This issue is discussed further in Section 5.5.3.1. It is also intriguing that, whereas Am/NIPAM and pure pNIPAM manifest reversibility within the time delay of the system, the inclusion of the SS, which inhibits the LCST, actually leads to a greater persistence of the aggregates against reversibility.

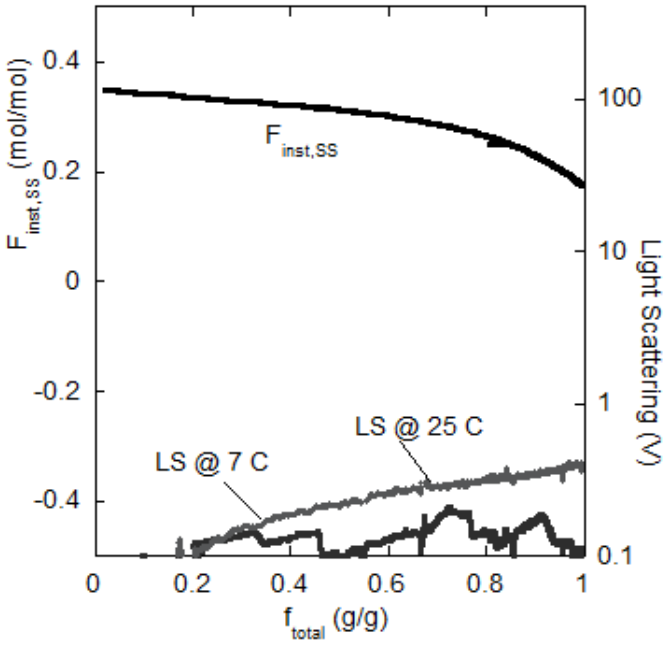

Figure 5.31: Light scattering versus total conversion for Reaction S5 indicates no LCST at any point in this reaction.

In contrast, Reactions S5 and S6 data display only single-phase behavior: both the SS and the NIPAM conversions show first-order kinetics for the entire reaction, and there is no inflection point in the resulting conversions. These two reactions show much smaller overall increase in LS, indicating that there is no LCST behavior in these reactions. In addition, the reactor solution did not visibly cloud at any time during these two reactions. Figure 5.31 shows the data from Reaction S5. This reaction behaves just as the first phase of Reactions S2 through S4: $F_{\mathrm{inst,SS}}$ decreases and is concave down. $F_{\mathrm{inst,SS}}$ ends the reaction at about 17%. The SGA light scattering signals indicate no LCST. Note that the highest temperature reported in the SGA detector in this reaction is 25 °C, below the expected LCST even for a homopolymer. By itself, the lack of LCST at 25 °C would not be notable. In an off-line measurement, the end product of this reaction was verified to have no LCST below 74 °C, in 10 mM NaCl.

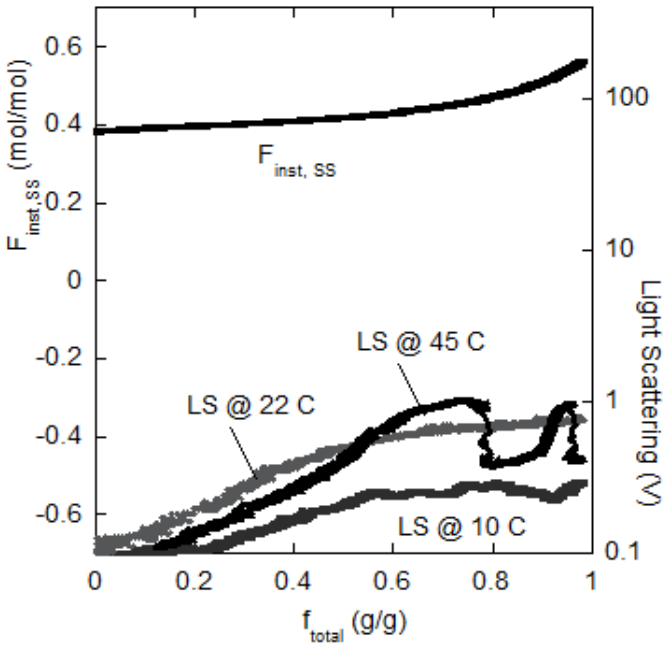

Figure 5.32: Conversion data from ACOMP indicates that the instantaneous conversion of SS begins at 40% for Reaction S6, and increases. LCST is not seen in this reaction.

By contrast, Figure 5.32 for Reaction S6 indicates that $F_{\mathrm{inst,SS}}$ is concave up and increasing in Reaction S6. It is unsurprising, then, that this reaction does not have an LCST. The increase in LS at 45 °C in this reaction is small, and does not indicate an LCST. As in Reaction S5, the end product of this reaction was verified to have no LCST below 74 °C. Reactions S5 and S6, taken together, indicate that the azeotrope for this comonomer pair is found between 50/50 and 70/30 NIPAM/SS initial molar ratio. This is close to, but slightly different from, the azeotrope of the Am/SS pair, previously found to be between 80% and 70% initial SS composition [132].

Figure 5.27 also shows M_w and η_r for Reaction S2 before the LCST. A_2 effects are not important in this region, so M_w was calculated without a correction for A_2. Values of A_2 were estimated from those reported for the Am/SS system [13], giving values of $2A_2cM_w$ in the detectors no larger than 0.30 (Reaction S4). Both M_w

and η_r follow typical paths for free radical polymerization reactions, in which both decrease with conversion. While the sharp increase in raw LS at the LCST indicates the formation of high mass aggregates, η_r does not show any such qualitative change at the LCST and continues its slow decrease. Figure 5.33 shows raw viscosity and LS signals versus total conversion for several reactions. Reactions S2 and S5 each have an LCST, while Reaction 6 has no LCST; all three show a simple increase in raw viscosity with conversion, and no abrupt or qualitative changes when the LCST is reached. The indifference of viscosity to LCST in this section can be explained by the fact that only those copolymer chains produced after the LCST is reached participate in the aggregates that signal the LCST. Since the intrinsic viscosity of collapsed aggregates is very low, they do not contribute appreciably to the viscosity signal. The LS from the aggregates, in contrast, is extremely high, so that even a small population of collapsing, aggregating chains after the LCST is reached can generate large LS signals.

Because of the effect that LCST has on apparent M_w, Table 5.8 reports M_w and η_r just before the onset of LCST for those reactions that showed an LCST, and at the end of the reaction for those reactions that did not. The general trend of decreasing M_w and increasing η_r with increasing polyelectrolyte linear charge density are typical of copolymeric polyelectrolytes [13, 14].

It is quite remarkable that in Reactions S2 through S4 that SS has such a strong effect on the copolymer behavior in 10 mM NaCl solutions that LCST is suppressed until SS content is almost negligible, at $F_{\text{inst,SS}} = 4\% \pm 1\%$. While the measured values are greater than zero, the LCST clearly tolerates only very little SS in these conditions. A similar threshold has been observed before, but without this precision [133]. Since this value of $F_{\text{inst,SS}}$ is observed for a wide range of initial compositions it appears to be a critical value for the reaction conditions in 10 mM

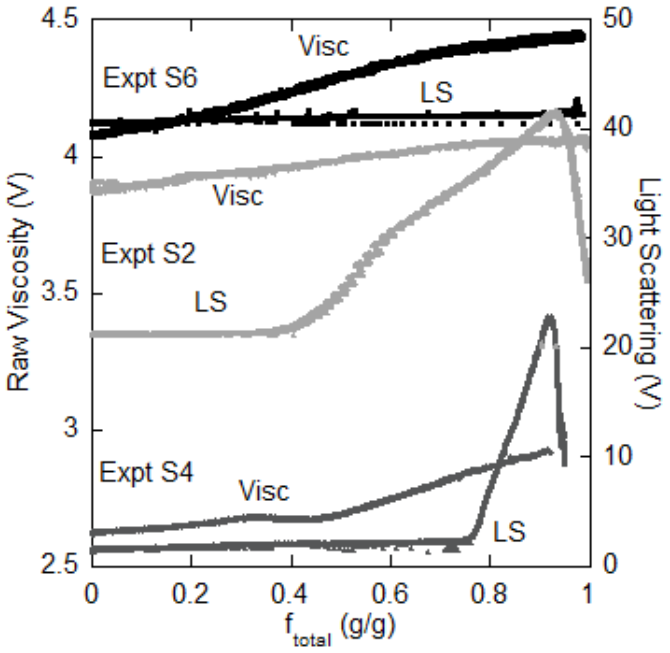

Figure 5.33: The raw viscosity signal shows no anomalous behavior when plotted against conversion. The light scattering is also plotted for each reaction in order to indicate the onset of LCST for that reaction.

ionic strength in the reactor (and detector train). Presumably, different reaction conditions (such as a different ionic strength solvent) could produce a different critical ionic content. It is demonstrated below that higher content SS copolymers in fact do have an LCST, but at much higher ionic strength than 10 mM. A model of increasing hydrophilic content of the polymer chains, and electrostatic charge repelling against chain collapse, could probably predict such a critical ionic content. A deeper study of charge versus hydrophilicity alone is currently underway, using different charged comonomers and Am.

There are three immediate simple explanations for the presence of SS suppressing the LCST of the pNIPAM. The first is that this suppression is a "dilution" of NIPAM monomers away from each other along the chain. Other NIPAM copolymer systems have shown such behavior [134, 135]. The second is that an inter-molecular interaction with a charged polymer increases pNIPAM solubility. The third is that

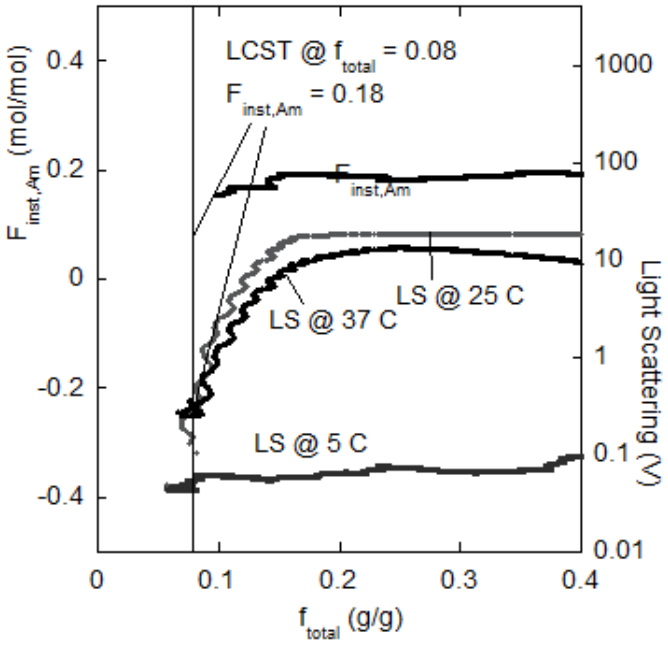

Figure 5.34: Light Scattering versus total conversion for reaction S8, pNIPAM copolymer with Am. LCST turns on almost immediately. Again, the increase in light scattering due to LCST is so large that a logarithmic scale is needed.

it is due to intra-chain charge-charge repulsion of the SS monomers and/or the high affinity of the SS monomers for water. Evidence is now provided to reject the first two possibilities, and supporting the third.

Reaction S8, a copolymerization of NIPAM with Am, rejects the possibility that this suppression is merely a dilution of the NIPAM monomers (figure 5.34). In this reaction, the LCST behavior appears at 7% total conversion (comparable to the homopolymer) and at $F_{\text{inst,Am}} = 18\%$, which drifts very little over the course of the reaction. If there is any simple dilution effect, it becomes prevalent at much higher comonomer content than seen in Reactions S2 through S6. This cannot be the dominant effect in the NIPAM/SS copolymer system since suppression occurs down to $F_{\text{inst,SS}} = 5\%$. SGA is an ideal tool for probing what level of Am the Am/NIPAM copolymers can tolerate before losing LCST behavior.

Figure 5.35 refutes the possibility that interchain interactions between pNIPAM and pSS inhibit the LCST chain collapse. pNIPAM and pSS homopolymers from Reactions S1 and S7, respectively, were mixed together using three inputs of a four-way mixing pump. Total polymer concentration was held constant at $c = 0.1\,\mathrm{mg/mL}$ as pSS replaced pNIPAM. Two of the LS cells were held above the LCST (39 °C and 63 °C), and a third was held below the LCST. Above the LCST, the scattering due to pSS is negligible compared with that due to pNIPAM aggregates. Hence, the light scattering signals for 39 °C and 63 °C in Figure 5.35 have been divided by the mass fraction of pNIPAM present in order to account for the dilution of pNIPAM aggregates as they are replaced by pSS. The two LS signals above the LCST of the NIPAM homopolymer show very little change in light scattering per unit pNIPAM as the pSS is mixed in. The relatively small increase in scaled scattering at $x = 0.4$ suggests some additional interaction between the NIPAM and SS homopolymers, which is not pursued here. Whatever that interaction is, it does not inhibit the LCST behavior of the NIPAM homopolymer and the pNIPAM remains above the LCST no matter how much pSS is added.

The final possibility is that the charges on the SS residues in a given chain and/or the high affinity for water of SS inhibit the collapse and subsequent aggregation of that chain. This would suggest that there is some critical value of $F_{\mathrm{inst,SS}}$ above which the chain is unable to collapse and aggregate, such as that seen in Reactions S2 through S6 above. This critical value should be, a priori, dependent on ionic strength, since at high screening, the polyelectrolyte behavior resembles that of a neutral polymer, and it was shown that pNIPAM tolerates a high percentage of Am without suppressing the LCST.

Figure 5.36 provides further evidence of this intramolecular effect. The end product of Reaction 5 was mixed with NaCl using three inputs of a four-way mixing

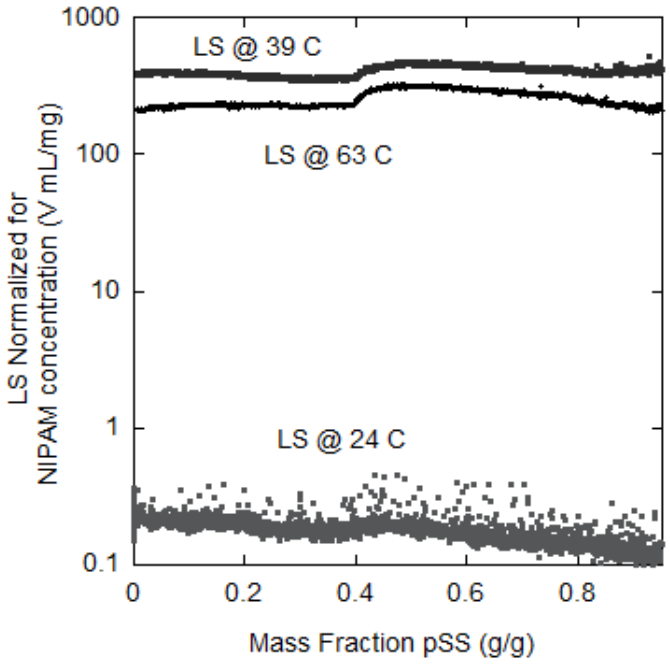

Figure 5.35: Light scattering of a blend of NIPAM and SS homopolymers. The raw LS voltages for 39 °C and 63 °C have been normalized for the mass concentration of pNIPAM present.

pump. The result was passed through the SGA in series mode, with each detector set to a different, fixed temperature. Because the voltage responses of the LS cells differ, the signals were normalized to each other by taking baselines both of water and of polymer with no NaCl. The water baseline was subtracted off, and the resulting signal was divided by the polymer-only baseline. The y-axis in Figure 5.36 therefore is proportional to an effective aggregation number. Recall that this sample did not show any LCST in 10 mM NaCl. The samples at 57 °C and 63 °C show LCST behavior appearing at 0.4 M NaCl. The samples at 24 °C and 12 °C do not show an LCST at any NaCl concentration up to 1 M. The displacement of LCST to higher temperature is consistent with NaCl screening intra-chain charge-charge repulsion. Below the critical ionic strength, electrostatic repulsion from the negative charges in the SS prevents the collapse and aggregation of the chains. At and above the critical ionic strength, the Debye screening length is short enough to allow collapse. Referring to Figure

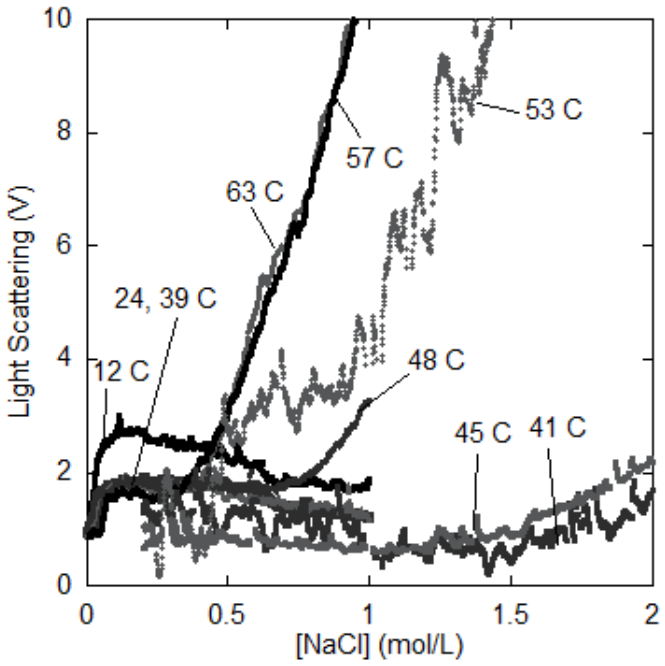

Figure 5.36: Addition of NaCl allows LCST behavior in the end product of Reaction S5, which showed no LCST behavior in 10 mM NaCl.

5.32, it is seen that $F_{\text{inst,SS}}$ for Reaction S5 varies from 18% to 35%. Hence, pNIPAM can tolerate at least 18% molar SS and still exhibit an LCST at high enough ionic strength. This is about four times as much SS content as for the copolymers in 10 mM NaCl. A quantitative model for the charge and ionic strength type behavior observed in this section can be developed when more extensive results are available.

5.5.3.1 Reversibility

Finally, the issue of short-term reversibility is considered again. Further investigations are ongoing concerning the stability and reversibility of pNIPAM aggregates on timescales longer than a few days, as previous studies have indicated that the chain collapse and aggregation of pNIPAM are not fully reversible [136]. In addition, the problem of long-term stability has only been partially investigated, and there is no reason to assume that the pNIPAM aggregates are in equilibrium. The SGA system in this section can be used on end-products or aliquots running with a peristaltic

pump to LS cells at different temperatures for dissociation kinetic studies.

Frisken has reported that NIPAM homopolymer in water can self cross-link [137], which would lead to irreversible aggregates. It was reported in Reference [137] that when NIPAM self cross-links, the observed M_w does not change upon heating through the LCST, but rather remains much larger than observed here. Cross-linking is not seen here in the homopolymer: off-line light scattering measurements show a marked increase in light scattering upon heating the final product of Reaction S1. In contrast, as noted above, the aggregation in the reactor during Reactions S2, S3, and S4 appears to be irreversible on the experimental time scales of this dissertation. Further off-line investigation with the end products of these reactions showed that the aggregation is irreversible on the time scale of several days. This is an interesting finding. Irreversible aggregation is a known problem in the protein folding literature [138], but is unreported in the synthetic stimuli-responsive polymer literature.

5.5.4 Conclusion

Detection of LCST behavior during polymer synthesis has been demonstrated with a new embodiment of ACOMP instrumentation. This opens many possibilities for understanding and optimizing the development of stimuli-responsive polymers. While this dissertation uses only free radical polymerization, the ACOMP technique is independent of the reaction chemistry, and has been used in a very wide array of reactions. One potentially fruitful area will be the application of this SGA approach to controlled polymerization techniques, allowing one both to understand the fundamental physical processes controlling the LCST and to tailor the LCST behavior and the specific chemical architecture of the resulting polymer.

Charged comonomers suppress LCST-induced chain collapse and aggregation in a way that neutral comonomers do not. This suppression is an intra-chain effect,

and is strongly dependent on ionic strength. That is, both the critical value of $F_{\text{inst,SS}}$ at which suppression of LCST begins and the associated temperatures may be a function of the Debye screening length of the solution, persistence length, and possibly other length scales and details of linear charge distribution in the copolymer chains. Preliminary evidence is given here for what would be surmised for copolymeric polyelectrolytes; i.e. due to increased screening higher ionic strength increases the critical value of $F_{\text{inst,SS}}$ at which an LCST can appear. This can be examined by running the copolymer Reactions S2 through S6 again in higher ionic strength solvent. Evidence is provided of irreversible aggregation of copolymer polyelectrolytes in the reactor.

5.6 Cationic comonomer: Q9

5.6.1 Introduction

Thermosensitive polymers have broad application for all sorts of things, including drug delivery and protein folding modeling. pNIPAM is known to undergo a coil-to-globule transition at 32 °C. In addition, several authors have demonstrated that copolymerizing NIPAM with hydrophilic or hydrophobic comonomers can raise or lower the temperature of this transition [4, 15, 76, 91]. Not as much work has been done regarding ionic comonomers. Due to the charge, these should have a much stronger effect on the transition temperature. Our lab has previously shown [87] that a copolymer with as much as 5% (mol/mol) styrene sulfonate (SS) can have an LCST in low ionic strength solution. Further, chains with higher SS content can undergo LCST in higher salt environments.

In this section, I copolymerize NIPAM with [2-(acryloyloxy)ethyl]-trimethylammonium chloride (Q9), a cationic monomer. In addition to reversing the sign of the charge, this introduces another change relative to the SS study. Where the NIPAM/SS free

radical polymerization is a very high drift reaction [13,87], the NIPAM/Q9 free radical polymerization reaction has a low but non-zero drift [14].

Heyda has recently developed a model to describe the LCST of polyelectrolytes based on ionic content [139] and added small molecule salts. In that work, the model is mathematically valid for chains of low charge fraction, and for both positive and negative charges along the chain. Heyda verified this model for chains of charge fraction $\chi \leq 7.6\%$ in ionic strength solutions of $C_s \leq 0.1\,\mathrm{mol/L}$. The particular charged monomer they used in that work was 1-Ethyl-3-vinylimidazolium bromide (EVImBr), with a net charge of $z = +1$ per monomer. This model gives the change in LCST as

$$\Delta T = (k_B T_0 \rho_g)(4\Delta S(\chi))(\alpha^2/c_s) + \frac{m_\chi}{(\Delta S(\chi))}\chi + \frac{m}{\Delta S(\chi)}c_s \tag{5.25}$$

The three fit parameters in this model are: ρ_g, the molecular density of the polymer globules, describing electrostatic interactions; a thermodynamic slope with respect to the fraction χ of charged monomer $m_\chi = \frac{\partial \Delta G}{\partial \chi}$, representing hydrophobic effects; and $m_\chi^{'} = \partial S_0/\partial\chi$, the change in entropy change with respect to χ, also representing hydrophobic effects. $m = \partial\Delta G/\partial C_s$ is the thermodynamic slope with respect to the ionic strength. This is not a fit parameter in Heydas model; it is derived from the slope $\Delta T/C_s$ of the pNIPAM homopolymer. $\Delta S(\chi) = \Delta S_0 + m_\chi^{'}\chi$ is the change in entropy during the transition of the copolymer. ΔS_0 is the change in entropy during the transition of the homopolymer, and is fixed in Heydas work at $15.0\,\mathrm{J\,K/mol}$. In Heydas work, m_χ was set to zero for the specific salt KBr.

This section further verifies this model under those conditions using Q9, and provides data for conditions at both higher ionic strength solutions and with higher charge content.

Table 5.10: The batch reactions used in the Q9 study.

ID	Initial composition (mol Q9/ mol Np)	Temperature (°C)	Ionic Strength (mM NaCl)
Q1	50/50	60	100
Q2	50/50	27	100
Q3	20/80	27	100

5.6.2 Materials and Methods

NIPAM (97% pure) and Q9 monomer 80% solution with 800 ppm MeHQ inhibitor, NaCl (99.0%), Ethylenediaminetetraacetic acid (EDTA) and potassium persulfate (KPS, 99+%) were purchased from Aldrich. Tetramethylethylenediamine (TEMED, min 99%) was purchased from Spectrum. All reagents were used as received unless otherwise noted. Purified water was obtained from a ELGA Purlab Ultra system, with a resistivity of 18.2 MΩ cm. All liquid samples were filtered with a Millipore Millex 0.22 µm syringe filter before use. Because the reactions were run in aqueous solution, it was preferred to run them at close to ambient temperature in order to avoid LCST-driven aggregation in the reactor. The TEMED was used as a redox catalyst to allow the the reaction to progress at ambient temperature. The EDTA was used as a chelation agent to remove the MeHQ from the solution. In all reactions, 8 mg/mL of total reactor solution EDTA was used. This was added and thoroughly mixed into the diluted Q9 solution immediately before adding the Q9 to the reactor solution.

The reactions were all free radical reactions. A series of batch reactions were carried out in order to confirm the reactivity properties of the NIPAM/Q9 pair. In each of these reactions, a pre-determined quantity of both monomers was added to the reaction in solution, and brought to temperature. The initiator was added, and the reaction was monitored. These reactivities were used to inform the input parameters for the batch reactions. The batch reactions are summarized in Table 5.10.

Table 5.11: The semi-batch reaction used in the Q9 study.

ID	Initial composition (mol Q9/mol Np)	Flow rate (mL/min)	Final Composition (mol Q9/ mol)	Temperature (°C)	Ionic Strength (mM NaCl)
Q4	50/50	0.1	0/100	27	100

In the semi-batch reaction, a pre-determined quantity of both monomers was added to the reaction solution. Again, the initiator was added. Instead of simply monitoring the reaction, however, additional NIPAM monomer was added from a reservoir. This added monomer served to replace monomer as the reaction consumed it. The result is the synthesis of polymers with a variety of compositions. The semi-batch reaction is summarized in Table 5.11.

Absolute continuous online monitoring of polymerizations (ACOMP) was used to conduct and monitor Reactions Q2 through Q4. [93,98]. In this section , an HPLC pump (LC-10AD Shimadzu) extracted reactor solution at the rate of 0.1 mL/min from the reactor. This stream was pumped to a high-pressure mixing tee, where it was diluted with 1.9 mL/min of solvent from a solvent reservoir. This produced a dilution factor of 0.05. The diluted stream was then passed at 2.0 mL/min to a train of detectors. The detectors used were single capillary viscometer (Validyne, Northridge CA), multi-angle light scattering (MALS; BiMw-A, Brookhaven), UV-Vis diode array spectrophotometer (SPD-M20, Shimadzu), a differential refractometer (RID-10A, Shimadzu), and a home-built second-generation (SGA) light scattering flow cell detector, in that order.

The SGA detector in this case has three flow cells. These flow cells heat the sample immediately before it passes through a single-angle light scattering cell. The sample temperature is measured directly at the light scattering cell. Each cell was held at ambient temperature, 45 °C, and 70 °C, in that order. No LCST behavior was expected during the batch reactions Q2 and Q3, though the SGA detector was used to confirm or deny this expectation. LCST was expected, however, during Reaction

Q4, and the SGA detector was used online to measure this behavior.

The final product of all reactions was kept for further analysis. During Reaction Q4, several samples were taken from the waste line for further analysis.

Simultaneous multiple sample light scattering (SMSLS) [100, 101] was used to measure the LCST of several samples in parallel, under different ionic strengths. In each of these, the polymer concentration was diluted 100-fold from the final products of Reactions Q2 and Q3, and 6-fold from the samples taken from Reaction Q4. NaCl was added to a final concentration of 1 mM to 4.24 M. The temperatures were ramped at a rate of 1 °C/min from ambient temperature to 95 °C. Following that ramp, the temperatures were allowed to cool passively to ambient temperature.

5.6.3 Results and Discussion

5.6.3.1 Batch reactions

Reaction Q2 (50% Q9) does not have an LCST in the low-salt environment. This reaction produced chains with compositions in the range $30\% \leq F_{\text{inst,NIPAM}} \leq 45\%$, so this low-ionic strength result is unsurprising. One weakness with the batch reactions is that the Q9 reacted poorly. This produced lower Q9 content chains than intended, making the full analysis of the resulting chains difficult. Figure 5.37 shows this: the concentration of Q9 decreases to only about half of the initial concentration. This difficulty can be overcome by using a batch reaction method to push the reaction from chains of high Q9 content to chains of lower Q9 content, ultimately to NIPAM homopolymers. This was the goal of Reactions Q5 and Q6, discussed in Section 5.6.3.2. These reactions were also able to measure the onset of the LCST during the reactions. As a result of this data, we can quickly estimate at what composition the LCST turns on.

Reaction Q3 (20% Q9) showed an LCST of between 40 °C and 70 °C in 0.1 M NaCl, beginning quite early in the reaction (Figure 5.38). This is surprising, given

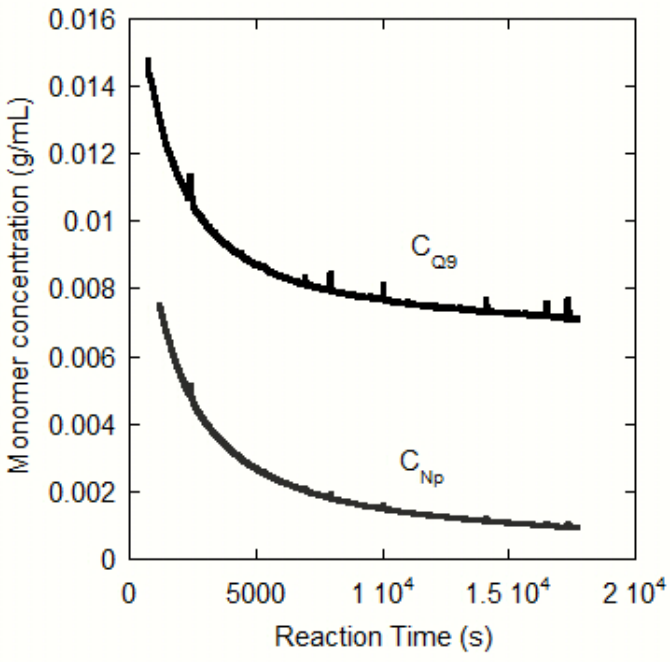

Figure 5.37: The computed monomer concentrations from Reaction Q2 show that the NIPAM was nearly fully converted. Only about half of the Q9 was converted into polymer.

the Q9 composition of that reaction, and the overall reactivity. Even if only about half of the Q9 was reacting, this would produce chains of $F_{\text{inst,Q9}} = 10\%$; this is well above the 5% threshold we previously found [87]. This discrepancy can be resolved by examining the $F_{\text{inst,Q9}}$ data in more detail, as in Figure 5.39. Because the Q9 reacts so poorly, the Q9 content is actually between 3.0% and 3.5% very early in the reaction. Most of the polymer mass is synthesized in that early portion, so any LCST displayed by this content is easily measurable by SMSLS. After this period of low-Q9 chains, the reaction produces a compositionally disperse population of chains. Each value of $F_{\text{inst,Q9}}$ will give rise to a different LCST. These can be distinguished with the addition of NaCl to the solution. This technique was previously used in the NIPAM/Am system [91], and is further discussed in Section 5.6.3.4.

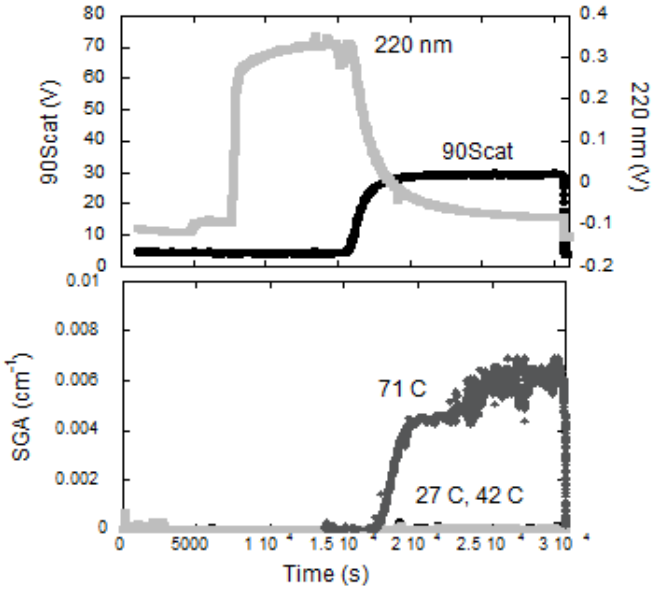

Figure 5.38: The ACOMP UV and light scattering data show that polymerization takes place in Reaction Q3. The SGA data is able to report that these polymer chains have an LCST between 40 °C and 70 °C, and that this begins shortly after the reaction itself begins.

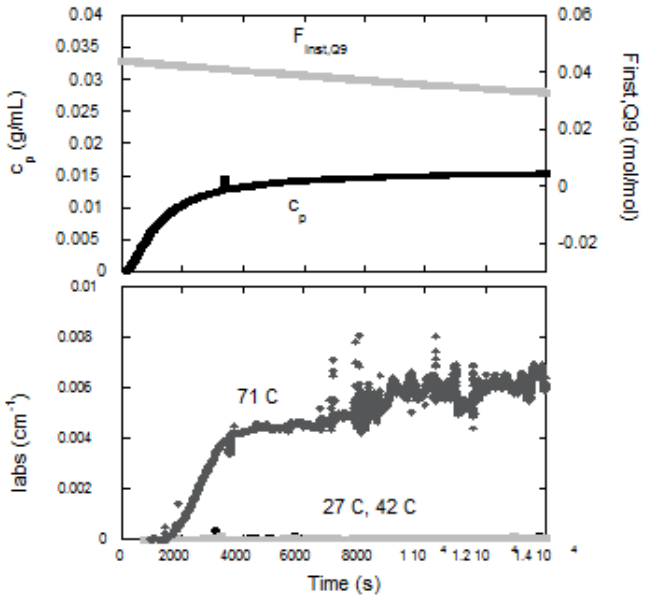

Figure 5.39: The computed monomer concentrations indicate that most of the polymer is synthesized early in Reaction Q3, and that very little of that early polymer is high in Q9 content. The $F_{\text{inst,Q9}}$ data from Reaction Q3 allows direct comparison between the Q9 content in the chains and the onset of the LCST during the reaction. This allows us to see that the LCST behavior tolerates as much as $F_{\text{inst,Q9}} = 0.04$. The noise in the 71 °C SGA signal beginning aroudn 8000 s is likely due to larger aggregates flowing through the detector at random intervals.

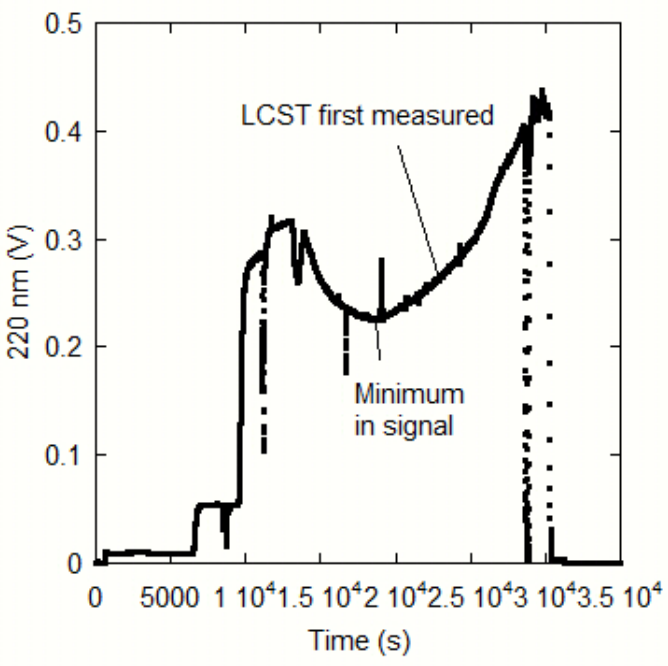

Figure 5.40: Raw UV data from Reaction Q4. The UV signal decreases initially as in the batch reactions. In the semi-batch reaction, however, the signal reaches a minimum and begins to increase. This minimum occurs because the Q9 monomer absorbs much more weakly than the NIPAM monomer.

5.6.3.2 Semi-batch reaction

Figure 5.40 shows the raw data from the semi-batch reaction. Comparison of the composition data with the SGA data in Figure 5.41 indicates that the LCST drops below 70 °C only after some chains of approximately $F_{\text{inst,Q9}} = 2\%$ have been synthesized. This estimate provides an additional confirmation of the composition in the early portion of the batch reactions.

One interesting feature of the raw UV data in Figure 5.40 is that the UV signal decreases initially, hits a minimum, then increases. This is in sharp contrast to the behavior of the UV signal from the batch reactions, and is a clear signal of the semi-batch reaction process for this pair of monomers. NIPAM absorbs more strongly in the UV than does Q9. So when a given molar concentration of Q9 monomer reacts,

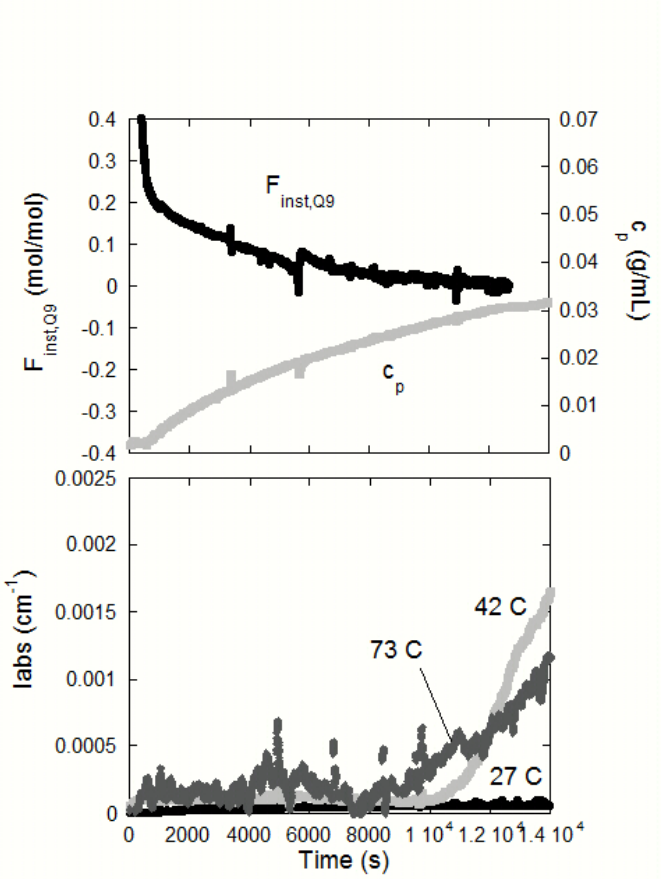

Figure 5.41: The instantaneous molar fraction of the chains in the semi-batch reaction drops very quickly from Q9 homoplymer to approximately 20% Q9 in the first 10 minutes of the reaction. It then falls more slowly over the rest of the reaction. The SGA detectors are able to detect LCST beginning at around $F_{\mathrm{inst,Q9}} = 0.02$.

and is replaced by NIPAM monomer, the result is an increase in UV. When no Q9 is left to react, the added NIPAM will be replaced only reacting NIPAM, so the UV signal will neither increase nor decrease. This eqilibrium is never achieved in this reaction.

5.6.3.3 GPC

One concern that the poor Q9 reactivity creates is that these reactions may actually be producing blends of homopolymers, rather than true copolymers. Figure 5.42 shows a GPC trace of the end product of Reaction Q1, which helps to confirm that the Q9 is incorporated into the polymer chains. This figure compares the signal due to the initial Q9 monomer to the signal due to the polymer and the reamaining Q9 monomer at the end of the reaction. In this case, the polymer and monomer are not well separated, indicating that this was a poor selection of column for this system. An exact quantitative estimate of the conversion is difficult, but we can estimate an upper and lower bound for the conversion. The light scattering signal indicates that the polymer is finish eluting at 800 s. Because there is a 30 s delay between the light scattering detector and the RI detector, this corresponds to 830 s in the RI detector. We can integrate the RI signal between 830 s and the Q9 monomer peak at 844 s, and compare this integral between the GPC injections with monomer only and the end product. This integral evaluates to 0.287 V s for the sample containing monomer only. The integral for the end product is 0.174 V s. These integrals imply a Q9 conversion of $1 - \frac{0.174}{0.287} = 0.40$. Alternatively, we can integrate the entire front half of the monomer signal from 780–840 s, and try to subract out the signal due to the polymer. The integral of the front half of the monomer peak (780–844 s) is 0.375 V s. The integral of the front half of the polymer peak (700–780 s) is 0.182 V s. The integral of the end product from 780 s to 844 s is 0.489 V s. This method therefore estimates the Q9 conversion as $1 - \frac{0.489 - 0.182}{0.375} = 0.18$ We can therefore conclude that somewhere between

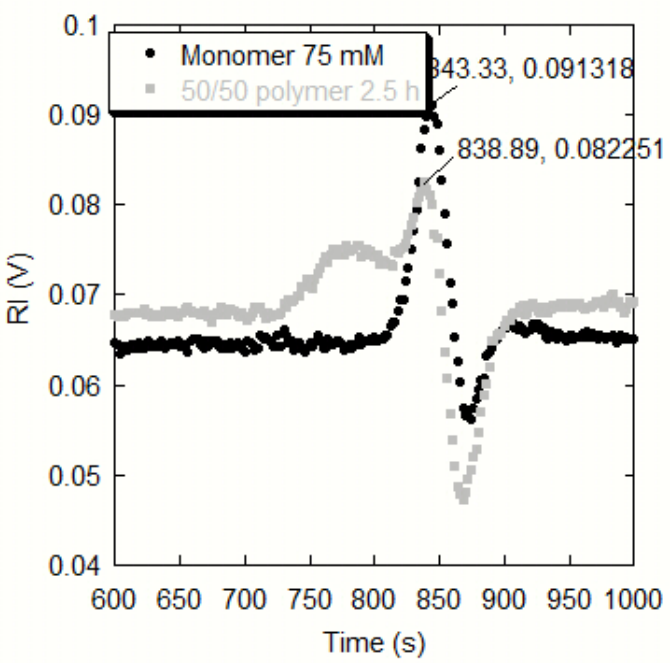

Figure 5.42: GPC of the end product of Reaction Q1 shows the polymer signal eluting almost on top of the Q9 monomer signal. The front half of the monomer line has decreased in size. The presense of the polymer line makes a quantitative estimate difficult, but we can estimate the conversion as being between 18 % and 40 %.

18 % and 40 % of the initial Q9 monomer converted into polymer. This is broadly consistent with the finding from the ACOMP UV data that apporoximately half of the Q9 monomer converted. Further, this GPC trace shows only one populations of polymer chains, which makes us reasonably confident that this is a population of true copolymers, rather than two populations of homopolymers.

5.6.3.4 SMSLS

Figure 5.43 shows the LCST of the end products of Q2 and Q3 as a function of ionic strength. The LCST of Q2 seems to fall linearly with added NaCl across the full range of ionic strengths. The LCST rises as NaCl is added from 0 M to 100 mM NaCl. After that point, the LCST decreases in an approximately linear fashion with added NaCl. This increase in LCST at very low ionic strength is similar to behavior

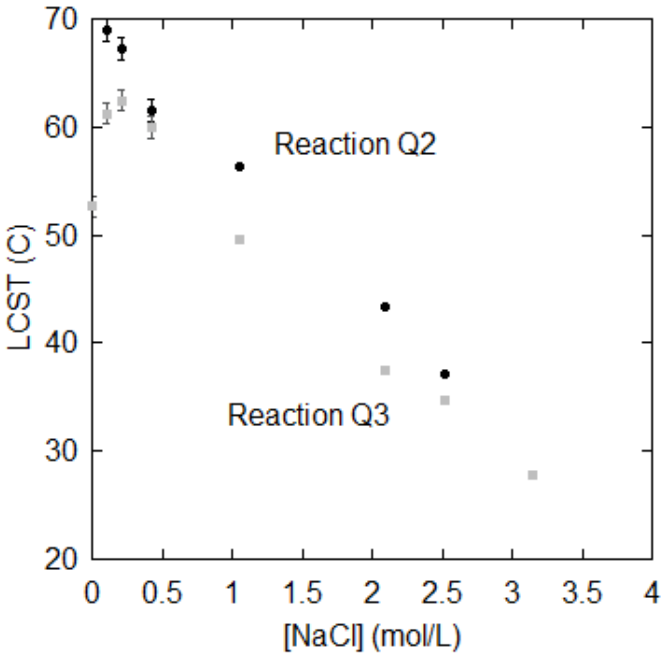

Figure 5.43: The LCST's of reactions Q2 and Q3 as a function of ionic strength. Above 100 mM NaCl, both shows an approximately linear decrease with added NaCl.

previously observed in pNIPAM homopolymer with other added salts [5].

The aliquots taken from the waste stream of the semi-batch reactions are able to provide a more detailed view of the effect of charge content on LCST. Table 5.12 shows the LCST of these samples in 17 and 100 M NaCl. A Q9 content of 2% suppresses the LCST in 17 mM NaCl; a Q9 content of 7% supresses the LCST in 100 mM NaCl. Below that electrolyte content, the LCST decreases as Q9 content decreases. The effect of Q9 content is much larger than the effect of Am on LCST.

Adding NaCl to these high-Q9 samples allows us to screen the charges on the Q9, and induce the LCST. Figure 5.44 shows the LCST of the Reaction Q4 aliquots in 1 M NaCl. 1 M NaCl is sufficient to induce an LCST in the Reaction Q4 samples with $F_{\mathrm{inst,Q9}} < 17\%$. The LCST appears to be roughtly independent of Q9 content above $F_{\mathrm{inst,Q9}} = 5\%$. Below this value, the LCST falls sharply with Q9 content. This is consistent with the idea that the salting-out effect is independent

Table 5.12: The samples taken from the waste stream of Reaction Q4. Times are taken relative to the addition of the initiator and the beginning of the NIPAM monomer flow. The uncertainties in the LCST's are derived from the method desribed in Section 5.4.3.4.

Sample	Time (s)	Q9 content (mol/mol)	LCST (17 mM) (°C)	LCST (100 mM) (°C)
Q4s1	300	0.67	> 100	> 100
Q4s2	1540	0.17	> 100	> 100
Q4s3	2974	0.12	> 100	> 100
Q4s4	4880	0.068	> 100	> 100
Q4s5	6794	0.043	> 100	83.3 ± 1.0
Q4s6	9450	0.023	> 100	53.6 ± 2.0
Q4s7	11658	0.0078	> 100	44.4 ± 1.0
Q4s8	13724	< 0.001	42.9 ± 0.5	40.9 ± 0.5
Q4s9	15150	< 0.001	41.4 ± 0.5	38.7 ± 0.5

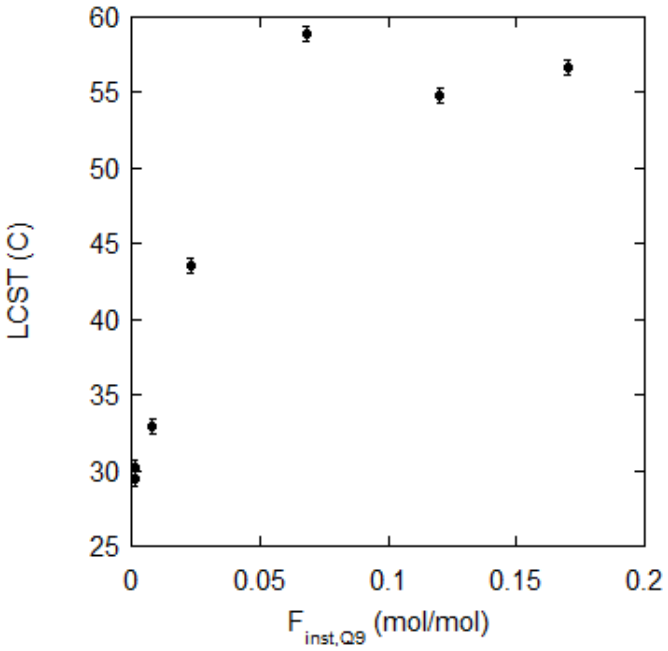

Figure 5.44: In 1 M NaCl, samples with $F_{\mathrm{inst,Q9}}$ as high as 17% show an LCST. The LCST falls very sharply as the Q9 content drops below 5%.

of composition. The samples with $F_{\text{inst,Q9}} > 5\%$ fail to have an LCST in lower ionic strength solutions because their LCST is above the boiling point of those solutions. More speculatively, this result suggests that $F_{\text{inst,Q9}} = 5\%$ is a real physical threshold. Further experiments would help to confirm or deny that idea.

5.6.3.5 Conclusions

I have synthesized copolymers of N-isopropyl acrylamide (NIPAM) and [2-(acryloyloxy)ethyl]-trimethylammonium chloride (Q9). These copolymers show lower critical solution behavior characteristic of NIPAM copolymers. In this case, the presense of the charged Q9 strongly suppresses the LCST behavior. However, the LCST behavior is compatible with the presence of some Q9 in the polymer chains. Increasing the ionic strength of the solution lowers the LCST of the chains. Semi-batch reactions allow me to synthesize chains with very braod comonomer comositions; these chains show a wide distribution of LCST's.

Chapter 6

Conclusion

I have developed and commissioned a new detector, called Second-Generation ACOMP (SGA). This is a flow-through detector for measuring temperature-driven aggregation of polymers using light scattering. I have used this new detector to observe the onset of LCST behavior in poly(NIPAM)-based copolymers during synthesis. This is the first time this has been done.

Using this technique, I have reproduced earlier measurements of the LCST of NIPAM/Am random copolymers.

Offline measurements of LCST using Simultaneous Multiple Sample Light Scattering (SMSLS) have reproduced past measurements of the effect of added NaCl on the LCST of NIPAM homopolymers. SMSLS has also measured, for the first time, the effect of added NaCl on NIPAM/Am copolymers. This confirms that adding NaCl to a solution can turn on LCST behavior of polymers with high Am content. The hydrophilic content of such polymers is so high that LCST behavior is not seen at any temperature in pure water; adding NaCl can bring the LCST to nearly any desired temperature for NIPAM/Am polymers of nearly any composition.

I have demonstrated that copolymers with some ionic content can have an LCST if the ionic content is low but non-zero. I have also demonstrated that adding salt can induce an LCST in copolymers with moderate ionic content. Copolymers

containing the anionic monomer SS and the cationic monomer Q9 have similar LCST behaviors; as a result, there seems to be little difference due to the sign of the charge.

Finally, I have used the semi-batch polymerization technique to sweep through all possible compositions in a single polymerization synthesis reaction. This allows rapid characterization of the LCST-composition relationship. I have demonstrated that the LCST's resulting from these semi-batch polymers are the same as those resulting from the batch polymers with the same composition.

References

[1] Mülhaupt, R., "Hermann staudinger and the origin of macromolecular chemistry", *Angewandte Chemie International Edition* **43** (2004), no. 9, 1054–1063.

[2] Schild, H. G., "Poly(n-isopropylacrylamide): experiment, theory and application", *Progress in Polymer Science* **17** (1992), no. 2, 163–249.

[3] Taylor, L. D. and L. D. Cerankowski, "Preparation of films exhibiting a balanced temperature dependence to permeation by aqueous solution. lower consolute behavior", *J. Polym. Sci., Polym. Chem. Ed.* **13** (1975), 2551–70.

[4] Priest, J. H., S. L. Murray, R. J. Nelson, and A. S. Hoffman, "Lower critical solution temperatures of aqueous copolymers of n-isopropylacrylamide and other n-substituted acrylamides", *ACS Symp. Ser.* **350** (1987), 255–64.

[5] Zhang, Y., S. Furyk, D. E. Bergbreiter, and P. S. Cremer, "Specific ion effects on the water solubility of macromolecules: PNIPAM and the hofmeister series", *Journal of the American Chemical Society* **127** (2005), 14505–14510.

[6] Witten, T. A. and P. A. Pincus, *Structured fluids: polymers, colloids surfactants*, first ed., Oxford University Press, 2004.

[7] Laurent, B. A. and S. M. Grayson, "Synthetic approaches for the preparation of cyclic polymers", *Chemical Society Reviews* **38** (2009), no. 8, 2202–2213 (en).

[8] Jia, Z. and M. J. Monteiro, "Cyclic polymers: Methods and strategies", *Journal of Polymer Science Part A: Polymer Chemistry* **50** (2012), no. 11, 2085–2097 (en).

[9] Dotson, N., R. Galvan, R. Laurence, and M. Tirrell, *Polymerization process modelling*, Advances in Interfacial Engineering, John Wiley & Sons, New

York, 1996 (English).

[10] Hiemenz, P. C. and T. P. Lodge, *Polymer chemistry*, second ed., CRC Press, Boca Raton, FL, 2007.

[11] O'Shaughnessy, B. and J. Yu, "Autoacceleration in free radical polymerization", *Physical Review Letters* **73** (1994), no. 12, 1723–1726.

[12] Fineman, M. and S. D. Ross, "Linear method for determining monomer reactivity ratios in copolymerization", *Journal of Polymer Science* **5** (1950), no. 2, 259–262.

[13] Alb, A. M., A. Paril, H. Çatalgil-Giz, A. Giz, and W. F. Reed, "Evolution of composition, molar mass, and conductivity during the free radical copolymerization of polyelectrolytes", *The Journal of Physical Chemistry B* **111** (2007), 8560–8566.

[14] Gonzàlez Garcìa, G., T. Kreft, A. M. Alb, J. C. de la Cal, J. M. Asua, and W. F. Reed, "Monitoring the synthesis and properties of copolymeric polycations", *The Journal of Physical Chemistry B* **112** (2008), 14597–14608.

[15] Mumick, P. S. and C. L. McCormick, "Water soluble copolymers. 54: N-isopropylacrylamide-co-acrylamide copolymers in drag reduction synthesis, characterization, and dilute solution behavior", *Polymer Engineering & Science* **34** (1994), 1419–1428.

[16] Alb, A. M., P. Enohnyaket, M. F. Drenski, R. Shunmugam, G. N. Tew, and W. F. Reed, "Quantitative contrasts in the copolymerization of acrylate- and methacrylate-based comonomers", *Macromolecules* **39** (2006), no. 24, 8283–8292.

[17] Reed, W., "Class notes for molecular biophysics (physics 621/321)", August 2003.

[18] Manning, G. S., "Limiting laws and counterion condensation in polyelectrolyte solutions i. colligative properties", *The Journal of Chemical Physics* **51** (1969), no. 3, 924–933.

[19] Weast, R., *Handbook of chemistry and physics*, 46th ed., The Chemical Rubber Company, 1965.

[20] Kreft, T. and W. F. Reed, "Experimental observation of crossover from non-condensed to counterion condensed regimes during free radical polyelec-

trolyte copolymerization under high-composition drift conditions", *The Journal of Physical Chemistry B* **113** (2009), no. 24, 8303–8309.

[21] Sorci, G. A. and W. F. Reed, "Electrostatically enhanced second and third virial coefficients, viscosity, and interparticle correlations for linear polyelectrolytes", *Macromolecules* **35** (2002), no. 13, 5218–5227.

[22] Jackson, J. D., *Classical electrodynamics*, 3rd ed ed., Wiley, New York, 1999.

[23] van de Hulst, H. C., *Light scattering by small particles*, first ed., Dover Publications, New York, 1981.

[24] Stowe, K., *Introduction to statistical mechanics and thermodynamics*, John Wiley & Sons, New York, 1984.

[25] Zimm, B. H., "Apparatus and methods for measurement and interpretation of the angular variation of light scattering; preliminary results on polystyrene solutions", *The Journal of Chemical Physics* **16** (1948), no. 12, 1099–1116.

[26] Kerker, M., *The scattering of light and other electromagnetic radiation*, first ed., Physical Chemistry: a Series of Monographs, no. 16, Academic Press, New York, 1969.

[27] Berne, B. J. and R. Pecora, *Dynamic light scattering with applications to chemistry, biology, and physics*, Dover Publications, Inc., 2000.

[28] Michelson, I., *The science of fluids*, van Nostrand Reinhold Company, New York, 1970 (English).

[29] Winnik, F. M., H. Ringsdorf, and J. Venzmer, "Methanol-water as a cononsolvent system for poly(n-isopropylacrylamide)", *Macromolecules* **23** (1990), 2415–16.

[30] Schild, H. G., M. Muthukumar, and D. A. Tirrell, "Cononsolvency in mixed aqueous solutions of poly(n-isopropylacrylamide)", *Macromolecules* **24** (1991), no. 4, 948–952.

[31] Winnik, F. M., H. Ringsdorf, and J. Venzmer, "Interaction of surfactants with hydrophobically-modified poly(n-isopropylacrylamides). 2. fluorescence label studies", *Langmuir* **7** (1991), 912–17.

[32] Lowe, A. B., M. Torres, and R. Wang, "A doubly responsive AB diblock copolymer: RAFT synthesis and aqueous solution properties of poly

(n-isopropylacrylamide-block-4-vinylbenzoic acid)", *Journal of Polymer Science Part A: Polymer Chemistry* **45** (2007), no. 24, 5864–5871.

[33] Virtanen, J., C. Baron, and H. Tenhu, "Grafting of poly(n-isopropylacrylamide) with poly(ethylene oxide) under various reaction conditions", *Macromolecules* **33** (1999), no. 2, 336–341.

[34] Meng, H. and J. Hu, "A brief review of stimulus-active polymers responsive to thermal, light, magnetic, electric, and water/solvent stimuli", *J. Intell. Mater. Syst. Struct.* **21** (2010), 859–885.

[35] Roy, D., J. N. Cambre, and B. S. Sumerlin, "Future perspectives and recent advances in stimuli-responsive materials", *Progress in Polymer Science* **35** (2010), no. 1-2, 278–301.

[36] Huang, J. and X. Y. Wu, "Effects of pH, salt, surfactant and composition on phase transition of poly(NIPAm/MAA) nanoparticles", *Journal of Polymer Science Part A: Polymer Chemistry* **37** (1999), no. 14, 2667–2676.

[37] Bignotti, F., M. Penco, L. Sartore, I. Peroni, R. Mendichi, M. Casolaro, and A. D'Amore, "Synthesis, characterisation and solution behaviour of thermo- and pH-responsive polymers bearing -leucine residues in the side chains", *Polymer* **41** (2000), 8247–8256.

[38] Idili, A., A. Vallée-Bélisle, and F. Ricci, "Programmable pH-triggered DNA nanoswitches", *Journal of the American Chemical Society* **136** (2014), no. 16, 5836–5839.

[39] Izumi, A., R. Nomura, and T. Masuda, "Design and synthesis of stimuli-responsive conjugated polymers having azobenzene units in the main chain", *Macromolecules* **34** (2001), no. 13, 4342–4347.

[40] MacLachlan, H. J., M. Ginzburg, N. Coombs, T. W. Coyle, N. P. Raju, J. E. Greedan, G. A. Ozin, and I. Manners, "Shaped ceramics with tunable magnetic properties from metal-containing polymers", *Science* **287** (2000), no. 5457, 1460.

[41] McCulloch, B., G. Portale, W. Bras, and R. A. Segalman, "Increased order–disorder transition temperature for a rod–coil block copolymer in the presence of a magnetic field", *Macromolecules* **44** (2011), no. 19, 7503–7507.

[42] Zhu, Y., H. Liu, F. Li, Q. Ruan, H. Wang, M. Fujiwara, L. Wang, and G. Q. Lu, "Dipolar molecules as impellers achieving electric-field-stimulated

release", *Journal of the American Chemical Society* **132** (2010), no. 5, 1450–1451.

[43] Cheng, H. and M. Olvera de la Cruz, "Hydrophobic-charged block copolymer micelles induced by oppositely charged surfaces: Salt and pH dependence", *Macromolecules* **39** (2006), no. 5, 1961–1970.

[44] Guo, B.-L., J.-F. Yuan, and Q.-Y. Gao, "Preparation and release behavior of temperature- and pH-responsive chitosan material", *Polymer International* **57** (2008), no. 3, 463–468.

[45] Huo, D., Y. Li, Q. Qian, and T. Kobayashi, "Temperature-pH sensitivity of bovine serum albumin protein-microgels based on cross-linked poly(n-isopropylacrylamide-co-acrylic acid)", *Colloids and Surfaces B: Biointerfaces* **50** (2006), no. 1, 36–42.

[46] Kim, K. S. and B. Vincent, "pH and temperature-sensitive behaviors of poly(4-vinyl pyridine-co-n-isopropyl acrylamide) microgels", *Polymer Journal* **37** (2005), no. 8, 565–570.

[47] Mi Kyong, Y., S. Yong Kiel, S. C. Chong, and M. L. Young, "Effect of polymer complex formation on the cloud-point of poly(n-isopropyl acrylamide) (PNIPAAm) in the poly(NIPAAm-co-acrylic acid): polyelectrolyte complex between poly(acrylic acid) and poly(allylamine)", *Polymer* **38** (1997), no. 11, 2759–2765.

[48] Roy, D., J. N. Cambre, and B. S. Sumerlin, "Sugar-responsive block copolymers by direct RAFT polymerization of unprotected boronic acid monomers", *Chemical Communications* (2008), no. 21, 2477–2479.

[49] Yao, Y., H. Shen, G. Zhang, J. Yang, and X. Jin, "Synthesis of poly(n-isopropylacrylamide)-co-poly(phenylboronate ester) acrylate and study on their glucose-responsive behavior", *Journal of Colloid and Interface Science* **431** (2014), 216–222.

[50] Principi, T., C. C. E. Goh, R. C. W. Liu, and F. M. Winnik, "Solution properties of hydrophobically modified copolymers of n-isopropylacrylamide and n-glycine acrylamide: A study by microcalorimetry and fluorescence spectroscopy", *Macromolecules* **33** (2000), no. 8, 2958–2966.

[51] Kujawa, P. and F. M. Winnik, "Volumetric studies of aqueous polymer solutions using pressure perturbation calorimetry: A new look at the temperature-induced phase transition of poly(n-isopropylacrylamide) in water and d2o", *Macromolecules* **34** (2001), 4130–4135.

[52] Mao, H., C. Li, Y. Zhang, D. E. Bergbreiter, and P. S. Cremer, "Measuring LCSTs by novel temperature gradient methods: Evidence for intermolecular interactions in mixed polymer solutions", *Journal of the American Chemical Society* **125** (2003), 2850–2851.

[53] Zhang, Y., S. Furyk, L. B. Sagle, Y. Cho, D. E. Bergbreiter, and P. S. Cremer, "Effects of hofmeister anions on the LCST of PNIPAM as a function of molecular weight", *The Journal of Physical Chemistry C* **111** (2007), 8916–8924.

[54] Wu, C. and S. Zhou, "Laser light scattering study of the phase transition of poly(n-isopropylacrylamide) in water. 1. single chain", *Macromolecules* **28** (1995), 8381–8387.

[55] Wu, C. and S. Zhou, "Thermodynamically stable globule state of a single poly(n-isopropylacrylamide) chain in water", *Macromolecules* **28** (1995), 5388–5390.

[56] Wu, C. and S. Zhou, "First observation of the molten globule state of a single homopolymer chain", *Phys. Rev. Lett.* **77** (1996), 3053–3055.

[57] Li, M. and C. Wu, "Self-association of poly(n-isopropylacrylamide) and its complexation with gelatin in aqueous solution", *Macromolecules* **32** (1999), 4311–4316.

[58] Furyk, S., Y. Zhang, D. Ortiz-Acosta, P. S. Cremer, and D. E. Bergbreiter, "Effects of end group polarity and molecular weight on the lower critical solution temperature of poly(n-isopropylacrylamide)", *Journal of Polymer Science Part A: Polymer Chemistry* **44** (2006), no. 4, 1492–1501.

[59] Tong, Z., F. Zeng, X. Zheng, and T. Sato, "Inverse molecular weight dependence of cloud points for aqueous poly(n-isopropylacrylamide) solutions", *Macromolecules* **32** (1999), no. 13, 4488–4490.

[60] Lessard, D. G., M. Ousalem, and X. X. Zhu, "Effect of the molecular weight on the lower critical solution temperature of poly(n,n-diethylacrylamide) in aqueous solutions", *Canadian Journal of Chemistry* **79** (2001), no. 12, 1870–1874.

[61] Xia, Y., X. Yin, N. A. D. Burke, and H. D. H. Stover, "Thermal response of narrow-disperse poly(n-isopropylacrylamide) prepared by atom transfer radical polymerization", *Macromolecules* **38** (2005), 5937–5943.

[62] Zimm, B. H., "The scattering of light and the radial distribution function of high polymer solutions", *The Journal of Chemical Physics* **16** (1948),

1093.

[63] Kubota, K., S. Fujishige, and I. Ando, "Single-chain transition of poly(n-isopropylacrylamide) in water", *Journal of Physical Chemistry* **94** (1990), 5154–5158.

[64] Schild, H. G. and D. A. Tirrell, "Microcalorimetric detection of lower critical solution temperatures in aqueous polymer solutions", *Journal of Physical Chemistry* **94** (1990), 4352–4356.

[65] Ding, Y., X. Ye, and G. Zhang, "Microcalorimetric investigation on aggregation and dissolution of poly(n-isopropylacrylamide) chains in water", *Macromolecules* **38** (2005), no. 3, 904–908.

[66] Tang, Y., Y. Ding, and G. Zhang, "Role of methyl in the phase transition of poly(n-isopropylmethacrylamide)", *Journal of Physical Chemistry B* **112** (2008), no. 29, 8447–8451.

[67] Siano, D. B., J. Bock, P. Myer, and P. L. J. Valint, "Light scattering and fluorescence study of hydrophobically associating polymers", *Polym. Mater. Sci. Eng.* **57** (1987), 609–12.

[68] Ringsdorf, H., J. Venzmer, and F. M. Winnik, "Fluorescence studies of hydrophobically modified poly(n-isopropylacrylamides)", *Macromolecules* **24** (1991), 1678–86.

[69] Jana, S., S. P. Rannard, and A. I. Cooper, "Structure-LCST relationships for end-functionalized water-soluble polymers: an "accelerated" approach to phase behaviour studies", *Chemical Communications* (2007), 2962–4.

[70] Prigogine, I. and R. Defay, *Chemical thermodynamics*, John Wiley & Sons Inc, New York, 1954.

[71] Cowie, J. M. G. and V. Arrighi, *Polymers: chemistry and physics of modern materials*, third ed., CRC Press, Boca Raton, FL, 2008.

[72] Huggins, M. L., "Theory of solutions of high polymers", *Journal of the American Chemical Society* **64** (1942), no. 7, 1712–1719.

[73] Flory, P. J., "Treatment of disordered and ordered systems of polymer chains by lattice methods.", *Proceedings of the National Academy of Sciences of the United States of America* **79** (1982), no. 14, 4510–4514.

[74] Flory, P. J. and W. R. Krigbaum, "Statistical mechanics of dilute polymer solutions. II", *The Journal of Chemical Physics* **18** (1950), no. 8, 1086–

1094.

[75] Freitag, R. and F. Garret-Flaudy, "Salt effects on the thermoprecipitation of poly-(n-isopropylacrylamide) oligomers from aqueous solution", *Langmuir* **18** (2002), no. 9, 3434–3440.

[76] Kujawa, P., F. Tanaka, and F. M. Winnik, "Temperature-dependent properties of telechelic hydrophobically modified poly(n-isopropylacrylamides) in water: Evidence from light scattering and fluorescence spectroscopy for the formation of stable mesoglobules at elevated temperatures", *Macromolecules* **39** (2006), no. 8, 3048–3055.

[77] Tiktopulo, E. I., V. E. Bychkova, J. Ricka, and O. B. Ptitsyn, "Cooperativity of the coil-globule transition in a homopolymer: Microcalorimetric study of poly(n-isopropylacrylamide)", *Macromolecules* **27** (1994), no. 10, 2879–2882.

[78] Kawasaki, H., S. Sasaki, H. Maeda, and K. Nishinari, "Effect of the introduced charge on the thermal behavior of n-isopropylacrylamide gels in water and NaCl solutions", *Langmuir* **16** (2000), no. 7, 3195–3199.

[79] Ben-Naim, A. and M. Yaacobi, "Effects of solutes on the strength of hydrophobic interaction and its temperature dependence", *The Journal of Physical Chemistry* **78** (1974), no. 2, 170–175.

[80] Yaacobi, M. and A. Ben-Naim, "Solvophobic interaction", *The Journal of Physical Chemistry* **78** (1974), no. 2, 175–178.

[81] Heyda, J. and J. Dzubiella, "Thermodynamic description of hofmeister effects on the LCST of thermosensitive polymers", *The Journal of Physical Chemistry B* (2014).

[82] Hermans, J. J. and S. Levinson, "Some geometrical factors in light-scattering apparatus", *J. Opt. Soc. Am.* **41** (1951), no. 7, 460–464.

[83] Kreft, T. and W. F. Reed, "Predictive control and verification of conversion kinetics and polymer molecular weight in semi-batch free radical homopolymer reactions", *European Polymer Journal* **45** (2009), no. 8, 2288–2303.

[84] Alb, A. M. and W. F. Reed, "Simultaneous monitoring of polymer and particle characteristics during emulsion polymerization", *Macromolecules* **41** (2008), no. 7, 2406–2414.

[85] Alb, A. M. and W. F. Reed, "Fundamental measurements in online polymerization reaction monitoring and control with a focus on ACOMP", *Macromol. React. Eng.* **4** (2010), 470–485.

[86] Florenzano, F. H., R. Strelitzki, and W. F. Reed, "Absolute, on-line monitoring of molar mass during polymerization reactions", *Macromolecules* **31** (1998), no. 21, 7226–7238.

[87] McFaul, C. A., A. M. Alb, M. F. Drenski, and W. F. Reed, "Simultaneous multiple sample light scattering detection of LCST during copolymer synthesis", *Polymer* **52** (2011), no. 21, 4825–4833.

[88] Estey, T., J. Kang, S. P. Schwendeman, and J. F. Carpenter, "BSA degradation under acidic conditions: A model for protein instability during release from PLGA delivery systems", *Journal of Pharmaceutical Sciences* **95** (2006), no. 7, 1626–1639.

[89] Chodankar, S., V. K. Aswal, J. Kohlbrecher, R. Vavrin, and A. G. Wagh, "Structural evolution during protein denaturation as induced by different methods", *Physical Review E (Statistical, Nonlinear, and Soft Matter Physics)* **77** (2008), no. 3, 031901–9.

[90] Bagger, H. L., L. H. Øgendal, and P. Westh, "Solute effects on the irreversible aggregation of serum albumin", *Biophysical Chemistry* **130** (2007), no. 1-2, 17–25.

[91] McFaul, C. A., M. F. Drenski, and W. F. Reed, "Online, continuous monitoring of the sensitivity of the LCST of NIPAM-am copolymers to discrete and broad composition distributions", *Polymer* **55** (2014), no. 19, 4899–4907.

[92] Wu, C. and X. Wang, "Globule-to-coil transition of a single homopolymer chain in solution", *Phys. Rev. Lett.* **80** (1998), 4092–4094.

[93] Brousseau, J.-L., H. Çatalgil-Giz, and W. F. Reed, "Automatic, simultaneous determination of differential refractive index of a polymer and its corresponding monomer", *Journal of Applied Polymer Science* **77** (2000), 3259–3262.

[94] Zhang, J. and R. Pelton, "The surface tension of aqueous poly(n-isopropylacrylamide-co-acrylamide)", *J. Polym. Sci., Part A: Polym. Chem.* **37** (1999), 2137–2143.

[95] Chiklis, C. K. and J. M. Grasshoff, "Swelling of thin films. i. acrylamide-n-isopropylacrylamide copolymers in water", *J. Polym. Sci., Part A-2* **8** (1970), 1617–26.

[96] Mao, H., C. Li, Y. Zhang, S. Furyk, P. S. Cremer, and D. E. Bergbreiter, "High-throughput studies of the effects of polymer structure and solution components on the phase separation of thermoresponsive polymers", *Macromolecules* **37** (2004), 1031–1036.

[97] Kreft, T. and W. F. Reed, "Predictive control of average composition and molecular weight distributions in semibatch free radical copolymerization reactions", *Macromolecules* **42** (2009), no. 15, 5558–5565.

[98] Alb, A. M. and W. F. Reed, "Recent advances in automatic continuous online monitoring of polymerization reactions (ACOMP)", *Macromolecular Symposia* **271** (2008), no. 1, 15–25.

[99] Doty, P. M., B. H. Zimm, and H. Mark, "An investigation of the determination of molecular weights of high polymers by light scattering", *The Journal of Chemical Physics* **13** (1945), no. 5, 159–166.

[100] Drenski, M. F. and W. F. Reed, "Simultaneous multiple sample light scattering for analysis of polymer solutions", *Journal of Applied Polymer Science* **92** (2004), no. 4, 2724–2732.

[101] Drenski, M. F., M. L. Brader, R. W. Alston, and W. F. Reed, "Monitoring protein aggregation kinetics with simultaneous multiple sample light scattering", *Analytical Biochemistry* **437** (2013), no. 2, 185–197.

[102] Paril, A., A. M. Alb, A. Giz, and H. Çatalgil-Giz, "Online monitoring of 4-vinylbenzene sulfonic acid sodium salt - acrylamide copolymerization in water", *Macromolecular Symposia* **275-276** (2009), 266–274.

[103] Enohnyaket, P., T. Kreft, A. M. Alb, M. F. Drenski, and W. F. Reed, "Determination of molecular mass during online monitoring of copolymerization reactions", *Macromolecules* **40** (2007), no. 22, 8040–8049.

[104] Dalkas, G., K. Pagonis, and G. Bokias, "Control of the lower critical solution temperature-type cononsolvency properties of poly(n-isopropylacrylamide) in water-dioxane mixtures through copolymerisation with acrylamide", *Polymer* **47** (2006), no. 1, 243–248.

[105] Giz, A., H. Çatalgil-Giz, A. Alb, J.-L. Brousseau, and W. F. Reed, "Kinetics and mechanisms of acrylamide polymerization from absolute, online monitoring of polymerization reaction", *Macromolecules* **34** (2001), 1180–1191.

[106] Stockmayer, W. H., "Distribution of chain lengths and compositions in copolymers", *The Journal of Chemical Physics* **13** (1945), no. 6, 199–207.

[107] Liu, H. Y. and X. X. Zhu, "Lower critical solution temperatures of n-substituted acrylamide copolymers in aqueous solutions", *Polymer* **40** (1999), no. 25, 6985–6990.

[108] Barker, I. C., J. M. G. Cowie, T. N. Huckerby, D. A. Shaw, I. Soutar, and L. Swanson, "Studies of the "smart" thermoresponsive behavior of copolymers of n-isopropylacrylamide and n,n-dimethylacrylamide in dilute aqueous solution", *Macromolecules* **36** (2003), no. 20, 7765–7770.

[109] Hahn, M., E. Gornitz, and H. Dautzenberg, "Synthesis and properties of ionically modified polymers with LCST behavior", *Macromolecules* **31** (1998), no. 17, 5616–5623.

[110] Hoare, T. and R. Pelton, "Calorimetric analysis of thermal phase transitions in functionalized microgels", *Journal of Physical Chemistry B* **111** (2007), no. 6, 1334–1342.

[111] Laukkanen, A., L. Valtola, F. M. Winnik, and H. Tenhu, "Formation of colloidally stable phase separated poly(n-vinylcaprolactam) in water: A study by dynamic light scattering, microcalorimetry, and pressure perturbation calorimetry", *Macromolecules* **37** (2004), no. 6, 2268–2274.

[112] Tanaka, F., T. Koga, and F. M. Winnik, "Temperature-responsive polymers in mixed solvents: Competitive hydrogen bonds cause cononsolvency", *Physical Review Letters* **101** (2008), no. 2, 028302.

[113] Tsubouchi, T., K. Nishida, and T. Kanaya, "Lower critical solution temperature type of phase separation in aqueous mixture of polyelectrolytes", *Colloids and Surfaces B: Biointerfaces* **56** (2007), no. 1-2, 265–269.

[114] Smith, A. E., X. Xu, S. E. Kirkland-York, D. A. Savin, and C. L. McCormick, "Schizophrenic self-assembly of block copolymers synthesized via aqueous RAFT polymerization: From micelles to vesicles. paper number 143 in a series on water-soluble polymers.", *Macromolecules* **43** (2010), no. 3, 1210–1217.

[115] Murthy, N., M. Xu, S. Schuck, J. Kunisawa, N. Shastri, and J. M. J. Fréchet, "A macromolecular delivery vehicle for protein-based vaccines: Acid-degradable protein-loaded microgels", *Proceedings of the National Academy of Sciences of the United States of America* **100** (2003), no. 9, 4995–5000.

[116] Kim, K. T., J. J. L. M. Cornelissen, R. J. M. Nolte, and J. C. M. v. Hest, "Polymeric monosaccharide receptors responsive at neutral pH", *Journal of the American Chemical Society* **131** (2009), no. 39, 13908–13909.

[117] Wallace, G. G., G. M. Spinks, L. A. P. Kane-Maguire, and P. R. Teasdale, *Conductive electroactive polymers: Intelligent polymer systems*, third ed., CRC Press, Boca Raton, 2009.

[118] Goodby, J. W., "Mesogenic molecular crystalline materials", *Current Opinion in Solid State and Materials Science* **4** (1999), no. 4, 361–368.

[119] Mataga, N., "Possible ferromagnetic states of some hypothetical hydrocarbons", *Theoretical Chemistry Accounts: Theory, Computation, and Modeling (Theoretica Chimica Acta)* **10** (1968), no. 4, 372–376.

[120] Burba, C. M., S. M. Carter, K. J. Meyer, and C. V. Rice, "Salt effects on poly(n-isopropylacrylamide) phase transition thermodynamics from NMR spectroscopy", *The Journal of Physical Chemistry B* **112** (2008), no. 34, 10399–10404.

[121] Foster, E. J., E. B. Berda, and E. W. Meijer, "Metastable supramolecular polymer nanoparticles via intramolecular collapse of single polymer chains", *Journal of the American Chemical Society* **131** (2009), no. 20, 6964–6966.

[122] Jeon, H. J., D. H. Go, S.-y. Choi, K. M. Kim, J. Y. Lee, D. J. Choo, H.-O. Yoo, J. M. Kim, and J. Kim, "Synthesis of poly(ethylene oxide)-based thermoresponsive block copolymers by RAFT radical polymerization and their uses for preparation of gold nanoparticles", *Colloids and Surfaces A: Physicochemical and Engineering Aspects* **317** (2008), no. 1-3, 496–503.

[123] Lutz, J.-F., Ö. Akdemir, and A. Hoth, "Point by point comparison of two thermosensitive polymers exhibiting a similar LCST: is the age of poly(NIPAM) over?", *Journal of the American Chemical Society* **128** (2006), no. 40, 13046–13047.

[124] Roberts, C. J., "Kinetics of irreversible protein aggregation: Analysis of extended lumry-eyring models and implications for predicting protein shelf life", *The Journal of Physical Chemistry B* **107** (2003), no. 5, 1194–1207.

[125] Norwood, D. P. and W. F. Reed, "Comparison of on-line single-capillary and bridge capillary viscometric detectors for size exclusion chromatography", *International Journal of Polymer Analysis and Characterization* **4** (1997), no. 2, 99–132.

[126] Stineman, R. W., "A consistently well-behaved method of interpolation", *Creative Computing* **6** (1980), no. 7, 54–57.

[127] Synergy Software, "Using smooth curve fits", `http://www.synergy.com/Tools/curvefitting.pdf`, pp. 29–32.

[128] Bjornsson, T. J. . H. and I. M. O. G. Grothendieck, "stinepack: Stineman, a consistently well behaved method of interpolation", http://cran.r-project.org/web/packages/stinepack/index.html, October 2012.

[129] Henning, J., "stineman(x, y, xi, yp)", `http://www.mathworks.com/matlabcentral/fileexchange/36800-interpolation-utilities/content/stineman.m`, September 2014.

[130] Wagon, S., "Stineman.nb", `http://library.wolfram.com/infocenter/Articles/1933/`, 1995.

[131] Tauer, K., D. Gau, S. Schulze, and H. Hernandez, "Transient-thermal and isothermal studies of thermo-sensitive polymer solution with ultrasound resonator technology", *Polymer* **49** (2008), 5452–5457.

[132] Kreft, T. and W. F. Reed, "Direct monitoring of the cross-over from diffusion-controlled to decomposition-controlled initiation in free radical polymerization", *Macromolecular Chemistry and Physics* **209** (2008), no. 24, 2463–2474.

[133] Nowakowska, M., K. Szczubialka, and M. Grebosz, "Modifying the thermosensitivity of copolymers of sodium styrene sulfonate and n-isopropylacrylamide with dodecyltrimethylammonium chloride", *Colloid Polym. Sci.* **283** (2004), 291–298.

[134] Siu, M.-H., G. Zhang, and C. Wu, "Effect of comonomer distribution on the coil-to-globule transition of a single AB copolymer chain in dilute solution", *Macromolecules* **35** (2002), no. 7, 2723–2727.

[135] Geever, L. M., D. M. Devine, M. J. D. Nugent, J. E. Kennedy, J. G. Lyons, A. Hanley, and C. L. Higginbotham, "Lower critical solution temperature control and swelling behaviour of physically crosslinked thermosensitive copolymers based on n-isopropylacrylamide", *European Polymer Journal* **42** (2006), no. 10, 2540–2548.

[136] Garcia-Salinas, M. J., M. S. Romero-Cano, and F. J. de las Nieves, "Colloidal stability of a temperature-sensitive poly(n-isopropylacrylamide/2-acrylamido-2-methylpropanesulphonic acid) microgel", *Journal of Colloid and Interface Science* **248** (2002), no. 1, 54–61.

[137] Gao, J. and B. J. Frisken, "Influence of reaction conditions on the synthesis of self-cross-linked n-isopropylacrylamide microgels", *Langmuir* **19** (2003),

no. 13, 5217–5222.

[138] Roberts, C. J., "Non-native protein aggregation kinetics", *Biotechnology and Bioengineering* **98** (2007), no. 5, 927–938.

[139] Heyda, J., S. Soll, J. Yuan, and J. Dzubiella, "Thermodynamic description of the LCST of charged thermoresponsive copolymers", *Macromolecules* **47** (2014), no. 6, 2096–2102.

Biography

Colin Alfred McFaul was born April 1, 1983, in Seattle WA. In June of that year, he moved with his parents and older brother to Huntington Beach CA. He attended K-8 at Saints Simon and Jude School in Huntington Beach. In 1997, the family moved to Mission Viejo CA. Colin attended Santa Margarita Catholic High School in Rancho Santa Margarita CA, graduating in 2001. That year, he moved to Chicago IL to begin his studies at the University of Chicago. He was awarded an AB in Physics from the University of Chicago in June 2005. From then until September of that year, he lived in Santiago, Chile. Upon his return to Chicago, he worked at the University of Chicago from November 2005 to June 2007 in a lab researching EPR imaging of the oxygenation of tumors in mice. On April 22, 2007, he married Eleanor (Nora) Elana Friedman. In June of 2007, they moved from Chicago to New Orleans LA, where they live today with their three cats Hodag, Tony, and Okra, and a deaf American Bulldog named Marilyn Monroe.